

Electronic and structural dynamics in DNA single strands

Présentée le 14 mai 2021

Faculté des sciences de base
Laboratoire de spectroscopie ultrarapide
Programme doctoral en photonique

pour l'obtention du grade de Docteur ès Sciences

par

Benjamin BAUER

Acceptée sur proposition du jury

Prof. J.-E. Moser, président du jury
Prof. M. Chergui, directeur de thèse
Prof. B. Kohler, rapporteur
Prof. A. Cannizzo, rapporteur
Prof. C. Bostedt, rapporteur

To my friends and family, for all their help, support and inspiration.

Acknowledgements

The thesis you are holding in your hands right now (or reading on a screen) was not possible without the contributions of several people over the last four years.

First of all I want to thank Dr. Malte Oppermann. Malte co-supervised my thesis, planned and coordinated the project. He made sure our laser setup was operational and invested a lot of time and energy in the lab. He worked closely with me on the project and had always an open ear for discussions. Without him this project would have been impossible. Thanks for the close supervision and the careful proofreading of the manuscript, which improved the quality of the work. I also want to thank Prof. Majed Chergui my thesis adviser for the help on the project and making the project possible.

With my thesis committee (Prof. Bern Kohler, Prof. Andrea Cannizzo, Prof. Christoph Bostedt and Prof. Jacques-Eduard Moser) I had a nice and fruitful scientific discussion on my work. Thanks for taking the time to carefully read and evaluate my work and make valuable suggestions.

My work was based on previous works. I want to thank my predecessors for pushing the field scientifically but also technically forward. We were a small team working nicely together on the 20kHz team. I want to thank the master students Livia, Ianina and Francois for the enjoyable time together in the labs as well as in the office. I especially want to thank Livia who I had the honour to supervise her on a semester project. We shared the office for two years and had a great time together. Furthermore I want to thank Thomas Rossi, I spend two years with him as a office and lab mate. Thanks introducing me to the many details of PhD life at EPFL and for the profound discussion be it scientifically or on everyday topics. A special thanks goes to Lars with whom I not only share the passion for ultrafast spectroscopy but also for outdoor sports. Thanks for taking me with you on our outdoor trips. I want to thank my fellow PhD colleagues who shared the time with me in LSU namely, Oliviero, Fabio, Lars, Lijie, Thomas, Luca, Serhii, Dominik, Jose, Tania, Boris, Ludmilla and Hui-Yuan and our master students Livia, Ianina, Francois, Stéphane and Arash. Thanks also to our Post-docs who helped me with their knowledge, namely Hugo, Natalia, Joanna, Kathrin, Rolf, Michele, Chris, Thomas Raphael, Francesco, Jeremy and Rebecca. I want to thank Annick for her kind help with many organisational things.

I also want to thank our collaborators. Prof. Heinis kindly granted us access to his static CD spectrometer and Xudong and Zsolt introduced us to it. Prof. Jacques-Eduard Moser granted

us access when our UvVis spectrometer was broken and Etienne and Andrés introduced us to the device. Furthermore I want to thank Rahul for his simulations that contributed to the project as well as for the fruitful discussions on his results.

I want to thank the LUMES team with whom we shared space for the collegiality and the nice time we spend, namely Francesco, Gianmaria, Enrico, Paolo and Shiam as well as the LSE team Alberto, Silvan and Gigi.

As experimentalists we are heavily dependent on technical support. Representatively for all the people from the mechanical and electronic workshop who helped me out in many occasions on a quick manner and gave me high quality solutions I want to thank Christophe, Guillaume, Benjamin and Supardi.

I want to thank my friends and family for their emotional support over the last four years and freeing my mind from work.

Special thanks goes to Bernd with whom I shared an apartment for three years. I also want to thank the whole Konstanz-crew for making the last ten years very special and sometimes crazy.

I want to thank my parents, my brothers, my sister and their families for the wonderful time and emotional support.

A very special thanks goes to Angie. Thank you very much for your love and helping me out especially during the last intensive year of my PhD thesis. I also want to thank Sarah for her help and support.

And last but not least I want to thank you for your interest in my work.

Lausanne, 17 April 2021

B. B.

Abstract

The absorption, conversion and transport of electronic energy in molecular aggregates is at the heart of many important natural and artificial photochemical systems, including organic solar cell materials, photosynthetic light-harvesting complexes and DNA oligomers. The photochemical function of these systems is built on the interactions between their aggregated chromophores, which determine the dynamic evolution of their photoexcited states. In this thesis, DNA oligomers are investigated as multi-chromophoric model systems, where the coupling of individual nucleobases is key to their photoprotection mechanism against high-energy ultraviolet (UV) radiation. In this respect, the pairing and stacking interactions of the nucleobases enable the formation of exciton states with charge transfer character, which govern the photochemical dynamics in DNA. In this thesis, the electronic and structural dynamics of adenine single strands are studied with broadband, polarization-controlled transient absorption spectroscopy in the deep-UV. This spectral region gives direct access to the excited state dynamics encoded in the UV-transitions of the nucleobases and by comparing different base-sequences, strand-lengths, solvent environments, and photoexcitation conditions, the role of the base-stacking interaction in energy and charge transfer processes in DNA systems is investigated.

By comparing adenosine homopolymers of different strand lengths, it is found that the initially formed charge-transfer (CT) exciton spans two stacked bases, whereas the maximum charge separation sensitively depends on the structural arrangement and solvation shell of the stack. Importantly, these aspects also determine the lifetime of the excitons: in dimers with large inter-base distances, charge recombination dynamics are a factor of two slower than in closely packed oligomers with 20 bases. Through transient absorption anisotropy experiments in deuterated buffer solutions, an intra-strand proton transfer is identified as the main quenching process governing the CT exciton lifetime and its structural relaxation to a minimum-energy configuration on the 10 ps scale is observed.

2-aminopurine (2AP) is used as a sensitive local structural probe as its strong fluorescence is quenched via stacking. By integrating 2AP in adenine strands charge and energy transfer processes are studied. Varying the base sequence reveals that two coupled 2AP bases play an important role in the excited state dynamics. By comparing the dynamics after direct excitation of 2AP and indirect excitation via adenine bases, the fast energy transfer from

adenine to 2AP is observed. A charge transfer state, responsible for the quenching of 2AP's strong emission, is detected.

Keywords: DNA dynamics, electronic and structural dynamics, adenine, 2-amino purine, charge transfer state, proton transfer, charge recombination, energy transfer, transient absorption spectroscopy, anisotropy, time-resolved spectroscopy

Kurzzusammenfassung

Die Absorption, Umwandlung und der Transport von elektronischer Energie in molekularen Aggregaten ist das Herzstück vieler wichtiger natürlicher und künstlicher photochemischer Systeme, einschließlich organischer Solarzellenmaterialien, photosynthetischer Lichtsammelkomplexe und DNA-Oligomeren. Die photochemische Funktion dieser Systeme beruht auf den Wechselwirkungen zwischen ihren aggregierten Chromophoren, die die dynamische Entwicklung ihrer photoangeregten Zustände bestimmen. In dieser Arbeit werden DNA-Oligomere als multichromophore Modellsysteme untersucht, bei denen die Kopplung der einzelnen Nukleobasen der Schlüssel zu ihrem Photoprotektionsmechanismus gegen hochenergetische ultraviolette (UV) Strahlung ist. Dabei ermöglichen die Paarungs- und Stapelungswechselwirkungen der Nukleobasen die Bildung von Exzitonenzuständen mit Ladungstransfercharakter, die die photochemische Dynamik in der DNA steuern. In dieser Arbeit wird die elektronische und strukturelle Dynamik von Adenin-Einzelsträngen mit breitbandiger, polarisationsaufgelöster transientser Absorptionsspektroskopie im tiefen-UV untersucht. Dieser Spektralbereich ermöglicht einen direkten Zugang zur Dynamik der angeregten Zustände, die in den UV-Übergängen der Nukleobasen kodiert sind. Durch den Vergleich verschiedener Basensequenzen, Stranglängen, Lösungsumgebungen und Photoanregungsbedingungen wird die Rolle der Base-Stacking-Wechselwirkung bei Energie- und Ladungstransferprozessen in DNA-Systemen untersucht.

Durch den Vergleich von Adenosin-Homopolymeren verschiedener Stranglängen wird festgestellt, dass das anfänglich gebildete Ladungstransfer (CT)-Exziton zwei gestapelte Basen überspannt, während die maximale Ladungstrennung empfindlich von der strukturellen Anordnung und der Lösungsmittelhülle des Stapels abhängt. Wichtig ist, dass diese Aspekte auch die Lebensdauer der Exzitononen bestimmen: In Dimeren mit großen Basenabständen ist die Ladungsrekombinationsdynamik um den Faktor zwei langsamer als in dicht gepackten Oligomeren mit 20 Basen. Durch transiente Absorptionsanisotropie-Experimente in deuterierten Pufferlösungen wird ein Intra-Strang-Protonentransfer als Hauptrekombinationsprozess identifiziert, der die CT-Exzitononen-Lebensdauer bestimmt, und seine strukturelle Relaxation zu einer Minimum-Energie-Konfiguration auf der 10 ps-Skala beobachtet.

2-Aminopurin (2AP) wird als empfindliche lokale Struktursonde verwendet, da seine starke Fluoreszenz durch Stapelung gelöscht wird. Durch den Einbau von 2AP in Adeninstränge

werden Ladungs- und Energietransferprozesse untersucht. Die Variation der Basensequenz zeigt, dass zwei gekoppelte 2AP-Basen eine wichtige Rolle in der Dynamik des angeregten Zustands spielen. Durch den Vergleich der Dynamik nach direkter Anregung von 2AP und indirekter Anregung über Adeninbasen wird der schnelle Energietransfer von Adenin zu 2AP beobachtet. Ein Ladungstransferzustand, der für die Fluoreszenzlöschung der starken Emission von 2AP verantwortlich ist, wird nachgewiesen.

Stichwörter: DNS Dynamik, elektronische und strukturelle Dynamik, Adenin, 2-Amino Purin, Ladungstransferzustand, Protonentransfer, Ladungsrekombination, Energietransfer, Transiente Absorptionsspektroskopie, Anisotropie, Zeitaufgelöste Spektroskopie

Contents

Acknowledgements	i
Abstract (English/Deutsch)	iii
1 Introduction	1
2 Background	5
2.1 Photochemistry of multichromophoric systems	5
2.1.1 Multichromophoric systems	5
2.1.2 Excited state deactivation of multichromophoric systems	8
2.1.3 Excitation energy transfer	10
2.1.4 Photoinduced electron transfer	14
2.1.5 Excimer and exciplexes	17
2.2 Photochemistry of DNA	19
2.2.1 Molecular structure of DNA	19
2.2.2 Photodamage and -repair mechanism in DNA	21
2.2.3 Electronic states of DNA	23
2.2.4 Excited state dynamics in adenosine monomers	25
2.2.5 Excited state dynamics of 2AP	28
2.2.6 Excited state dynamics in adenosine multimers	29
3 Methods	33
3.1 Static spectroscopic techniques	33
3.1.1 Static UV-vis spectrometer	33
3.1.2 Static photoemission	34
3.1.3 Static circular dichroism spectrometer	34
3.2 Transient absorption spectroscopy	35
3.2.1 Measurement principle	35
3.2.2 Transient absorption setup in the deep-UV	36
3.2.3 Flow cell and Wire-guided liquid jet	38
3.2.4 Anisotropy	40
3.2.5 Spectral calibration	41
3.2.6 Instrument response function	41
3.3 Fluence dependence	42

3.4	Data procedures	42
4	Excited state dynamics in adenine single strands	45
4.1	Introduction	45
4.2	Experimental details	46
4.3	Results	49
4.3.1	Early transients and static spectra	50
4.3.2	Global analysis	51
4.3.3	20-mer excited in the low energy tail of the absorption spectrum.	53
4.4	Discussion	55
4.4.1	Excited state formation	55
4.4.2	Charge-transfer state relaxation	56
4.4.3	Direct excitation of charge-transfer state	57
4.5	Conclusion	59
5	Structural dynamics and intrastrand proton charge transfer	61
5.1	Introduction	61
5.2	Experimental details	62
5.3	Results	62
5.3.1	Static spectra and population dynamics of oligomers in a heavy water solution	62
5.3.2	Anisotropy	66
5.4	Discussion	70
5.4.1	Electronic states of oligomers in heavy water solution	70
5.4.2	Structural dynamics	72
5.5	Conclusion	74
6	Energy and charge transfer between adenine and 2AP bases in a single strand	77
6.1	Introduction	77
6.2	Experimental details	78
6.3	Results	80
6.3.1	Static characterisation of the samples	80
6.3.2	Population dynamics after exciting the 2AP bases	83
6.3.3	Population dynamics after exciting the adenine bases	85
6.3.4	Anisotropy	92
6.4	Discussion	97
6.5	Conclusion	101
7	Conclusion and outlook	103
	Bibliography	105

A Appendix	121
A.1 Drawing of the wire-guided liquid-jet	121
A.2 UV-vis spectra before and after the 2AP time resolved experiments	123
CV	125

1 Introduction

Multichromophoric systems are systems consisting of several chromophores interacting via fundamental interactions [1]. Those interactions tune the properties of the whole molecule. Therefore, studying the impact of inter-chromophoric interactions on multichromophoric systems is paramount to understand how they modify their properties. Model systems are the ideal playground for answering those questions. One example of such model systems is perylene bisimide aggregates (PBI) [2]. DNA with its covalently linked nucleobases is a multichromophoric system as well. Its properties are governed by the fundamental photophysics of each nucleobase, as well as by intrastrand base stacking and interstrand base pairing. Furthermore, the solvent environment as well as salt concentrations can change the ordering of the energy levels and therefore change how the molecule works fundamentally [3] [4]. There is also an inherent interest in DNA photophysics as DNA photostability is essential for life. Regardless of its strong absorption cross section with high energy photons, DNA is surprisingly photostable and the quantum yield of harmful photoproducts is low [5] [6].

Static methods are powerful tools to unravel fundamental photochemical questions but only deliver a time averaged picture of the involved photophysics. As the fastest dynamics that govern the properties of molecules take place on the femtosecond and picosecond timescale, scientists need to use tools that can resolve dynamical processes [7]. The advent of ultrafast technology enables the development of ultrafast analogues like transient absorption spectroscopy for static absorption or time resolved fluorescence. An ultrafast process in a molecule can be triggered by a short laser pulse and probed by a second one after a defined waiting time. With these techniques, we obtain access to the full temporal evolution of the species involved in photophysical dynamics.

These tools are used to study and understand the dynamics in multichromophoric systems. The dynamics in DNA are fascinating but as they are governed by multiple factors and different chromophores they are very complex. Adenine is therefore chosen in a controlled environment as a model system to study the impact of base stacking on the photophysics. Dipolar coupling of stacked bases causes excitons with a charge transfer character which leads to fundamentally different excited state dynamics [8]. The origin and dynamics of these charge transfer excitons

are studied in this thesis. The electronic energy landscape is strongly coupled to the molecule's nuclear degrees of freedom. Thus, the promotion to an electronically excited state and its electronic dynamics couple to the nuclear degrees of freedom, which drive local changes in the conformation of the molecule. Functional structural dynamics are a common feature of biological systems [9]. In order to investigate both electronic population dynamics as well as structural dynamics, broadband transient absorption anisotropy spectroscopy in the deep-UV is used. By having access to a supercontinuum in the deep-UV [10] [11] one can observe the bleached ground state transitions as well as the characteristic charge transfer excited state species simultaneously. Time resolved measurements are complemented with static characterisation to have a complete picture. Using the same methods, model strands consisting of adenine and 2-aminopurine, a fluorescent base analogue of adenine used as a local biological structural probe, are investigated. Energy transfer as well as charge transfer are studied in this model system.

In this thesis, first the general photophysical concepts are explained and a literature review on excited state dynamics in adenosine single strands is given. A brief overview of the experimental methods is followed by the presentation and interpretation of the measurements on adenine single strands.

After this introduction, **chapter 2** starts by explaining the photophysical concepts of multichromophoric systems. The forces and interactions, which are decisive for their properties, are introduced and pathways for excited state deactivation are explained, including energy and charge transfer. After an introduction to the concept of molecular excitons and exciplexes, the photochemistry of DNA is presented. Photodamage and -repair mechanisms in DNA are explained and a literature review on the electronic states, as well as the excited state dynamics, of adenosine single strands is given.

Chapter 3 briefly reviews the experimental and analysis methods used in the thesis. A brief introduction on the static characterisation methods is followed by a presentation of the deep-UV transient absorption anisotropy setup used for the time resolved measurements. The experimental procedures as well as the data treatment are shown.

In **chapter 4**, the main sample system investigated in this thesis, monomer dimer and 20-mer of adenosine monophosphate in physiological buffer solution, are introduced. A transient absorption (TA) study where adenosine is excited at its main absorption is presented. First, it is identified that in a strand, unlike in a dimer, due to the stronger dipolar coupling an exciton spanning over two bases is excited. A transiently formed charge transfer (CT) state is identified, which has full CT character in the 20-mer and only partial CT character in the dimer. The charge recombination in the dimer is approximately a factor of two slower. As Earth's atmosphere blocks UV radiation at adenosine absorption peak, the results of the previous TA study are compared with a second TA study where a multimer exclusive absorption tail overlaps with the terrestrial absorption spectrum. It is found that this excitation directly populates a CT state with partial CT character.

By changing the solvent from water to heavy water in **chapter 5**, a proton transfer is identified to play a key role in the charge recombination process. TA anisotropy is used to identify the time scale of the structural relaxation of the CT state.

In **chapter 6** the tools presented in chapter 3 and 4 are applied to model systems containing 2-amino purine (2AP). Static as well as time resolved measurements show the energy transfer from adenosine to 2AP bases. A direct excitation of 2AP bases leads to the same excited states which were populated in the other experiment by energy transfer. The bright excited state is quenched by neighbouring adenosine bases and a charge transfer state is identified.

Chapter 7 sums up the main results of the thesis and gives an outlook for further studies following the results of the thesis.

2 Background

In this chapter the photophysical concepts are explained, which are necessary to understand the findings of this thesis. The photochemistry of multichromophoric systems with an emphasis on energy and electron transfer processes are described. Afterwards the photochemical processes in DNA systems are explained. In this respect, I will focus on single-stranded adenosine and 2-aminopurine systems.

2.1 Photochemistry of multichromophoric systems

2.1.1 Multichromophoric systems

A chromophore is the part of a molecule where an electronic transition is localized that leads to a specific absorption signature [12]. In this context, the absorption of a chromophore is typically assumed to be mostly independent of the remaining molecule. However, molecular systems that contain several chromophores often display additional photochemical dynamics that are not observed for the individual chromophores. Instead, they are caused by the interactions between them within the molecule. The identification and investigation of these inter-chromophoric couplings and the resulting photochemical dynamics is the primary aim of this thesis.

Supramolecules versus large molecules A supramolecule is typically defined as an aggregate of molecular entities that only interact weakly [1], whereas a large molecule is a system where the individual sub-units interact strongly. In the context of this thesis, the degree of interaction can be determined in the view of the response to a photochemical excitation of the multichromophoric system, which is illustrated schematically in figure 2.1 for a two-component system. If an external stimulus (the absorption of a photon) leads to an excitation or charge separation localized on individual chromophores, we define the system as a supramolecule. If the same event leads to an excitation delocalized over the whole compound, the interaction between component A and B cannot be considered weak anymore and the

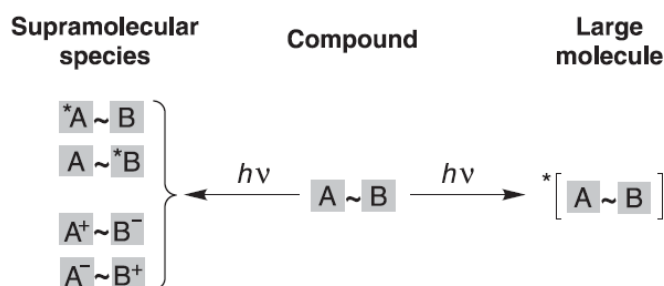


Figure 2.1: Illustration showing the behaviour of a multichromophoric system consisting of two units A and B following a photoexcitation. If the system behaves as a supramolecular species (left) the excitation is either localized on A or B or a charge is transferred between the two chromophores. If the system behaves as a large molecule, the excitation is delocalized over the whole system. Reprinted from [1] with permission from John Wiley and Sons.

system is regarded as a "large" molecule. Most multichromophoric systems are between these two limiting cases.

It should be noted that the definitions given above are convenient when investigating the interactions of subunits following photoexcitation. However, it should be noted that supramolecular chemistry is also a dedicated area of chemistry that studies molecular entities consisting of multiple molecules that are held together via non-covalent weak bonds. Typical supramolecular aggregates are the double helix of DNA or an enzyme with its substrate [13],[14]. However, this historical definition is not convenient in our context: One can find several examples of systems which have a similar structure and show qualitatively the same photophysics despite some of them being held together by weak intermolecular forces and others by covalent bonds [15]. Therefore, defining a supramolecule based on its photophysical properties rather than by its type of bonding seems to be more convenient in the context of this thesis.

Forces and interactions In this section the most important interchromophoric forces relevant in DNA systems are introduced. Further information can be found in "Physical chemistry" by Atkins et al. [16]. In multichromophoric systems we can generally distinguish inter- and intramolecular interactions. An interaction or force is intermolecular when the force acts between different molecules. Intramolecular forces on the other hand act between the atoms of an individual molecule. The most important intermolecular forces that govern the coupling of nucleobases in DNA systems are hydrogen bonds, dipole interactions, van-der-Waals forces and π -stacking.

Hydrogen bonds are an attractive force between a polar bound hydrogen atom in one molecule and an unbound electron pair of an atom in a nearby electronegative molecule. This interaction is typically weaker than a covalent bond but gives structure to proteins and is responsible for the high boiling point of water. In DNA systems, base pairs are connected and recognized via hydrogen-bonds, forming a double stranded helix [16].

The dipolar interaction between two polar molecules is

$$V = \frac{\mu_1 \mu_2 (1 - 3 \cos^2(\theta))}{4\pi\epsilon_0 r^3}. \quad (2.1)$$

μ_1 and μ_2 is the dipole moment of the molecule, θ the angle and r the distance between the two. ϵ_0 is the permeability of vacuum. The dipolar interaction is important in DNA to understand the Förster energy transfer, molecular Excitons and the van der Waals interaction.

The van der Waals interaction is an attractive interaction between two molecules with complete shells and scales as $1/r^6$, where r is the intermolecular distance. The van der Waals interaction contains three fundamental contributions, the Keesom interaction, Debye force and the London interaction. These are explained as follows [16]:

The Keesom interaction refers to the electrostatic interaction of two permanent dipoles. It thus describes the attractive force between two polar molecules and depends on their charge distributions, distance and mutual orientation.

The Debye force is the attractive interaction between a polar molecule with a permanent dipole and one which is polarizable. The permanent dipole of the former polarizes the latter one. The strength of the interaction thus depends on the magnitude of the permanent dipole moment and the polarizability of the second molecule.

The third attractive interaction is called dispersion or London interaction and acts between non-polarizable molecules. This becomes apparent when several non-polarizable molecules are in liquid phase at low temperatures proving that there is an attractive interaction as they would otherwise be in the gas phase. The electron density of any molecule is fluctuating, which leads to a small fluctuating polarization. The first polarization now induces a polarization in close molecules. This leads to an interaction and as a result to a lowering of the overall energy. Therefore the fluctuations are not random anymore but correlated. As mentioned before all three parts of the van der Waals interaction scale with $1/r^6$. For a derivation and an explicit description of the terms the reader can refer to [16].

In DNA strands bases have the tendency to arrange cofacially [17]. This behaviour is observed in aromatic systems containing π -electron systems and is often summarized as π -stacking. However recent reviews point out that there is no interaction specific for π -electron systems [18] [19]. Instead, reasons for aromatic systems to arrange cofacially are the van der Waals forces and the hydrophobic interactions between them. The hydrophobic interaction is briefly explained hereafter: When a non-polar molecule is placed in a polar solvent the solute is surrounded by a solvent cage [16]. The solvent molecules form hydrogen bounds, which is an exothermic process. Due to the structure of the solvent cage the possible configurations of solvent molecules are diminished and the entropy decreases. When several solutes share one solvent cage, the net entropy increases as the number of cage configurations rises. Therefore it is favorable for hydrophobic solutes to cluster and the process happens spontaneously.

2.1.2 Excited state deactivation of multichromophoric systems

Fermi's golden rule The transition rate $\Gamma_{i \rightarrow f}$, caused by an external perturbation, from one initial eigenstate $|i\rangle$ of a quantum system to a continuum of eigenstates $|f\rangle$, is described by Fermi's golden rule. The rate is dependent on the coupling between a single state and a continuum of states, which is described via a density function ρ . Here H' is the Hamiltonian of the perturbation. In the case of light-matter interaction H' will describe the perturbation of the matter by incident photons. A time-dependent perturbation $H'(t)$ will result in a time-dependent rate $\Gamma_{i \rightarrow f}(t)$ [20].

$$\Gamma_{i \rightarrow f} = \frac{2\pi}{\hbar} |\langle f | H' | i \rangle|^2 \rho(E_f) \quad (2.2)$$

Intramolecular relaxation pathways Before proceeding to the excited states of multichromophoric systems, isolated chromophores are discussed. The following section, based on the textbook "Wardle - Principles and Applications of Photochemistry" [21], presents the intramolecular relaxation pathways of their excited states. Photoexcited states are classified depending on their spin multiplicity $S = 2s + 1$, where s corresponds to the sum of unpaired electron spins. States where all spins are paired have a multiplicity of $S = 1$ and are called singlet states, whereas triplet states have two unpaired electron spins resulting in $S = 3$. The excited singlet and triplet states are each numbered with increasing numbers depending on the energy ordering of the states.

In a photoexcited state, an isolated molecule in solution can either decay via photophysical processes back to the ground state or may undergo a chemical reaction into another chemical species, whereby the original ground state will not be recovered.

Photophysical processes can be conveniently illustrated in Jablonski diagrams (see figure 2.2 for a simple example). Singlet (S_0 and S_1 and S_2) and the triplet (T_1) states are shown with their corresponding vibrational levels and possible photophysical decay paths. Intramolecular decay processes can then be divided into radiative and radiationless mechanisms. In figure 2.2 the bold down-pointing arrows are illustrating the radiative processes. Radiative relaxation is called fluorescence when the spin multiplicity remains unchanged and it is called phosphorescence when the multiplicity changes during the relaxation. Consequently, phosphorescence decays generally have smaller rates and are less bright compared to fluorescence. Internal conversion (IC) is a radiationless process where two states with the same multiplicity and the same energy are converted into each other. One example is the transformation of an electronically excited state ($S_1(v=0)$ whereby v is the vibrational level) into an electronic ground state with high vibrational excitation ($S_0(v>0)$). This is visualized in figure 2.2 on the left. The radiationless conversion of two isoenergetic states with changing multiplicity (eg. $S_1 \rightarrow T_1$) is called intersystem crossing (ISC in figure 2.2). For an isolated molecule in solution, the only available intermolecular relaxation mechanism is vibrational relaxation

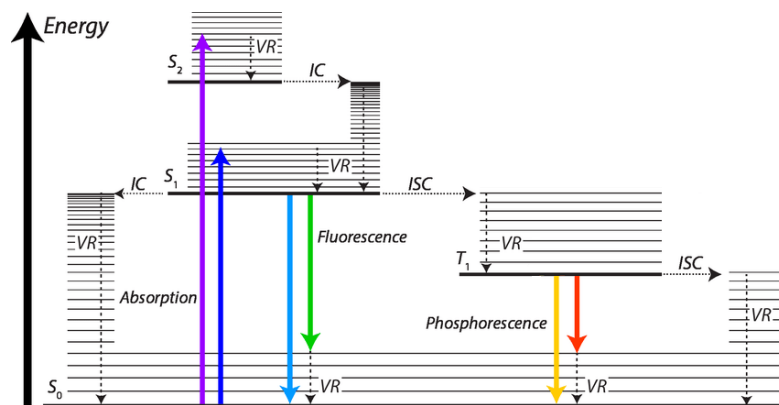


Figure 2.2: Jablonski diagram illustrating excitation and possible recovery paths. A molecule is excited, by absorbing a photon from the ground state (S_0) to an excited state. A vibrationally excited state can relax via vibrational relaxation (VR), undergo internal conversion (IC) into a different state with the same spin multiplicity or undergo intersystem crossing (ISC) into a state with different spin. Radiative transitions are fluorescence or phosphorescence. Reprinted and modified from [22].

(VR). During vibrational relaxation a vibrationally excited molecule transfers its excess energy to solvent molecules. The vibrational energy transfer takes place via collisions with the solvent molecules.

As is apparent from the Jablonski diagram, several relaxation mechanisms may act on an individual excited state. In this situation, faster mechanisms usually dominate over slower mechanisms. Internal conversion between two excited states happens typically faster ($\sim 10^{-14} - 10^{-11}$ s) than between S_1 and S_0 ($\sim 10^{-9} - 10^{-7}$ s). The reason being, that the energy spacing between two higher excited states is usually smaller than between the first excited and the ground state. Therefore the lowest excited state will rapidly be populated and fluorescence is for example mainly observed from the lowest excited state even if a higher excited state was originally populated. This finding is known as Kasha's rule [23]. VR can be observed in figure 2.2 after excitation, internal conversion and intersystem crossing. Relaxation processes can be assigned a rate k . The lifetime $^1\tau$ of the first excited state S_1 is the inverse of the sum of the rates of its relaxation mechanisms: fluorescence (k_f), internal conversion (k_{IC}) and intersystem crossing (k_{ISC}). the radiative lifetime $^1\tau_f$ is the inverse of k_f . Therefore the lifetime of the first excited state and its radiative lifetime will be identical in case of vanishing internal conversion and intersystem crossing. The quantum yield ϕ describes the fraction of molecules which decay via a given process. Therefore, the quantum yield of a given process is the ratio of the rate of the given process to the overall decay rate. As a function of lifetimes and for the specific case of fluorescence this leads to:

$$\phi_f = \frac{^1\tau}{^1\tau_f} \quad (2.3)$$

2.1.3 Excitation energy transfer

In multichromophoric systems, excited states initially localized on an individual chromophore may be quenched via interchromophoric decay channels. Among those are energy and electron transfer processes, which are presented in this and the following section, respectively. For DNA systems, excited state deactivation may also proceed via photochemical pathways. The most relevant in the context of this thesis are described in section 2.2.2.

In excitation energy transfer the excitation of an initially excited molecule or chromophore A, is transferred to another chromophore B. We call A the donor and B the acceptor, which is photosensitized by A. In total there are three different mechanisms of energy transfer to which I will refer hereafter [21]. The first is radiative energy transfer, in which one photon is emitted by A and absorbed by B. This transfer is called the trivial mechanism. As photons can travel far, a long distance energy transfer is possible via this channel. Additionally there are two nonradiative transfers. The Förster energy transfer works via a Coulombic mechanism, whereas the Dexter energy transfer proceeds via an electron exchange mechanism. Both mechanisms have the common pre-requisite that the emission spectrum of A has to overlap with the absorption spectrum of B.

Generally, non-radiative energy transfers can either be coherent or incoherent. If the transfer rate is faster than the reorganization of the solvent shell and the vibrational relaxation rate, a back transfer is possible. The energy is delocalized over the whole molecule and it is coherent. In case the relaxation processes are faster, the transfer can only work in one direction, the energy is localized and the transfer is incoherent. The energy transfer rate can be obtained from Fermi's golden rule (see formula 2.2) whereby V_{if} is the coupling between the donor and the acceptor, with the initial state $|i\rangle = \psi_A^* \psi_B$ and the final state $|f\rangle = \psi_A \psi_B^*$. The coupling term can be separated into the two independent contributions mentioned above and which will be discussed in detail in the following sections:

$$V_{if}^2 = V_{dip}^2 + V_{exch}^2. \quad (2.4)$$

Förster energy transfer

Förster energy transfer is based on dipole-dipole interaction which plays a role for distances in the range from 1 – 10 nm and can therefore be considered a long-range interaction [21] [24]. The interaction originates from the repulsive, electrostatic force between the electrons in the donor and the acceptor chromophores. The transition dipole moments of the donor and the acceptor interact which each other like two antennas. Therefore the physical principle behind the Förster energy transfer is the Coulomb interaction. One can describe the Coulomb interaction in a multipole expansion where the dipolar term is the dominant part. The

potential is given by (compare equation 2.1):

$$V_{dip} = \frac{\mu_A \mu_B (\cos(\beta_{AB}) - 3 \cos(\beta_A) \cos(\beta_B))}{4\pi\epsilon_0 r_{AB}^3}, \quad (2.5)$$

where r_{AB} is the vector connecting chromophore A and B, β_{AB} is the angle between the two transition dipole moments μ_A and μ_B , β_A the angle between r_{AB} and transition moment of A and β_B the angle between r_{AB} and transition moment of B. For better readability of the formula the geometric factor will be referred to as $\kappa = (\cos(\beta_{AB}) - 3 \cos(\beta_A) \cos(\beta_B))$. As we will consider molecules in solution we have to take into account the susceptibility of the dielectric medium ϵ . It is connected to the refractive index via $n = (\epsilon/\epsilon_0)^{1/2}$. Also the molecule itself shields the electric field and the Lorentz-factor has to be taken into consideration $f_L = \frac{n^2+2}{3}$. Putting these relations into Fermi's golden rule (equation 2.2) and taking into account that we are investigating absorption and emission bands leads to

$$k_{dip} = \frac{2\pi f_L^2}{\hbar\epsilon} \int \frac{|\langle \mu_{A^*A}(E) \rangle|^2 |\langle \mu_{BB^*}(E) \rangle|^2}{r_{AB}^6} \kappa^2 \rho_{AB}(E) dE. \quad (2.6)$$

The first dipole moment in the equation is associated with the radiative rate k_r and the second with the extinction coefficient $\epsilon(E)$. ρ_{AB} scales with the overlap of emission and absorption bands. This gives us the following simplified form for the dipole interaction rate:

$$k_{dip} = \frac{c^4 9000}{128\pi^5 N_A} \frac{\kappa^2 k_r \theta}{n^4 |\vec{r}_{AB}|^6} \quad (2.7)$$

where N_A is the Avogadro constant, c the vacuum speed of light and θ denotes the overlap integral of the normalized emission spectrum, with $\theta = \frac{\int F_A(\nu) \epsilon_B(\nu) \nu^{-4} d\nu}{\int F_A(\nu) d\nu}$. The efficiency of the transfer is therefore depends on the following three factors: First there needs to be a considerable spectral overlap between the donor and the acceptor, as expected. Second the emission line of the donor as well as the absorption line of the acceptor needs to be sufficiently strong. Third, staying in the antenna analogy one realizes that the spatial orientation between the two transition dipoles is crucial. Parallel dipoles show the most efficient transfer. As the efficiency scales with the oscillator strength of the absorption and emission bands one can see that a change in multiplicity of either the donor or the acceptor would strongly reduce the rate. The Förster theory thus describes the dependence of the efficiency of the energy transfer with respect to the distance between donor and acceptor, which scales with the 6th power of the distance. FRET is therefore often referred to as a molecular ruler, as it can be used to indirectly measure the distances between electrostatically coupled chromophores [16].

Dexter energy transfer

The second energy transfer mechanism is the Dexter or exchange mechanism [21]. At very short distances where the orbitals of two chromophores overlap, the probability of charge transfer increases strongly. As a consequence, it is possible that an electron from chromophore A is transferred to B, which is accompanied by a charge transfer from B to A. As this exchange is happening simultaneously it does not lead to ionization. The overall spin is conserved during the exchange but the multiplicity of each chromophore can change. An excited electron of the donor is exchanged with a ground state electron of the acceptor. As the associated orbitals have to overlap, the exchange mechanism usually only plays a role up to 1.5 nm. We also see a different distance dependence compared to the Förster mechanism. The rate for exchange is again described by Fermi's golden rule similar to the Förster mechanism with an overlap integral θ' :

$$k_{exch} = \frac{2\pi}{\hbar} V_{exch}^2 \theta'. \quad (2.8)$$

The potential decays exponentially depending on the distance between the two chromophores:

$$V_{exch} = |V_0| \exp(-\gamma(r_{AB} - r_0)). \quad (2.9)$$

γ is a constant describing the distance-dependent decay and r_0 is the minimal distance between the two chromophores.

Exciton interaction

Pioneering work to understand how coupling in molecular assemblies affects their excited states has been done by Frenkel, Kasha and Davidov [25] [2] by introducing the concept of molecular excitons. These describe collective excitations of the coupled chromophores, such that the resulting excited state is delocalized over several units. In the mathematical description, one models a monomer as a two level system consisting of ground and excited state. In a molecular aggregate with non-interacting monomers any excitation would remain localized on individual monomers. When introducing an interaction potential between the monomers the monomer wavefunctions do not describe the system anymore and we instead employ their linear combination in the framework of low-order perturbation theory. The resulting wavefunctions describing the eigenstates of the system with coupling interactions are called molecular excitons. Unlike in this context, in solid state physics the term exciton is used to describe a bound electron hole pair. As an idealized analogue to a single DNA strand of identical monomers, we will now consider the excitonic states of a linear chain of identical

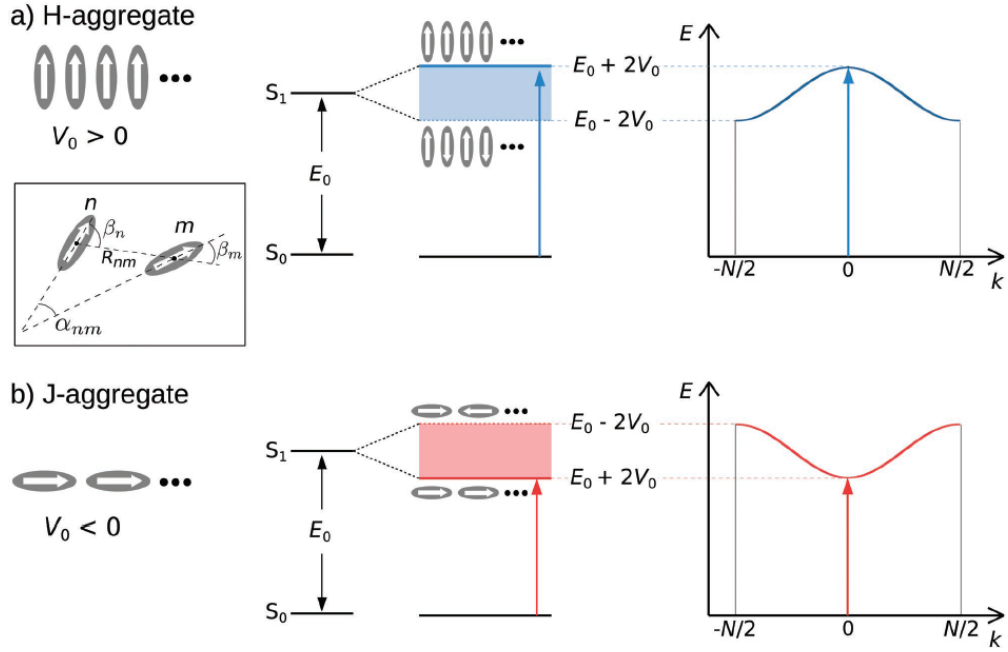


Figure 2.3: The arrangement of the transition dipole moments determines the shape of the exciton bands. In a) the transition dipole moments are oriented parallel to each other. The symmetric linear combination leads to the high energy state and the antisymmetric to the low energy state. The parallel arrangement is called H-aggregate. In b) the transition dipole moment are oriented in a head-to-tail fashion (J-aggregate). The symmetric linear combination leads to the low energy and the antisymmetric to the high energy state. H- and J-aggregates are two limiting cases and a spectrum of geometries that lie in between those two cases are possible. Reprinted from [2] with permission from John Wiley and Sons.

chromophores [2]. The exciton wavefunction of an idealized chain of monomers limited to nearest neighbour interactions, can be written as a linear combination of monomeric wavefunctions. The associated energy eigenvalues are then given by:

$$E(k) = E_0 + 2|V_0| \cos\left(k \frac{2\pi}{N}\right), \quad (2.10)$$

where E_0 is the energy eigenvalue of an isolated monomer, V_0 is the nearest neighbor dipolar interaction, N is the number of monomers and k is a quantum number labelling each excitonic state (can range between 0 and $N-1$). As a result, we get an exciton band spanning from $E(k=0) = E_0 + 2V_0$ to $E(k=\frac{N}{2}) = E_0 - 2V_0$ with a bandwidth of $4V_0$.

The coupling of the monomers is given by the dipolar coupling of their transition dipoles (c.f. equation 2.5). For $k=0$ we get a constructive and for $k=\frac{N}{2}$ a destructive interference of these transition dipole moments. As a result the constructive interference results in a fully dipole-allowed transition to a bright excitonic state and destructive interference leads

to a vanishing transition dipole moment and therefore a dark excitonic state. However, the energetic ordering of these two limiting cases depends on the sign of the dipolar coupling potential V_0 . As previously discussed, the associated dipole-dipole interaction depends on three different angles which determine the magnitude and the sign of the interaction. In figure 2.3 we can see this effect for the example of two limiting cases. A configuration where all the transition dipole moments are arranged parallel to each other is called an H-aggregate. There the fully symmetric linear combination of the monomer wavefunctions leads to a high energy bright state and the antisymmetric combination leads to the low energy dark state. This has direct consequences for the photochemistry of H-aggregates. Absorption will primarily populate the high energy state, which is shifted to higher energies compared to the monomer absorption (blue or hypsochromic shift). Typically, rapid internal conversion between the excitonic states then populates the lowest exciton state. This effect is called intraband scattering. As the low energy state is optically dark, H-aggregates usually display only weak fluorescence. If on the other hand the transition dipole moments are oriented in a head-to-head or head-to-tail fashion we call the arrangement a J-aggregate. In this geometry the symmetric combination of monomer wavefunctions leads to a bright low energy state which fluoresces and the antisymmetric combination results in an optically dark high energy state. The aggregate's absorption is therefore red shifted (batochromic shift) and the fluorescence decay rate is increased with respect to the individual monomer.

Above we looked at an idealized situation. Disorder of various nature can limit the delocalization of the exciton. If the energy difference to the average energy due to disorder is smaller than the interaction, we are in a strong coupling regime and a wave-like coherent energy transfer is possible. If on the other hand the energy differences dominate we are in a weak coupling regime and the exciton transfer can be described as an incoherent hopping mechanism [2].

2.1.4 Photoinduced electron transfer

Electron transfer describes the situation when a donor transfers an electron to an acceptor: $D + A \rightarrow D^+ + A^-$. In photoinduced electron transfer the donor is excited by a photon prior to the electron transfer. In order to understand the electron transfer one has to consider the donor-acceptor pair in a polar solvent. The equilibrium solvent configuration depends on the charge distribution of the donor-acceptor pair (see upper row of figure 2.4). For a charge transfer to take place, a solvent orientation has to be found which is compatible with the donor-acceptor pair before and after charge transfer (lower row of the figure). In this configuration the reactant and the product have the same energy. Due to fluctuations in the solvent such configurations are accessed and electron transfer can take place. As the charge is now transferred the equilibrium configuration of the solvent is different and the solvent cage reorganizes to the new minimum energy configuration.

To describe this mathematically Marcus theory is used. In Marcus theory the reactant and product states are described by parabolic potentials associated with the Gibbs energy as a

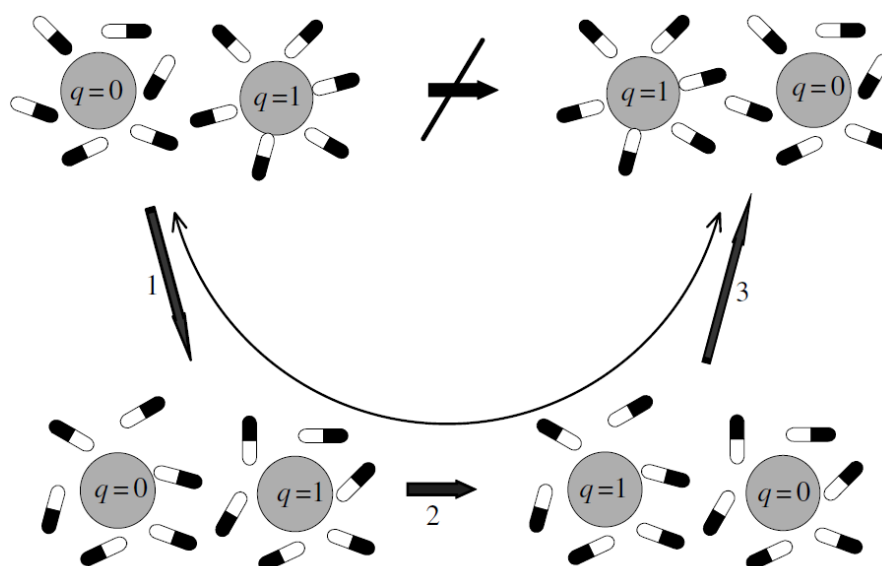


Figure 2.4: Schematic illustrating the solvent reorganisation necessary for electron transfer. The equilibrium configuration of the polar solvent for the reactant and the product are different so an electron transfer cannot take place directly (upper row). The solvent has to adopt a suitable orientation (1) for the electron transfer to take place (2). Afterwards the solvent can relax to its new equilibrium configuration (3). Figure reprinted from [26] with permission from Oxford Publishing Limited through PLSclear.

function of the reaction coordinate (see figure 2.5a). Here, the reaction coordinate describes the reorganization of the solvent environment. Chemical reactions happen spontaneously if they are exergonic, so the product state is lower in Gibbs free energy compared to the initial state. Therefore the Gibbs energy of the process is negative. It describes the tunnelling of one electron from the donor to the acceptor through a barrier. This barrier is partially determined by the ionization energies of the donor-acceptor pairs [16]. In order to access a configuration in which electron transfer can take place the donor-acceptor pair and its solvent environment have to structurally rearrange in order to reach an arrangement where the Gibbs energy parabolas intersect each other. This is shown in figure 2.5a.

To model the electron transfer we assume that it is fast compared to the nuclear motion. This means that during the transfer process the arrangement of the donor-acceptor pair and its solvent environment do not change significantly. At the equilibrium position of the reactant it is energetically not favorable to transfer an electron. Due to thermal fluctuations one can reach a configuration \ddagger where the reactant and the product intersect in Gibbs free energy (see figure 2.5a). The states are degenerate and an electron tunnelling can take place. Thereby the electron has to tunnel through a barrier with height V and a distance r which is the distance between the two molecules. The activation energy needed to arrive at the intersection of the two parabolas is called Gibbs energy of activation $\Delta^\ddagger G$. In the new equilibrium position of the product the Gibbs energy is lower than the one of the reactant. The difference is the

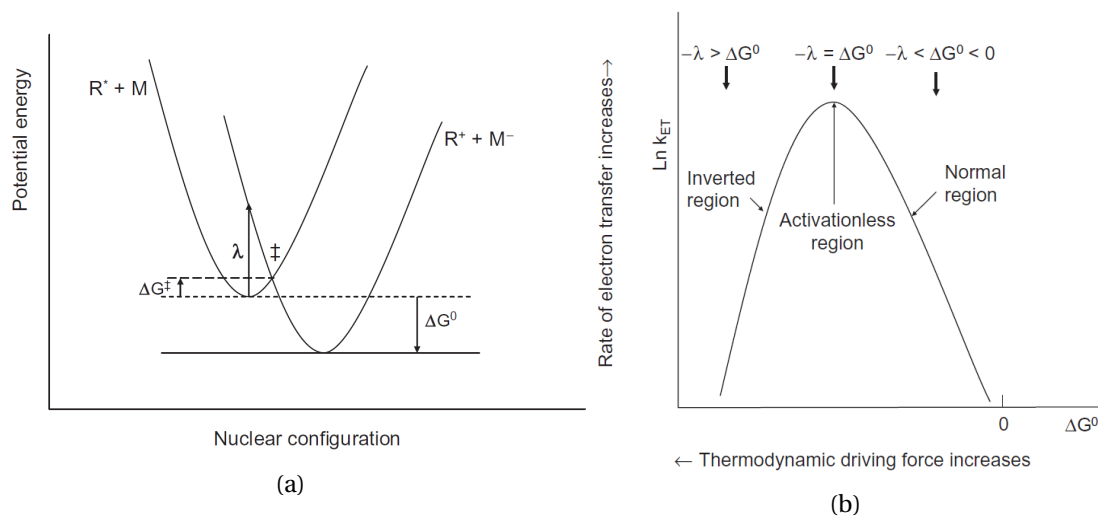


Figure 2.5: a) Gibbs energy of the donor-acceptor pair before (left parabola) and after (right parabola) the electron transfer as a function of the nuclear configuration, which is a measure for the donor-acceptor and solvent arrangement. In the equilibrium position the reactant is at a different nuclear configuration than the product. The electron transfer takes place at the intersection of both parabolas at \ddagger . The difference in Gibbs energy of the reactant between the equilibrium and at the intersection between the two parabolas is the Gibbs energy of activation $\Delta^\ddagger G$. The difference between the two equilibrium Gibbs energies is the standard Gibbs reaction energy ΔG^0 . The difference of Gibbs energy at the equilibrium configuration of the reactant between the reactant and the product is the reorganization energy λ . Figure reprinted from [21] with permission from John Wiley and Sons. b) Logarithmic rate of electron transfer as a function of the thermodynamic driving force. It displays the normal, the activationless and the Marcus inverted region. In the normal region the rate increases as the electron transfer gets thermodynamically more favorable. In the activationless region the barrier vanishes and the rate is the fastest. In the Marcus inverted region the nuclear configuration has to reorient again for an electron transport to take place. This is why the rate decreases even if the reaction gets thermodynamically more favorable. Figure reprinted from [21] with permission from John Wiley and Sons.

reorganization energy λ . The difference in Gibbs energy between both equilibrium positions of the reactant and the product is called standard Gibbs reaction energy ΔG^0 . The electronic coupling between donor and acceptor are described by the following expression:

$$\langle H_{DA} \rangle^2 = \langle H_{DA}^0 \rangle^2 e^{-\beta r} \quad (2.11)$$

where $\langle H_{DA}^0 \rangle^2$ is the electronic coupling when donor and acceptor are in contact. r is the distance between them and β is a parameter that describes the scaling of the tunnelling relative to the distance and is dependent on the solvent. As a rate for the electron transfer we get

$$k_{et} = \frac{2 \langle H_{DA} \rangle^2}{h} \sqrt{\frac{\pi^3}{4\lambda RT}} e^{-\frac{\Delta^\ddagger G}{RT}} \quad (2.12)$$

where R is the molar gas constant and $\Delta^\ddagger G = \frac{(\Delta G^0 + \lambda)^2}{4\lambda}$. We can see that if $-\lambda = \Delta G^0$ the activation Gibbs energy vanishes and there is no activation barrier (see figure 2.5b). We can also see that if the reaction Gibbs energy increases, the reorganization energy of the reaction becomes thermodynamically more favourable, but as the activation energy increases, the rate decreases. This is called the Marcus inverted region. When comparing molecules where the distance between the donor and the acceptor is kept identical but the reduction potential vary, one can simplify the transfer rate as a function of ΔG^0 :

$$\ln(k_{et}) = -\frac{1}{4\lambda} \left(\frac{\Delta^\ddagger G}{RT} \right)^2 + 1/2 \left(\frac{\Delta^\ddagger G}{RT} \right) + const. \quad (2.13)$$

When a molecule absorbs a photon it promotes an electron to a higher energy state. This molecule will be a good electron donor. But as it leaves an unoccupied low lying orbital it is also a good electron acceptor [21]. When going from the neutral donor acceptor pair to the pair where the electron transfer took place, the solvent reorganizes in order to shield the electric charge. The more polar the solvent, the stronger the shielding effect.

2.1.5 Excimer and exciplexes

A special type of molecular aggregate that is relevant in the context of this thesis is an excimer, which stands for excited dimer. It refers to an aggregate of two identical monomers that is only formed when one of them is in a photoexcited state, but is unstable when both of them are in the ground state. This is illustrated schematically in the potential energy curves in figure 2.6a. The two ground state monomers repel each other for short distances, which is represented by an exponential increase of their potential energy. A pair of an excited and a ground state molecule, on the other hand, shows a potential minimum at short distances and forms the

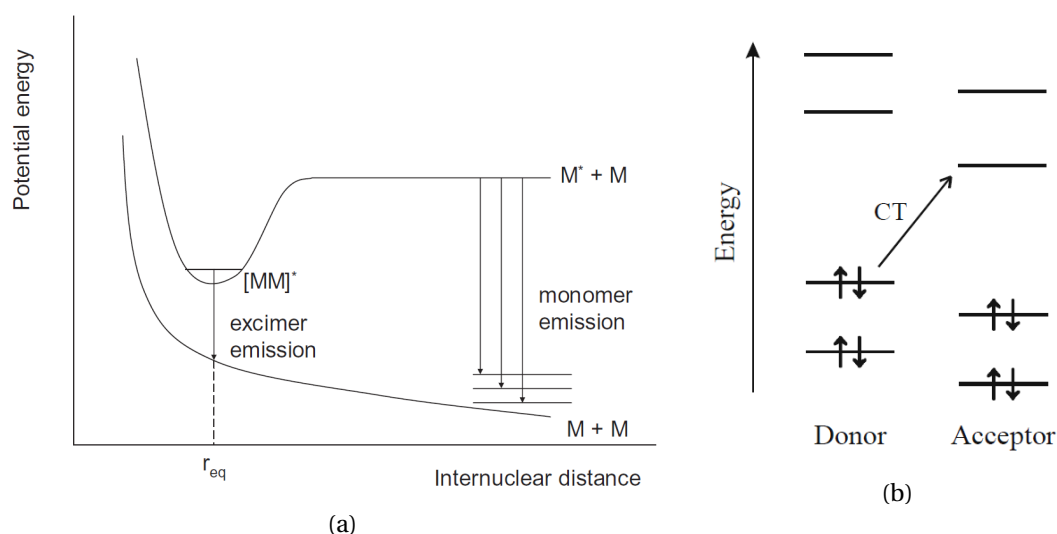


Figure 2.6: a) Potential energy curves of two ground state molecules M (lower curve) and an excited molecule M^* and a ground state molecule M or an excimer $[MM]^*$ relative to the internuclear distance. Figure reprinted from [21] with permission from John Wiley and Sons. b) Schematic showing a charge transfer excitation. Reprinted from [27] with permission from Taylor & Francis Group LLC-Books.

associated excimer state. As the ground state configuration of the pair is dissociative, the excimer dissociates after the return to the ground state. Excimers can be identified spectroscopically via the following characteristics. As the excimer state is lower in energy compared to the excited state of an individual monomer, the excimer state shows a redshifted emission spectrum compared to an individual monomer. In addition, any vibrational progression of the monomeric emission spectrum will vanish in the excimer emission, as the ground state is dissociative. Experimentally one can identify an excimer emission by recording the concentration dependent emission spectra of suitable monomers. At low concentrations no excimer emission is typically observed. At higher concentrations as monomers get closer to each other, an excimer emission band appears and the monomer band gets weaker in intensity. As a useful differentiation, an excimer formed by two different monomer species is called an exciplex, which stands for an excited complex.

Similar to a donor-acceptor pair, a photoexcited dimer may also undergo a (partial) electron transfer reaction, resulting in a so-called charge-transfer (CT) state. For such a CT transition, the starting and the final orbital are not on the same chromophore [27]. This can be seen in figure 2.6b where one orbital acts as an electron donor and the other as an electron acceptor. As an electric charge is moved, there is a strong change in dipole moment. Molecular aggregates can exhibit charge-transfer states and a new electronic transition appears in the absorption spectrum of the aggregate relative to the monomeric species [27]. Excimer and exciplex states can have a neutral or charge transfer-character and both play a role in the excited state dynamics of DNA molecules.

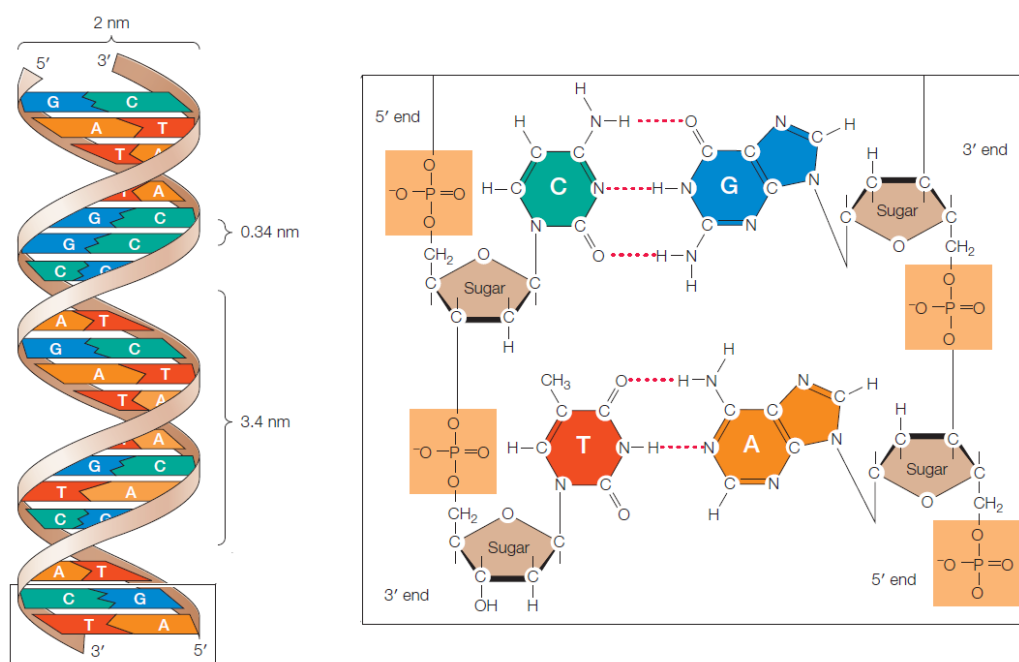


Figure 2.7: Structure of DNA: On the left a double strand of DNA. On the right the base pairing between the two strands is illustrated. Reproduced from [28] with permission of Oxford Publishing Limited through PLSclear.

2.2 Photochemistry of DNA

This section presents the basic structural and photochemical properties of DNA as well as the current state of research on the ultrafast dynamics of DNA systems. The primary aim of this thesis is to investigate the effect of intrastrand stacking on the excited state dynamics of DNA systems. I will therefore focus the literature review on DNA strands in physiological buffer solutions.

2.2.1 Molecular structure of DNA

A detailed description of the structure of DNA can be found for example in [28]: Deoxyribonucleic acid or short DNA is the biological molecule which stores the genetic information of all life forms. The building blocks of DNA are the four natural nucleobases: Cytosine (C), guanine (G), thymine (T) and adenine (A), of which C and T are called pyrimidines and G and A are called purines (see figure 2.7). Together with the sugar deoxyribose these nucleobases form the nucleosides. Nucleosides can in turn bind to a phosphate to form nucleotides. A DNA strand is composed of nucleotides that are covalently bound together at the sugar and the phosphate, resulting in the so-called the sugar-phosphate backbone.

Stacking interaction in single stranded DNA

Stacking, as elaborated in section 2.1.1 is the tendency of nucleobases to arrange cofacially. Adenine is the base where the probability of stacking is highest [29]. In an adenine dimer approximately 80% of the bases are stacked [8]. Therefore an adenine strand is the minimal model to investigate the effect of interactions between nucleobases in a single strand. Base stacking leads to long-lived states in adenine strands due to cooperative effects between the bases, as will be explained in section 2.2.6 [8]. Stacking, which increases the rigidity of a strand, is a cooperative effect. Only nearest neighbours can stack in a strand and non-adjacent bases cannot stack [29]. Nonetheless multiple domains of stacked bases separated by unstacked bases occur. A given base in a dimer can only have one nearest neighbour. This is why the probability for a base in a dimer to stack is lower than in a longer strand [30]. Therefore very short multimers are locally less rigid than longer strands. Double stranded DNA is more rigid compared to single stranded DNA due to the hydrogen bonding between the two strands (see next paragraph). As single stranded DNA is structurally less stabilized (only stacking is stabilizing the conformation but not hydrogen bonding) single stranded DNA has a shorter persistence length and can therefore have various secondary structure [31].

Molecular structure of double-stranded DNA

Natural DNA takes the form of a double stranded helix, where two single strands are connected via hydrogen bonds between nucleobases on opposite strands. In this way, the hydrogen-bonded nucleobases form so-called Watson-Crick base pairs. As the backbone is polar, the base pairs lie inside of the double strand in physiological conditions. The base pairing interaction achieves base-specificity through the number of hydrogen bonds (see chapter 2.1.1) that individual nucleobases can form: C and G have three and T and A only two hydrogen bonds. Thereby the bases C and G and T and A constitute the Watson-Crick base pairs. The structural stability of the double strand makes base stacking more probable compared to a single strand and each base pair has a stacking distance of 3.4 Å. Each base is rotated by a 36° pitch angle relative to its adjacent base. Therefore a full helix turn is completed after ~ 10.5 bases and a helix axial length of ~ 3.4 nm. The diameter of the double helix is approximately 2 nm.

Impact of solvation

The structure described above is the right-handed B-DNA which prevails under physiological conditions (see paragraph below). In such a solution counterions and deprotonated phosphate groups of the backbone are located close to each other. Water molecules are situated in the minor and major groove of the double helix (compare figure 2.7 left). There are also other forms of DNA which form under different solvent conditions. If DNA is dehydrated its shape becomes a right handed A-DNA helix and under high salt concentrations it forms Z-DNA, which corresponds to a more closely packed left-handed helix [32].

The fraction of bases that are stacked in a strand is controlled by the environment. Lowering the pH-value, using methanol as a co-solvent or increasing the temperature can facilitate unstacking [29], [33].

2.2.2 Photodamage and -repair mechanism in DNA

Photostability of biomolecules is paramount for their structural integrity in conditions with high-energy UV radiation. Even though our atmosphere already absorbs part of the incident UV-radiation, there is still a considerable amount of high energy photons reaching on the earth's surface. Mutations, which are modifications of the base-sequence of DNA, can have strong consequences for living organisms as they may disturb the synthesis of proteins from the genetic information. In this way, mutations can lead to proteins that cannot perform their biological function or may even be toxic to the organism. As a result cellular death can occur. In addition, mutations that take place on sequences responsible for cell growth can lead to cancer [28]. Mutations can be caused by chemicals or radiation [34]. Due to its large photon energy, UV radiation may excite highly energetic excited and thus reactive electronic states. Such states can be efficient precursors for photochemical reactions, involving the breakage or formation of chemical bonds, finally leading to mutations.

In this context it is important to point out that the first complex organisms evolved during primeval times, when UV exposure was significantly higher due to the absence of an absorptive atmosphere. It is therefore generally assumed that an exceptional photostability of DNA molecules might have played a central role in the evolution of living organisms [5]. Nevertheless, even at today's lower levels of UV exposure, photodamage of DNA cannot be completely avoided and living organisms display several molecular mechanisms to mitigate this damage. Below I will give short summary of common photoproducts and the repair mechanisms. The photophysics that lower the probability of photoproducts forming in the first place are described in the next chapter.

There are multiple photoproducts that play a role in the photodamaging of DNA. However, in the context of this thesis, I will describe only the four most relevant ones [35] (see figure 2.8). These are the cyclobutane pyrimidine dimer (CPD), the 6-4 lesion, the dewar valence isomer and the spore photoproduct. All of these belong to the class of pyrimidine dimers, accounting for the fact that harmful photoproducts mostly appear in pyrimidines [35]. In this respect, it should be noted that one can find photoproducts based on adenines but the yield is typically very low [36]. Generally, the yield of harmful photoproducts depends on both the type of base that is UV-excited and on its adjacent neighbouring bases. The photoreactivity of a DNA system is thus specific to its base sequence [36].

The photoproducts described below are shown in figure 2.8. The cyclobutane pyrimidine dimer is formed between two neighbouring pyrimidine bases in one strand. Thereby the double bond between carbon atom 5 and 6 of each pyrimidine is transformed into a single bond. Furthermore carbon atom 5 of one base and carbon atom 5 of the neighbouring base

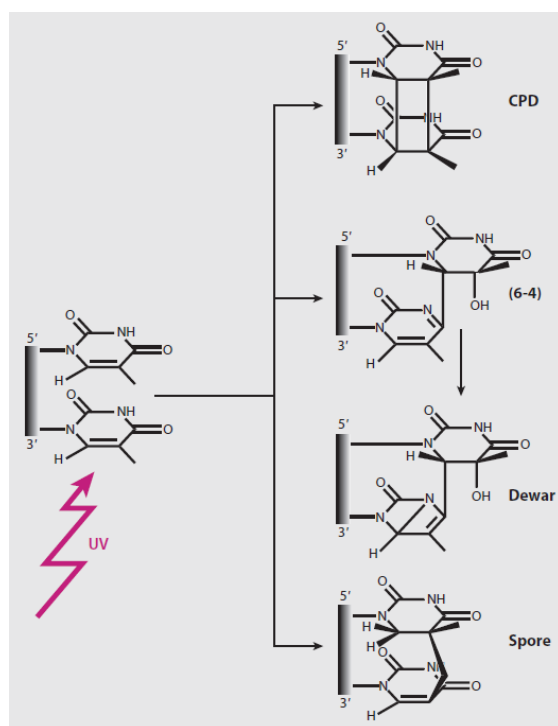


Figure 2.8: Structure of of the most common bi-pyrimidine photoproducts. Reprinted from [35] with permission from Annual Reviews.

are now connected by a single bond. The same is true for the carbon atoms 6 of both bases. Therefore both bases are now linked together by two single bonds. This photoproduct is the most relevant, shows the highest abundance and is induced by UV-C radiation [35]. It appears for all possible four pyrimidine pairings [37]. The above described mechanism is a $[2 + 2]$ cycloaddition, which can only take place via a photochemical pathway. However, it is still an open question if the photochemical path proceeds via a singlet or a triplet precursor state [35]. Thymine has the lowest lying triplet state compared to the other nucleobases. Therefore thymine could act as a triplet state energy sink, which could lead to an accumulation of mutations at this base [38]. UV pump - IR probe experiments on the other hand showed that the IR marker bands for cyclobutane rise in less than 1 ps [39]. This ultrafast photoproduct formation time is most likely too fast for an intersystem crossing to play a role and suggests a singlet excited state as a precursor. In addition, this time scale is too fast for any structural rearrangement in the excited state, such that, the quantum yield for this reaction to happen must be defined by the orientation of the two bases prior to the excitation.

The (6-4) photolesion is formed as well by two neighbouring pyrimidine bases in one strand. Thereby carbon atom 6 of the pyrimidine base at the 5' end of the backbone forms a bond with the carbon 4 atom of the pyrimidine base at the 3' end. The oxygen atom, which in the original base would be bound to the 3' base on the carbon 4 atom together with the hydrogen formerly bound to the nitrogen at the 3 position is part of an OH-group at the carbon 5 atom of the 5'

base. It is detected after irradiation with UV-C light [35]. However, the formation mechanism of the lesion is not fully understood. After excitation the rise time of the spectroscopic signature associated with the (6-4) photolesion is on the order of milliseconds [40]. This is much longer than the typical lifetimes of singlet or triplet excited states. Therefore, there has to be an intermediate species which does not show a signature in the UV-vis region from which the (6-4) photolesion evolves. One suggestion for this intermediate is an oxetane ring which has a smaller π -electron system [41]. Therefore the absorption would shift further into the UV and would not be present in the spectroscopy range of the experiments conducted thus far [41].

The dewar valence isomer is formed out of the (6-4) photolesion. It has a similar structure to the (6-4) photolesion but a bond between the nitrogen on the 3 position in the ring and the carbon on the 6 position of the 3' base. As the (6-4) photolesion absorbs around 325 nm, the dewar valence isomer can be formed photochemically [35]. Experiments with di-thymine model compound showed that it is formed in about 130 ps [42].

The spore photoproduct is only found in bacterial spores [35]. It appears after UV-A, B or C irradiation. The other photoproducts mentioned above are on the other hand almost not found in bacterial spores. The spore photoproduct is a pyrimidine dimer involving two thymine. Those are interconnected at the C5 atoms by a methyl bridge. The 5' end thymine has an additional hydrogen atom at the C6 atom.

In order to keep the genetic information unaltered organisms display multiple ways to repair damaged DNA [43]: All such mechanisms follow a similar principle. First the error in the sequence has to be identified, in a second step removed and in a third step the gap has to be filled with a DNA polymerase and the strand has to be reconnected by a DNA ligase. One of this mechanisms is the proofread mechanism. If during DNA replication a wrong base is inserted, the base will not be able to base pair with its complementary strand. This slows down the polymerase process, the base is cut out and the polymerase repeats the current position of the strand. Another mechanism is the so-called direct repair which works via the so-called photoreactivating enzyme. It is used to repair the above described pyrimidine dimers. An enzyme, the so-called photolyase binds to the pyrimidine dimer. After photoexcitation this enzyme can cleave the erroneous dimer. Furthermore there are the excision repair mechanisms. Thereby either a single base or in the case of a pyrimidine dimer several nucleotides get cut out of the strand after detection by a protein. The polymerase now starts to fill the missing gap starting at the 3' end of the gap using the information of the complementary strand. A DNA ligase is needed to connect the strand newly polymerized strand to the 5' end.

2.2.3 Electronic states of DNA

All DNA monomer building blocks show a strong and relatively broadband absorption feature centred around 260 nm (see figure 2.9a). It corresponds to a transition between the ground and the first excited singlet state, the $\pi\pi^*$ state.

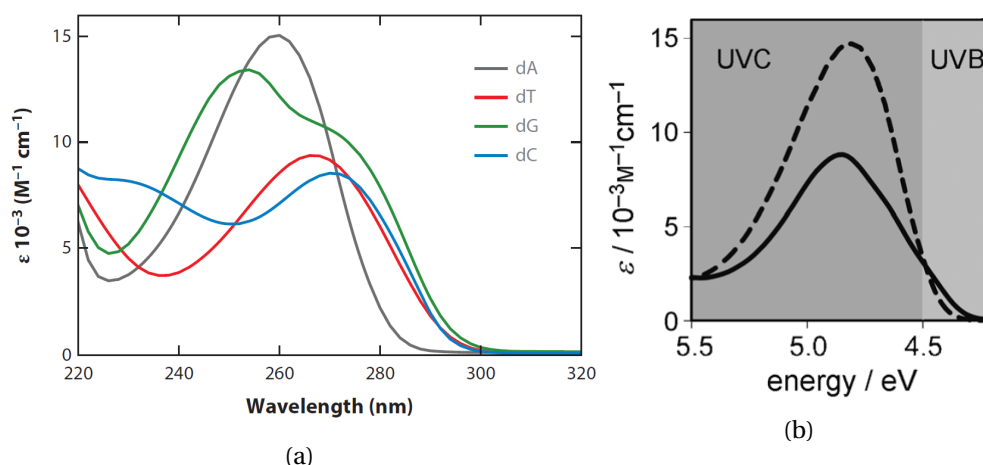


Figure 2.9: a) Absorption spectra from the natural DNA nucleosides in an aqueous solution. The absorption spectra of the following bases are shown: Deoxy-adenosine (dA) in grey, -thymidine (dT) in red, -guanosine (dG) in green and, -cytidine (dC) in blue. The figure is reprinted from [35] with permission from Annual Reviews. b) Molar absorption spectrum of dAMP (dashed) and (dA)₂₀ (solid line) from 5.5 eV (≈ 225 nm) to 4.25 eV (≈ 290 nm). The hypochromic effect leads to a blueshift in the absorption maximum as well as to less absorption per chromophore going from the monomer (dAMP) to the 20-mer. Reprinted from [46] with permission from John Wiley and Sons.

In Adenine monomers, theory has suggested three possible lowest lying transitions. The optically dark $n\pi^*$, and two bright $\pi\pi^*$ states, the L_a and the L_b state. Due to the different nature of the states, the solute-solvent interaction determines the energetic order of the states in solution. The lowest energy transition is thus L_a , whereby Fluorescence Anisotropy studies have shown, that whilst L_b may initially be populated in absorption, its population is transferred to L_a on an ultrafast timescale [44]. The fluorescence quantum yield is $\phi_f \sim 3 \times 10^{-4}$ [45].

As soon as DNA bases are in close contact, be it through a covalent bond in a single strand or just due to high concentrations, cooperative effects play a role. The quantum mechanical wavefunctions of the bases couple, which leads to molecular excitons [25]. In order to include a possible charge-transfer character, the exciton interaction can be written as the sum of the Coulomb, the Dexter exchange and the overlap interaction [47] (see chapter 2.1.3). One effect of the exciton interaction is the hypochromism, which can be observed in the absorption spectrum of DNA (see figure 2.9b). The coupling of the bases leads to a slight blue shift of the absorption maximum and a significantly lower absorption cross section per base [25]. Another cooperative effect is the absorption tail in the red part of the main absorption peak, which appears, as multiple bases are present in a strand. Theoretical studies suggest that this absorption is due to the direct excitation of ionic pairs resulting in excitonic states with a significant charge-transfer character [48]. Due to the CT character of these states, their electronic energy sensitively depends on solvent and structural configurations. This leads to

a strong inhomogeneous broadening of their associated absorption band compared to the neutral excitons. Lange et al. on the other hand suggest that the red part of the spectrum corresponds mainly to neutral $\pi\pi^*$ states and the low-energy tail of charge transfer states may be overlapping with the $\pi\pi^*$ transition [4].

Banyasz et al. found that the static fluorescence spectra change their shape when exciting above 275 nm, the crossing point of the absorption spectrum of dAMP and the multimer. Also the fluorescence quantum yield increases by an order of magnitude. They assigned this change to different excitations: Below the crossing point mainly bright excitons and above it CT states are excited [46].

2.2.4 Excited state dynamics in adenosine monomers

A hallmark of the lowest electronically excited states of all base monomers is their sub-picosecond lifetimes. The lifetimes have for example been obtained from transient absorption measurements, but also fluorescence upconversion measurements, which are only sensitive to bright states [30]. Figure 2.10 shows the time-resolved fluorescence measurements of the nucleosides and their associated nucleotides. For the purines the differences in lifetimes between nucleoside and nucleotide are negligible ($\tau_{dA/dAMP} = 0.13$ ps and $\tau_{dG} = 0.33$ ps, $\tau_{dGMP} = 0.34$ ps) in contrast to the Pyrimidines ($\tau_{dC} = 0.30$ ps, $\tau_{dCMP} = 0.45$ ps and $\tau_{dT} = 0.32$ ps, $\tau_{dTMP} = 0.50$ ps) [49].

The electronic excited state is converted into a vibrationally excited ground state due to ultrafast internal conversion via a conical intersection (CI). These are points in the energetic landscape where the potential energy surfaces of two electronic states cross so an efficient internal conversion can take place between them.

As this thesis focuses on adenine bases, this section presents further details on their excited state dynamics. For free adenine bases in solution, two tautomers are present. There is the 9H-adenine and the 7-H adenine, which differ in the position of the hydrogen atom, being at the 9 position in the former and at the 7 position in the later. As soon as the base is present as a nucleotide or nucleoside, tautomerism is eliminated and only 9H-bases occur. In the 9H-tautomer early time-resolved emission studies could find two time scales: One fast time scale which is limited to the instrument response of the experiment with $\sim 0.04 - 0.2$ ps [50], which refers to the initially excited state leaving the Franck-Condon region, as well as a second timescale associated with internal conversion to the ground state. This process was found to be slower in the gas phase ($0.75 - 1.3$ ps) [51], [52], [53] than in studies in aqueous solution ($0.18 - 0.43$ ps) [54], [55], [56]. As already stated above, the dynamics of the free base, the nucleoside and the nucleotide are very similar [50], [55], [44], [57].

Theory suggests two $\pi\pi^*$ and one $n\pi^*$ transition. The energy of those states is in the gas phase almost identical and the ordering depends on the level of theory [58], [59], [60]. Conical intersections (CI) connect them and population can be exchanged between the states [60],

[61]. The $\pi\pi^*$ states are assigned as L_a and L_b following Platt notation [62] with the transition dipole moment being parallel for L_a and perpendicular for L_b relative to the axis between the centre of one ring with the centre of the other ring (molecular axis) [44]. L_a is higher in energy and is optically brighter than L_b [60]. As a result the absorption spectrum is dominated by L_a . The deactivation takes places via a CI connecting L_a with the ground state, which is accessed via puckering of the C2-atom accompanied by an out-of-plane motion of the substituent [60], [63]. Theory states that L_b has a local minimum and therefore no internal decay pathway to the ground state can take place [60]. Nevertheless, conversion to L_a is possible via a small barrier. A recent time-resolved fluorescence study could find evidence for a conversion from L_b to L_a after 0.1 ps [44]. The $n\pi^*$ state has a very low oscillator strength [60]. A CI to the ground state could be found by puckering at the C-6 position, in a similar way to the CI for L_a described above [64].

In aqueous solution the energy of the $\pi\pi^*$ excitation is lowered relative to the $n\pi^*$ excitation, compared to the situation in the gas phase [65], [66]. In solution there is a mixture of 7H and 9H-adenine when they are present as free bases. 7H-adenine has an additional excited state lifetime of 8 ps [54], [56], [67]. This effect is called solvatochromism. It has been proposed, that the longer lifetime may be due to the CI being harder to access [68].

After reaching the electronic ground state via a CI all the excess energy is transferred to the vibrational degrees of freedom. The vibrationally excited electronic ground state has an excess energy of 4 eV, which corresponds to a temperature of 1000 K [69]. Subsequently the vibrational energy is transferred to the solvent until a thermal equilibrium is reached.

As a change in conformation is needed to reach a conical intersection little changes in structure can make them inaccessible. This can be seen at the example of 2-AP (see chapter 2.2.5) where a small change in structure fundamentally changes the photophysics.

Experimental signatures of vibrational cooling In the transient absorption data one can see a ground state bleach (GSB), stimulated emission (SE) and an excited state absorption (ESA) for the time steps when the electronically excited state is present. After the internal conversion one can see a red-shifted GSB absorption feature and an ESA feature, which corresponds to the vibrationally hot electronic ground state. This feature shifts over time to shorter wavelengths, as the vibrational cooling process transfers thermal energy to the solvent. An example from the literature can be seen in figure 2.11. Here early time steps are shown in blue and later time steps are shown in red. By having a broadband probe one can thereby monitor when the internal conversion takes place and how fast the vibrational cooling happens. The vibrational cooling in water has a time constant of about 2 ps for single nucleotides ($\tau_{AMP} = 2.05 \pm 0.07$ ps) [70], which monitored the GSB recovery at 252 nm.

Depending on the solvent, the dynamics of the vibrational cooling changes. It is important to note that changing the isotope of the solvent may have a direct impact on the cooling dynamics. For example, heavy water displays slower cooling than H_2O [29].

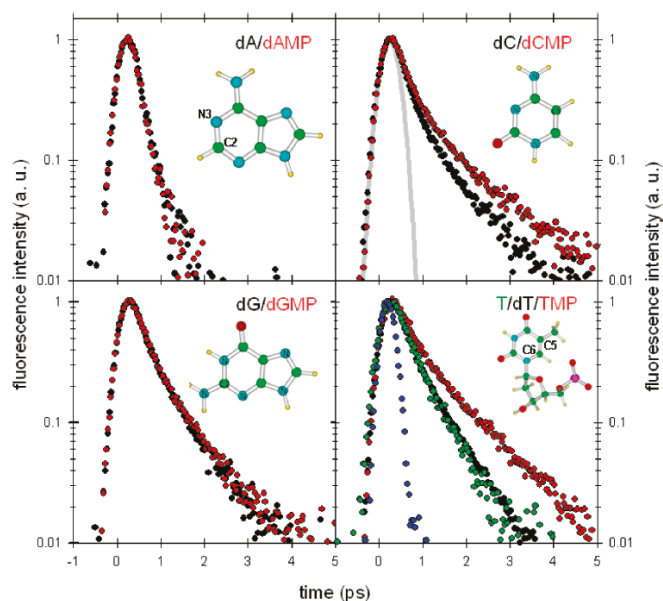


Figure 2.10: Time resolved fluorescence measurements of the nucleosides and the according nucleotides. The Purines show thereby no effect to the additional phosphate in contrast to the Pyrimidines. Reprinted with permission from [49]. Copyright 2010 American Chemical Society.

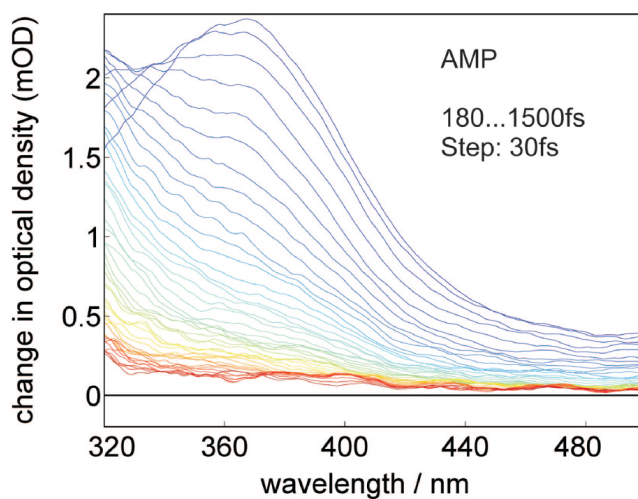


Figure 2.11: Broadband transient absorption spectra slices showing ESA of the hot electronic ground state. Time steps increase from blue to red. One can see the vibrational cooling. Reprinted adapted with permission from [71]. Copyright (2007) PNAS.

Note that the isotope substitution mainly modifies the reduced mass of the system, and thus impacts the vibrational frequencies of the solvent molecules. These results support the conclusion that the vibrational cooling happens mostly via the high-frequency modes of the solvent. Water thus has the fastest cooling rate among all solvents [72]. The ratio between the time constants associated with vibrational cooling, the so called kinetic isotope effect (KIE), in H_2O and D_2O is $\text{KIE} = \tau_{\text{H}_2\text{O}}/\tau_{\text{D}_2\text{O}} = 1.49 \pm 0.08$ [29].

2.2.5 Excited state dynamics of 2AP

2-aminopurine (2AP) is a fluorescent base analogue of adenine [73]: It is a structural isomer of adenine, which in the previously introduced labelling system can be called 6-aminopurine. Thus the sole difference between adenine and 2-aminopurine is the positioning of the amino group (NH_2). In case of adenine the amino group is attached to the position 6 in the pyrimidine ring and for 2-aminopurine at position 2. This minor change leaves the conformation of a strand where 2-aminopurine is incorporated, nearly unchanged [74]. The electronic structure, on the other hand, is changed in comparison to adenine in such a way that the non-radiative decay paths are less accessible and the fluorescence quantum yield is increased by orders of magnitude. Interbase interactions can quench the fluorescence which makes the quenching very sensitive to the environment. This is why 2AP is commonly used as a conformational probe. The 2AP monomer has a fluorescence quantum yield of 0.68, which is much higher than for adenine at $\sim 10^{-4}$ [75]. The fluorescence of 2AP peaks at 370 nm and its absorption peaks at 303 nm [75]. As this is redshifted compared to all other natural nucleobases one can excite 2AP selectively. When decreasing the polarity of the solvent, the fluorescence quantum yield decreases and the emission maximum shifts to lower wavelengths. Whilst the short excited state lifetime in adenine is due to internal conversion via a conical intersection, in 2AP the conical intersection is less accessible due to an energy barrier in the potential energy surface [59]. Therefore the excited state life-time in 2AP is longer and for the 2AP riboside takes a value of 11.6 ns [76]. In the nucleobase without the sugar, tautomerism plays a role and one can observe a bi-exponential decay with slightly different lifetimes [77]. The hydration of the base has a strong effect on its fluorescence lifetime and its quantum yield. This was studied in a supersonic molecular beam, where water-clusters with 2AP were formed [78]. The experiments demonstrated that hydration with a single water molecule changes the fluorescence lifetime from 156 ps in the gas phase to 14.5 ns. When 2AP is stacked, a second low intensity emission band, can be observed [79]. In circular dichroism experiments the excitonic coupling of 2APs in a stack was demonstrated [80]. 2AP incorporated in a strand shows a strongly reduced quantum yield as its fluorescence is quenched [81]. The energy of the excited state of 2AP is lower than those of any of the natural bases, so the quenching cannot take place via energy transfer. In natural DNA the quenching predominantly takes place via an intrastrand charge transfer with guanine [82]. However, it has been shown that all natural bases can quench the 2AP fluorescence, when they form a dimer with 2AP [83]. In the context of this thesis, it is particularly important that efficient charge transfer may take place in a 2AP-adenine dimer resulting in a reduction of 2AP by adenine [84]. Wan et al. then showed

in an ultrafast absorption and emission study that the fluorescence and absorption dynamics display different kinetics [85]. The authors conclude that a dark state has to be present in the deactivation dynamics, that is only visible in the transient absorption spectra but cannot be seen in the fluorescence decays.

2.2.6 Excited state dynamics in adenosine multimers

$\pi - \pi^*$ excitation

Stacking influences the excited state dynamics of DNA oligomers. As was discussed previously, excitation of their lowest energy absorption band initially populates excitonic states. Relaxation then leads to changes in their delocalization length, their inter-base conformation and typically to an increase in their CT character, with lifetimes in the 100s of ps range [70], [71], [86], [6], [48].

There has been a vivid discussion over how many bases couple excitonically in an adenine single strand. Different studies have claimed that photoexcitation leads to excitonic states delocalized over 2, 3 or 4 bases [29], [71], [87]. It was also speculated that on timescales shorter than 100 fs more bases could be involved but due to limitations in temporal resolution no experimental evidence could be provided [29]. In this context, Kadhane et al. gave experimental evidence that the coupling of adenine bases in the ground state in the $\pi\pi^*$ region is limited to two bases by analysing the amplitude of the CD signal as a function of the strand length [88]. In the region below 220 nm they could show that the coupling of the associated high-energy transition dipoles extends over up to eight bases.

The nature of the intermediates in the relaxation pathway have been a matter of discussion: Initially neutral exciton states were suggested to be the origin of the long lived states visible in time-resolved emission [89]. Various authors suggested 2-base exciton states with various degree of charge transfer [48], [70], [6]. Like in the previously introduced excimer states, a red-shifted emission could be observed in both static and in transient emission spectra of DNA strands [46]. This is caused by the stabilization of the excitonic states compared to the monomeric ones.

Importantly Bucher et al. [86] and Zhang et al. [90] have identified infra-red marker bands of ionized nucleobases in the relaxation dynamics of photoexcited heteropolymers and thereby verified the presence of charge transfer (CT) states in the photophysical relaxation pathways. This finding was corroborated by Borrego-Varillas et al. [91] who compared in their recent near-UV study the spectrum of adenosine cations and anions with the transient absorption spectrum of a photoexcited adenosine oligomer. The close agreement of the sum of the ion spectra with the transient spectra, showed that also in adenosine homopolymers CT states play a central role. The authors conclude that the evolution of the initially photoexcited neutral excitons into fully charge-separated CT states is complete after approximately three picoseconds. This interpretation is supported by molecular dynamics simulations [92].

In this context it is worth discussing in more detail a fluorescence anisotropy study of adenine homopolymers conducted by Banyasz et al. [46] after excitation at 266 nm the authors report an evolution of the fluorescence spectrum caused by the presence of a high-energy and a low-energy emission band with different decay dynamics. The high-energy band decays faster and displays a higher anisotropy than the low-energy band. In addition, the low-energy band shows a decrease in anisotropy on the sub-ps time scale, which the authors attribute to energy redistribution from bright neutral excitonic states to CT states. These dynamics change significantly for UV-A excitation, resulting in even lower, negative anisotropy values which typically implies a big angle between the originally excited and the fluorescing dipole moment. This suggests a strong out of plane component of the emitting CT state and can be interpreted as another strong indication for the charge transfer character of the exciton states. This assignment is also consistent with the higher fluorescent quantum yield and a strongly increased lifetime [46]. The exciton state has a lifetime, which is ~ 1000 times longer than that of the monomer, but only has a quantum yield which is ~ 10 times bigger. This suggests a state with low oscillator strength being the origin of the emission [30].

As was explained previously, molecular excitons are sensitive to the conformation as well as the solvation of the involved nucleobases [6]. In this context, Spata et al. conducted a QM/MM computational study on photoexcited adenine dimers in a solvated double-stranded DNA geometry [93]. The resulting exciton states showed different minimum energy configurations that were distinguished according to their CT character and inter-base distance: Neutral excitons, charge transfer excitons, neutral bonded excitons and charge transfer bonded excitons. The study suggests a picture where these configurations are populated transiently from the initially photoexcited exciton band. The involved changes in dimer conformation and CT character may explain the complexity of the experimentally observed relaxation dynamics [94].

Following from the above discussion, the dominant contribution to the electronic deactivation of photoexcited DNA oligomers on the 100 ps time scale is the decay of the formed CT states via charge recombination [70], [95]. For completeness it should be pointed out that several other photophysical pathways have been suggested in the past to explain the experimental data. A prominent suggestion is that a monomeric decay via a conical intersection remains accessible even in DNA oligomers [48], [96]. However, as the stacked bases are close to each other, steric hindrance slows down the process and may result in longer excited state lifetimes [48], [96], [29]. Figure 2.12 summarizes the above explained decay pathways. As described in chapter 2.2.3 a direct excitation of the charge transfer state is possible, when exciting with lower energy photons [41].

Moving from the photophysical dynamics of single-stranded to double-stranded DNA, base pairing interactions have to be taken into account. Single bases in an aqueous solution tend to stack rather than pair. As a consequence there does not exist a model system in aqueous solution but only in low polar solvents [30]. However, early ultrafast spectroscopic studies did not offer a conclusive picture concerning the role of base pairing in the excited state deactivation.

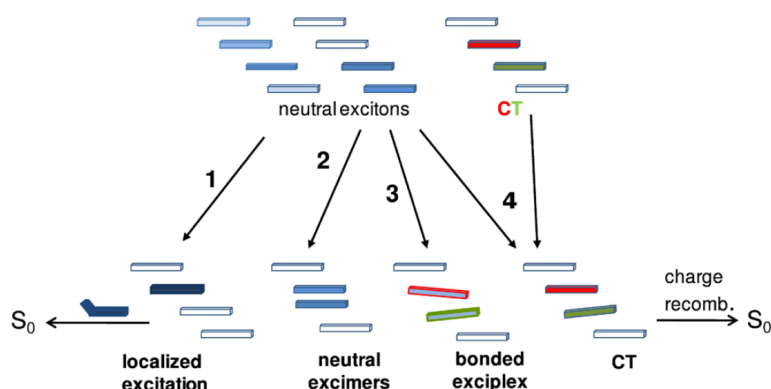


Figure 2.12: Various decay paths exist in adenine single strands. Depending on excited transition and the ground state conformation different dynamics take place. Unstacked bases can decay monomer-like, whereas in stacked regions the initially excited neutral exciton decays via charge transfer excimer states. A direct excitation of charge transfer states is also possible. The figure is reprinted with permission from [97]. Copyright 2016 American Chemical Society.

tion. The central question being whether base pairing opens fundamentally new relaxation channels or if it only perturbs the relaxation channels already existing in single strands [94], [98]. One change for example is, that the paired bases in a double strand experience a different solvent environment with a reduced exposure to the solvent. This could affect for example the vibrational cooling and in principle also the energy levels (compare chapter 2.2.4). The change in cooling dynamics can be observed for $(dA)_{18} \cdot (dA)_{18}$ structure measured by Chen et al. [99]. There, structure-dependent cooling times were measured: $\tau_{(dA)_{18} \cdot (dT)_{18}} = 4.7$ ps compared to $\tau_{(dA)_{18}} = 2.7$ ps and $\tau_{(dT)_{18}} = 2.8 \pm 0.12$ ps [99]. Another difference to the single strands is the change in structural rigidity and thus conformational ensemble. Due to the structural stabilization of the paired strands, stacking is more pronounced in double strands than in single strands, meaning that the ratio of stacked bases to the overall amount of bases is higher. Chen et al. measured, in the above mentioned publication, a life-time for the long living component of the ground state bleach recovery signal of $\tau_{(dA)_{18} \cdot (dA)_{18}} = 62 \pm 17$ ps [99]. This is almost three times faster than the life time measured by Su et al. in adenine single strands with $\tau_{exciton} = 183 \pm 6$ ps [29]. This is a strong evidence, that there is some quenching of long lived excited states. The life time of the charge transfer exciton state corresponds to the rate of charge recombination and scales with the redox potential of the bases involved [86]. Having a base with a different redox potential bound via a hydrogen bond may change the this recombination rate and thus quench this state. Bucher et al. found that base pairs linked via hydrogen bonds decay with a common lifetime [100]. In this context, Proton-Coupled Electron Transfer (PCET) has been established as a central deactivation mechanism in double strands [101], [102] [100]. Additionally to the electron transfer within one of the strands (intrastrand electron transfer), a proton transfer happens between two paired bases, according to this model. A sketch illustrating this transfer is shown in figure 2.13. In all models an electron is transferred from one base to a base in a single strand. In b) and c), additionally a proton is

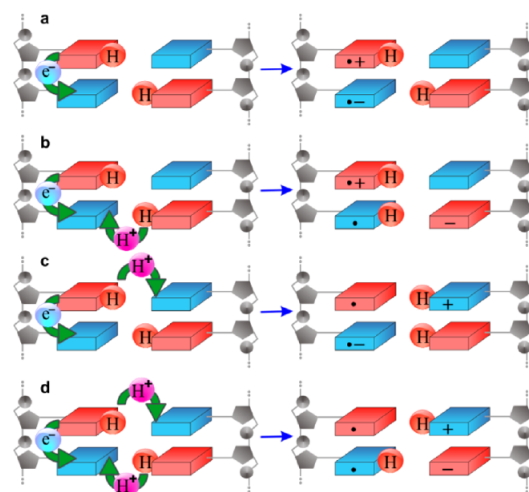


Figure 2.13: Schematic representation of the different mechanisms in Proton Coupled Electron Transfer (PCET). In all models one electron is transferred from one base to another in a single strand. Additionally to that a proton is transferred in b) and c) and two protons are transferred in d). The figure is reprinted with permission from [102] (<https://pubs.acs.org/doi/10.1021/jacs.5b03914>). Further permissions related to the material excerpted should be directed to the ACS.

transferred. Two protons are transferred in d).

3 Methods

In this chapter the methods, setups and procedures used for the measurements presented in the following chapters are described. First the static spectroscopy used to characterize the samples are introduced. Then the principle and the setups for the time resolved measurements are explained. The chapter finishes with a description of the data treatment and the samples used for the experiments.

3.1 Static spectroscopic techniques

3.1.1 Static UV-vis spectrometer

Static absorption spectra measure the macroscopic absorbance of a sample that is described by the Beer-Lambert law:

$$\log\left(\frac{I_0}{I_1}\right) = \epsilon \cdot c \cdot d, \quad (3.1)$$

whereby I_0 and I_1 are the initial, respectively the final, intensity of the light, ϵ is the molar extinction coefficient, c is the concentration and d is the distance over which the light travels through the sample. Microscopically, the absorption coefficient comprises the ground state transitions of the sample molecules.

Static UV-vis spectra were taken in a commercial high resolution UV-vis spectrometer (Shimadzu UV-3600). A halogen and a deuterium lamp is used as white light source to access a range from 185-3300 nm. The white light is monochromatized by two grating monochromators before passing the sample compartment. The absorption spectrum is recorded by scanning the wavelength range. A photomultiplier tube, an InGaAs and a PbS detector are used depending on the spectral range. The baseline of the spectrometer was recorded with an empty sample compartment. A measurement of the cuvette with the solvent was taken for each set of measurements and subtracted from the data.

3.1.2 Static photoemission

Static fluorescence spectra contain the radiative transitions from an excited state to the ground state. Static fluorescence spectra will contain, depending on the excitation wavelength, the solvent and the recorded emission range, the Raman line (in our case the Stokes line) of the solvent. By analysing their spectra we can learn about the nature of the excited state. Excimer states for example show a characteristically broad emission. Furthermore, by comparing the signal strength of two samples with the same concentration or absorption we get information about the radiative quantum yield. In this way, we may identify the contribution of non-radiative decay pathways in the relaxation of the excited state.

Static emission spectra were recorded with a commercial spectrofluorophotometer (Shimadzu FR-5301 PC). The excitation photons come from a Xenon lamp and pass a monochromator and can be set in a range between 220-900 nm. The fluorescence is recorded by scanning the wavelength range from 220-750 nm and is detected via a photomultiplier. Before each set of measurements the cuvette with the pure solvent was recorded at the respective excitation wavelength in order to subtract the pure solvent response.

3.1.3 Static circular dichroism spectrometer

CD indicates the difference in absorption between left and right circularly polarized light [103] in chiral molecular systems. On a microscopic level, it measures the helicity of charge displacements associated with photoinduced transitions. Chiral chromophores themselves can show CD. Furthermore, the excitonic coupling between chromophores, depending on their relative geometry, can lead to a CD signal. Therefore two or more coupled chromophores in a defined geometry can show a characteristic CD signal. This is routinely used to characterise the global structure of biological samples in solution as for example β -sheet and α -helix structures as well the B-Helix of DNA show characteristic CD spectra in the far ultraviolet region. CD measurements in this thesis are used to confirm the excitonic coupling in each measured sample as well as to investigate its dependence on different solvents. The CD spectra of the investigated samples were also used as an additional diagnostic to check their structural integrity before and after experiments.

Static circular dichroism (CD) spectra were recorded with a commercial CD spectrometer (Jasco J-810). The light source is a xenon lamp and the detector a photomultiplier tube. Spectra can be recorded from 163 to 900 nm. The light is monochromatized by passing twice through a set of a prism and two slits. These prisms not only select the wavelength but also clean the polarization so the light is linearly polarized. A photoelastic modulator (PEM) is used to turn the linearly polarized light into either left or right circularly polarized light. In a PEM, mechanical stress is periodically induced in a quartz block which leads to birefringence in the crystal. In this way, the polarization of the light is periodically modulated from left to right circular polarized light. When the detector measures the absorption for one wavelength, the average signal corresponds to the static absorption and the modulation of the signal to

the circular dichroism. A spectral calibration with a holmium oxide calibration standard was performed.

3.2 Transient absorption spectroscopy

3.2.1 Measurement principle

In order to investigate femtosecond dynamics a so-called pump-probe scheme is applied. In this approach, that is employed in multiple time-resolved spectroscopic techniques, two ultrashort events are used in order to first trigger a process and then probe the process. The former is called the pump and the latter the probe event. For optical experiments in the context of this thesis pump and probe pulses both originate from an ultrafast mode-locked laser system (see chapter 3.2.2). An intense laser pulse is used to excite a sample whereas a second, weaker laser pulse investigates the sample after a selectable waiting time. By controlling the optical path length difference between the two pulses one can vary the time difference between the two pulses. Thus one collects temporal snapshots of the ultrafast dynamics. In transient absorption one monitors the absorption spectrum of the probe pulse. By blocking the pump pulses with an optical chopper one reduces the repetition rate of the pump arm typically by two. Thus one can compare the changes in optical absorption of the sample induced by the pump, the so-called differential absorption ΔA . It is calculated by the following formula:

$$\Delta A = -\log\left(\frac{I_p}{I_u}\right). \quad (3.2)$$

Here I_p and I_u refers to pump and unpumped intensity of the probe spectrum. To further improve the signal-to-noise ratio one can record a reference beam that does not go through the excited sample and account for the fluctuations of the probe spectrum. One then divides each probe spectrum $I_{probe\ i}$ by the reference spectrum $I_{ref\ i}$:

$$I_{probe\ corr\ i} = \left(\frac{I_{probe\ i}}{I_{ref\ i}}\right). \quad (3.3)$$

A high number of single shots (for the measurements presented in this thesis 30 000) are recorded per scan, pump-probe delay and pump polarization. The data acquisition electronics sort the spectra in pumped and unpumped reference or signal spectra. After the sorting each group of spectra are averaged and saved. In the post processing the averaged pumped and the averaged unpumped spectra are divided by the associated averaged reference spectra according to formula 3.3. i stand for the pumped or unpumped spectra. In order to address for systemic fluctuations in the spectrum one can apply the B-matrix procedure [104], [105]. The B-matrix is a matrix with the dimensions of pixels the signal times the pixels of the reference. It scales the fluctuations of each reference pixel to the fluctuations of a signal pixel. By this not only one but multiple pixel of the reference accounts for fluctuations on a signal pixel. Thus

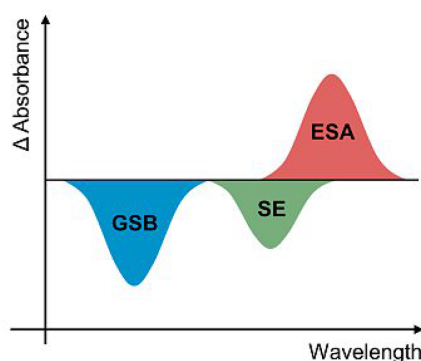


Figure 3.1: Schematic sketch showing the ground state bleach (GSB), the stimulated emission (SE) and the excited state absorption (ESA) feature. The figure is reprinted from [106].

the B-matrix maps the correlation of different regions in the spectrum and a more advanced noise suppression may be achieved.

In transient absorption (TA) measurements the pump pulse only ever excites a small fraction of the sample molecules. As a result, a typical TA spectrum contains three main contributions: excited state absorption (ESA), ground state bleach (GSB) and stimulated emission (SE) (see fig. 3.1). The ESA contribution is caused by a new excited state species that usually has a different absorption spectrum. The excited state species may show new absorption bands compared to the ground state species. This signal has a positive sign in TA. By monitoring the ESA signal dynamics one can investigate the evolution of the excited state population. Where the ground state molecule shows an absorption band, the absorption may be lowered compared to the ground state absorption. The ground state population is reduced by the excitation, thereby reducing the ground state absorption of the sample. One says the ground state absorption is bleached and the associated signal is called ground state bleach (GSB), which has a negative sign in transient absorption data. The dynamics of the GSB recovery signal shows the repopulation of the ground state species. In addition, the probe pulse can stimulate the emission of a photon from an excited sample. The stimulated emission (SE) signal has a negative sign in TA.

3.2.2 Transient absorption setup in the deep-UV

The time-resolved data discussed in this thesis were recorded on a transient absorption setup, which had been discussed in detail elsewhere [10], [11], [106], [107] and will therefore only be described briefly. To resolve a given signature one needs a sufficient signal to noise ratio. If the setup and the samples are stable over time, acquiring more shots improves the signal quality. To limit measurement time for achieving a certain signal to noise ratio, it is advantageous to have a high repetition rate and to have low pulse-to-pulse fluctuations. The setup presented in this section was implemented with the aim to optimize these properties [10], [11] and is usually referred to as the 20 kHz setup.

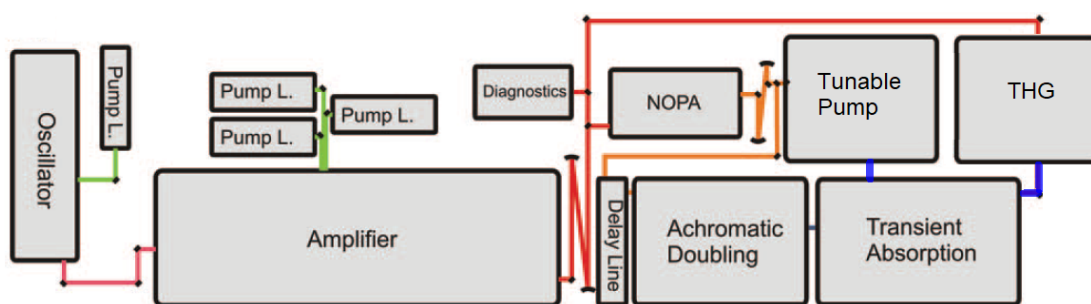


Figure 3.2: Schematic of the 20kHz Ti:Sa chirped pulse amplification setup. Shown is the Oscillator, the Amplifier with its three pump lasers, the NOPA, the achromatic doubling, the narrow band doubling and the transient absorption station. The figure is reprinted and modified from [10], with the permission of AIP Publishing.

A schematic of the setup can be seen in figure 3.2. The 20kHz setup is seeded by a commercially available mode locked titanium-sapphire oscillator (Halcyon, KMLabs), which is pumped by a frequency doubled Nd:YAG (neodymium-doped yttrium aluminium garnet) Verdi laser. It provides mode-locked femtosecond pulses with a repetition rate of 75MHz and a bandwidth covering at least 40nm full width at half maximum (FWHM) at a central wavelength of around 800nm. These pulses seed a regenerative titanium-sapphire chirped pulse amplifier (CPA), which works at a repetition rate of 20kHz and is pumped by three separate Q-switched Nd:YVO₄ (neodymium-doped yttrium orthovanadate) solid state lasers. This scheme has two advantages. Compared to Nd:YAG, these laser can achieve lower fluctuations due to their single-mode operation, but the employed models were also built to provide an extra low shot noise of <0.3% root mean square (RMS). Additionally the intensity fluctuations of the three individual pump sources are uncorrelated. Therefore the fluctuations of the overall pump light sum up to a factor of $\frac{1}{\sqrt{3}}$ compared to pumping with a single laser. Pump pulse fluctuations are the main source for intensity fluctuations of pulses out of a CPA system. We drive the amplification process in a saturation regime, which makes the amplifier output even less sensitive to pump intensity instabilities. The setup provides pulses with an energy of approximately 0.6mJ with a shot-to-shot stability of < 0.1 RMS (root mean square) and a repetition rate of 20kHz.

As a simple and stable pump source in a pump-probe experiment we can directly use the 800nm, frequency double to 400nm or triple to 266nm pulses. Hereby we can also easily achieve pump pulse energies that are higher than the powers we obtain by narrow band doubling of the NOPA (non-collinear optical parametric amplifier) output (see paragraph below).

NOPA, Achromatic doubling and narrow doubling The setup provides tunable pump pulses and broadband probe pulses in the deep-UV. To achieve this, a commercially available NOPA (non-collinear optical parametric amplifier, TOPAS white, light conversion) is used. A white light continuum is generated in a sapphire plate. This serves as seed light for a two stage parametric amplification process in a BBO (beta barium borate) crystal. This provides broadband

intense white light pulses with spectra that span approximately 500–760 nm and have a pulse energy of $13\ \mu\text{J}$. One part of these pulses can get frequency doubled in a thick BBO crystal to provide a narrow band deep-UV optical pump. By turning the crystal one changes the phase matching condition, different wavelength components are frequency doubled and one gets a tunable deep-UV pump from the broadband NOPA output. By implementing a chirped mirror compressor in front of the BBO one can compress the pulses in time and get higher conversion efficiency in the BBO and therefore higher achievable pump powers for the experiment.

To get a broadband deep UV probe one has to convert the broadband visible into a broadband UV spectrum. In the frequency doubling process the phase matching condition has to be fulfilled for all wavelengths. To achieve this, one spatially chirps the spectrum in a pair of prisms and then focuses on the BBO with an off axis parabola (OAP). Each wavelength component thereby enters the BBO under an angle that satisfies the phase matching condition [108] [109]. As a result, we have pulses in the deep-UV spanning from approximately 250 – 380 nm.

In combination with a variable delay stage and a shot-to-shot data acquisition system this these optical components constitute a time resolved 2DUV pump-probe setup [10], [11].

Acquisition system Before the the probe beam is focussed into the sample, a part of the broadband continuum is split to be used as reference. For this purpose reflective neutral density filter (1 mm thickness, 0.3 OD optical density) is used. The reference beam is used to record spectrally resolved intensity fluctuations in the probe beam. The probe and reference beam are each focused via an off-axis parabola into a multimode fibre. The inner diameter of the fibres were $400\ \mu\text{m}$ for the data presented in chapter 4 and $105\ \mu\text{m}$ for chapter 5 and 6 . The fibres are connected to a grating spectrometer. Thus the inner diameter of the fibres are equivalent to the entrance slid width of the spectrometer and determine the spectral resolution. The spectrometer (Chromex 250is) is equipped with a 150 grooves/mm grating and two complementary metal-oxide semiconductor (CMOS) detector arrays with 512 pixels each. The probe and reference beams are horizontally offset, travel over the same optics and are each collected at the related detector array. The detectors are readout shot-to-shot at 20 kHz.

3.2.3 Flow cell and Wire-guided liquid jet

In the scope of this thesis the setup is used to look at sample in transmission to do transient absorption measurements. When working with samples in solution one has to renew the sample continuously. Otherwise one could measure an artefact due to the accumulation of long lived states or damaged sample [8]. Therefore one typically works with flow cells, which have the drawback that they induce additional dispersion and birefringence. Additionally the glass can burn at high pump power in the deep-UV.

To avoid these problems, one may either employ an optimised flow cell design with very

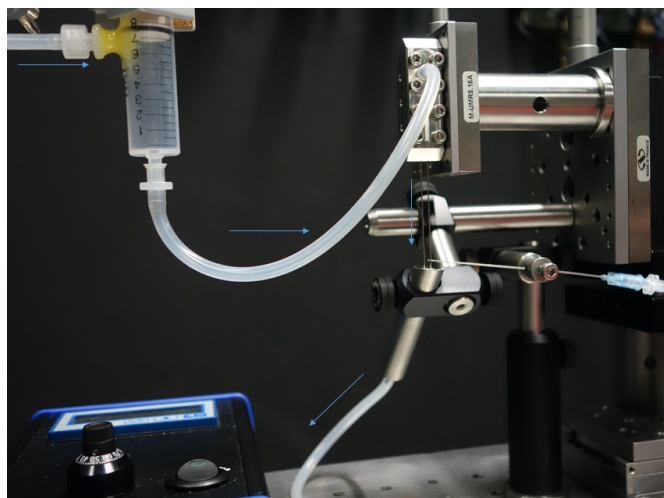


Figure 3.3: Image of the wire-guided liquid jet. The blue arrows indicate the flow direction of the sample. The damper (left high), the sandwich block with the wires (centre), the catcher (centre low), the needle (centre) and the gear pump (left low) can be seen.

thin glass windows [110] or by using a wire-guided liquid jet (e.g. [111], [112], [113]), which inherently does not show these issues. Figure 3.3 shows an image of the wire-guided liquid jet. There the sample flows down as a liquid curtain between two wires. The pulses don't have to travel through glass windows, which solves the problem with burning glass, avoids additional dispersion and lowers the coherent artefact¹ coming from the interaction between the pulses and the glass.

The wire guided liquid jet setup built for this thesis was mainly inspired by the publication of Picchiotti et. al [111] but also some concepts were taken from [112] and [113].

The centrepiece of the setup is a sandwich block composed of a front and a back part (for drawing of the front part see figure A.1 in the attachment). Both parts have a small U-shaped groove, which fixes a U-shaped wire. The combination of groove and wire also serves as a sealing. The front part of the sandwich block has a little hole with a nipple where a tubing can be attached. Through this hole the sample is entering the sandwich block. The sample is exiting the blocks at the lower end as a liquid curtain between the two wires and is collected in a catcher. For a flow as smooth as possible, the wires have to be as close to the catcher as possible while not touching it. The catcher is connected with tubings to a micro annular gear pump, which pumps the sample into a syringe. It works on the one hand as a damper for vibrations and on the other hand as a reservoir for the sample. From the reservoir the sample is pumped into the sandwich blocks again. As this system is a closed loop, except of the region where the curtain flow is, one can control the volume flow rate and thereby the thickness of

¹The term "coherent artefact" describes an unwanted feature mostly around time zero whose origin is not the examined sample but for example the sample cell or the solvent. Its origin can be two photon absorption or cross phase modulation induced by the overlap of the pump and the probe pulses [114]. For the duration of the artefact it is difficult to extract meaningful information out of the measurement data

the liquid sheet by the pump speed. Higher pump speeds thus lead to thicker liquid sheets. The thickness of the liquid sheet with the volume flow rate used in this thesis was estimated to be $\sim 200\ \mu\text{m}$ [107]. At the open part of the liquid jet solvent can evaporate. This leads to concentration changes of the sample under examination and can even lead the flow to run dry. To compensate this, a syringe pump, which can precisely add a specified amount of liquid at a very low rate is used. For aqueous solutions the evaporation rate in our setup is $3.6\ \mu\text{l}/\text{min}$. For D_2O solutions the evaporation rate was $1.7\ \mu\text{l}/\text{min}$. Knowing the evaporation rate of one solvent under given conditions, one can estimate the evaporation rate of an unknown solvent by multiplying the known rate with the ratio of the vapor pressures. One has to keep in mind that only the solvent and not the sample or salts of a buffer evaporate and therefore only purified solvent has to be added by the syringe pump. Apart from the advantages, the liquid jet introduces a new source of noise, as the sheet can change in thickness or can get unstable.

3.2.4 Anisotropy

Anisotropy is a simple but powerful tool to investigate dynamics in molecules. In a homogeneous sample the transition dipole moments are randomly oriented. By exciting the sample with polarized light, the chromophores, whose transition dipole moments are oriented parallel to the incident light, are excited with a higher probability. This is called photo-selective excitation or photoselection. The probability for the excitation scales with $\cos^2 \theta$, where θ is the angle between the chromophore's transition dipole moment and the polarization of the linearly polarized light. The initial anisotropy r_0 of a single chromophore is [76]

$$r_0 = \frac{2}{5} \frac{3 \cos^2(\beta) - 1}{2}, \quad (3.4)$$

where β is the angle between the excited and probed transition dipole moment. Thus the initial anisotropy is between 0.4 for a parallel transition relative to the excited transition and -0.2 for a perpendicular transition. Processes that can lead to a change in anisotropy are rotational diffusion, energy transfer between chromophores, changes in the electronic states (for example CT character), or the structural rearrangement of a molecule. Therefore, one can investigate these phenomena with an anisotropy study.

The anisotropy r is calculated from the experimental data by using [115]

$$r = \frac{\Delta OD_{\parallel} - \Delta OD_{\perp}}{\Delta OD_{\parallel} + 2\Delta OD_{\perp}}. \quad (3.5)$$

ΔOD_{\parallel} and ΔOD_{\perp} are the parallel and the perpendicular polarized change in absorption of the probe relative to the pump polarization. The signal which is insensitive to polarisation

effects and only depends on the population dynamics is calculated via

$$\Delta OD_{MA} = 1/3(\Delta OD_{\parallel} + 2\Delta OD_{\perp}). \quad (3.6)$$

The same signal can be recorded when measuring under an angle of 54.75° between pump and probe polarizations, which is also called the magic angle. How ΔOD_{\parallel} and ΔOD_{\perp} are experimentally obtained is explained in the following. The polarisation of the probe is set up perpendicular to the optical table. A Glan-Laser polarizer is used after the sample in order to clean the detected polarization and to not affect the time resolution of the setup. The polarisation of the pump pulse is adjusted by a motorized half-wave plate. The wave plate needs to be calibrated relative to the probe polarization before each set of measurements. For this purpose the probe polarizer is placed in between the half-wave plate and a power meter. By recording the power transmitted through the polarizer and fitting the values to a \cos^2 -function one can determine the parallel and perpendicular polarization of the pump relative to the probe polarization.

3.2.5 Spectral calibration

Before each set of measurements a spectral calibration of the detector needs to be performed. For this purpose probe and reference spectra with and without a calibration liquid in the beam path are recorded. By subtracting the spectra with the liquid from the blank spectra one can identify the absorption peaks of the calibration liquid. For the deep-UV spectral region holmiumoxide shows up to 6 sharp absorption peaks. The wavelength of each of the peaks are known and by performing a linear fit a mapping between each detector pixel and the corresponding wavelength is found.

3.2.6 Instrument response function

To determine the temporal resolution of the setup an instrument response function (IRF) is taken. In aqueous solutions in the deep-UV a strong and instantaneous two photon absorption in the solvent can be observed [116] (see figure 3.4 a)). The two photon absorption signal in a water jet was measured and the obtained kinetic traces were fitted with a Gaussian at each probe wavelength. Such a representative trace together with a Gaussian fit can be seen in figure 3.4 b)). The IRF is typically between 100fs and 300fs (full width half maximum (FWHM)) over the whole spectral range (see figure 3.4 c)). The IRF may vary depending on the pumping conditions, e.g. pumping with the tripled fundamental, or the doubled NOPA output, or using different thicknesses for the non-linear crystal. As a measure for the quality of the Gaussian fit the R^2 value of the related fit is shown in figure 3.4 d)). In figure 3.4 a) one can also estimate the chirp of the probe pulse. Wavelengths around 285 nm arrive the earliest and wavelengths around 365 nm the latest with a time difference of approximately 2.5 ps. The chirp stems from the strong group velocity dispersion in the deep UV. The achromatic doubling scheme in this setup is optimized for optimal phase matching condition but not for shortest probe pulses

resulting in a chirped probe pulse. The data get chirp corrected during the data treatment as can be seen in section 3.4.

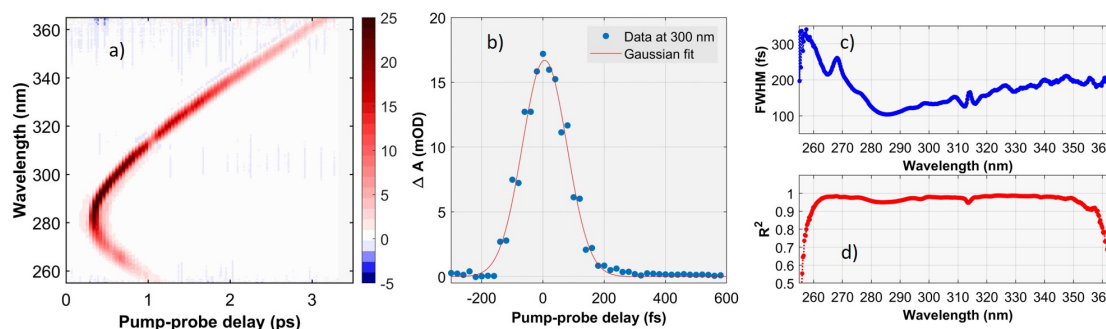


Figure 3.4: Instrument response function (IRF) pumped at 288 nm. a) shows the spectrally resolved transient absorption signal for time delays close to the pump-probe overlap. b) shows an exemplary time trace at a probe wavelength of 300 nm. c) shows spectrally resolved the FWHM of a Gaussian fit to the data in a) and d) shows the respective R^2 value as a measure of the goodness of the fit.

3.3 Fluence dependence

To get a high signal one aims at measuring as many excited molecules as possible. To achieve that one can adapt either the concentration or the thickness of the sample as well as vary the pumping conditions. When pumping the sample one has to make sure that the measurement is done in a linear regime, meaning that the signal strength scales linearly with the pump power. Furthermore, ionization of the sample or the solvent can happen which changes the transient absorption signals. Strong pump pulses can for example ionize a water molecule and lead to a solvated electron whose spectral signature can overlap with the signatures of the observed sample [30]. To make sure one stays in the linear regime a fluence dependence is performed. For this the TA spectrum for a fixed pump-probe delay is recorded as a function of the pump power. As long as the signal strength scales linear with the pump power one is in the linear regime.

3.4 Data procedures

All data are imported via a Matlab script. Dark spectra, that are recorded before every scan with no light on the detector, are subtracted from the data. Furthermore an offset, extracted from the counts on pixels where the probe spectrum is not present, is subtracted from all spectra. The spectra are divided by their reference spectra and the B-matrix algorithm (see above) can be applied. A preliminary pump-probe spectrum is calculated and a pronounced TA band is selected and its amplitude is used in order to perform a parity and outlier correction. Due to rare sorting issues in the acquisition a flip in parity can appear in the data. By controlling the parity of all the spectra, these errors can be accounted for, by multiplying those spectra with

a factor of -1. If the pump-probe signal in one scan and time delay differs substantially, for example by more than 100%, the outlier correction algorithm will identify this data point as an outlier and reject the related spectrum. The pump-probe spectrum is calculated via

$$\Delta A = \frac{1}{\ln 10} \frac{I_p - I_u}{I_u}, \quad (3.7)$$

which is the first order Taylor expansion of equation 3.2. The average signal before time zero can optionally be subtracted as another background subtraction. To account for the group velocity dispersion of the probe pulse a chirp correction is performed. At time zero the two photon absorption cross correlation signal shows a very prominent signal. A representative set of time-wavelength points on the chirp is chosen and a third order polynomial is fitted to describe the chirp function. The time vector for each pixel is calculated and the pump-probe spectra are extrapolated and shifted on a grid. Finally the anisotropy and magic angle data are calculated according to equations 3.5 and 3.6.

To gain insights from complex time-wavelength-resolved measurements an advanced data analysis is needed. For this purpose a global fit is applied [117], [118]. In this thesis a global lifetime analysis is used. For this a mathematical model is used to describe the data. Global analysis is simultaneously fitting several exponential decays, resulting in a life time τ and a wavelength dependent exponential pre-factor for each exponential. The wavelength dependent exponential pre-factor is called decay associated spectrum (DAS). The experimental data are recorded with a limited time resolution, so the fitting function is a multi-exponential model convoluted with the IRE. Two possible fitting functions are used in global life time analysis, one that assumes a series of exponential decays and one that assumes a parallel set of exponential decays. Those mathematical models correspond to a series of coupled states or a collection of uncoupled individual states. This analysis is used to quantify the data and make different datasets comparable. To make a statement about reaction mechanism further information are required. In a target analysis a complex reaction scheme can be fitted to the data, where for example a branching from one initial species to two independent intermediates could take place. It should be noted, that global analysis assumes time independent DAS. Spectral shifts as they are present for example with vibrational cooling can therefore not be accounted for in global lifetime analysis [117]. Nonetheless one can mathematically account for them with an additional exponential temporal decay that will result in an additional spectrally shifted DAS. Those DAS and their associated lifetimes have no photophysical meaning. In this thesis OPTIMUS, an Matlab based implementation for global analysis by Slavov et al. [119], is used to analyse the time resolved transient absorption spectra.

Besides global analysis singular value decomposition (SVD) is a tool to analyse the data. SVD is another mathematical approach to analyse the data and quantify its spectro-temporal dynamics. Applied to time wavelength dependent data, it decomposes the data as a sum of prefactors each multiplied with a spectrum and a lifetime [117]. It can be used as an estimation

how many decay components one data set has. Furthermore it can be used for noise filtering, as components with a small prefactor likely are noise contributions.

To fit the anisotropy data, each anisotropy band is averaged. All bands are fitted with an multiexponential model whereas the decay times are global. If for example the anisotropy of the ESA has three decay components and the one of GSB shows two, two lifetimes of the ESA are identical with those of the GSB.

4 Excited state dynamics in adenine single strands

Photo stability of DNA bases is paramount to life. In order to determine the photo-chemical pathways in DNA oligomers and their crucial role in photo-damage control of the genome, broadband deep-UV (250-360 nm) transient absorption spectroscopy is applied covering the bleached ground state transitions as well as excited state signatures simultaneously. It was identified that the excitation of an adenine single strand close to the maximum of its main absorption peak (266 nm) leads to an exciton which spans over two bases. Surprisingly this exciton cannot be identified in a dimer thus leading to the conclusion that the structural rigidity of the multimer enables stronger dipolar coupling which is necessary for the exciton formation. The transiently formed charge transfer (CT) state has a full CT character in the multimer whereas the CT character is only partial in the dimer. As the atmosphere of the earth blocks all radiation at the adenine's main absorption band it is not a good model for terrestrial photo-protection. Adenine multimers show a tail in the absorption spectrum which has considerable overlap with the terrestrial solar spectrum. To bridge the gap towards the biologically more relevant case experiments with excitation at 285 nm had been performed. Thereby a CT state gets directly populated. The experiments provide the first evidence of the strong inhomogeneous broadening of the CT state, which resembles the CT state of the dimer after exciting at 266 nm. The charge recombination rates are determined by the structure of the strand and not by the nature of the CT state.

4.1 Introduction

The stability of our genetic code, the DNA, is essential for life. When a DNA molecule absorbs electromagnetic radiation, the molecule is in an excited state, which is prone to chemical reactions. Such a chemical reaction can lead to a mutation, which may have fatal consequences. In the past two decades, many studies had been performed to elucidate the photochemical decay pathway after photoexcitation [35] [6] [120]. Due to the strong absorption of the atmosphere in the UV-C region, barely any significant radiation around 266 nm reaches the earth at sea level. DNA has its main absorption peak around 260 nm but an absorption tail, associated to collective states in the multimer, absorb until beyond 300 nm. Under these circumstances

it becomes clear that the photostability of DNA under natural conditions is determined by the photochemistry associated with its UV-A absorption. However not much is known about this region because the absorption is weak and most studies have so far focussed on the more easily accessible 260 nm band. A literature review on the excited state dynamics can be found in paragraph 2.2.3 and the following paragraphs. To be able to study the dynamics of these processes many groups performed pump-probe studies, mainly based on commercially available mode-locked Titanium Sapphire (Ti:sapphire) lasers. All nucleobases show a strong absorption peak around 266 nm, which is easily accessible by the third harmonic of Ti:sapphire lasers. Regardless of DNA bases having a strong absorption at 266 nm, photochemical events at that wavelength cannot mimic the photochemistry happening after the absorption of a solar photon on earth. In addition, DNA absorbs well beyond 300 nm having a significant overlap with the terrestrial solar spectrum [35]. In this chapter, the aim is to identify and confirm the nature of the electronic transition responsible for the absorption. Furthermore, the dynamics following this excitation will be studied and kinetics and reaction intermediates will be compared to the dynamics induced with 266 nm excitations to identify common behaviour. This chapter therefore focusses on two aspects. First we consolidate the current picture of the photochemical dynamics of the $\pi\pi^*$ excited states in adenine homopolymers via the unique bandwidth of the employed deep-UV transient absorption setup. Second, we gain detailed new insights into the role of solvation in the formation and relaxation of charge-transfer states that dominate the photochemistry of this model system.

4.2 Experimental details

The sample system investigated in this chapter are mono and multimers of deoxyadenosine monophosphate (dAMP). It is the deoxy-nucleotide of adenine as already explained in chapter 2.2.1. Samples were purchased from Sigma-Aldrich (2'-Deoxyadenosine 5'-monophosphate (dA₁)) and from biomers.net (dimer (dA₂) and 20-mer (dA₂₀)) and used without further purification. The dimer (dA₂) and multimer (dA₂₀) consist of dA₁ as building blocks, where the phosphate group is covalently linked to the deoxyribose at the 3' carbon of the next dA₁, from which a single strand is formed with a sugar phosphate backbone (see figure 4.1). The samples were used without any further purification. By measuring the samples in a static UV-vis spectrometer (UV-3600, Shimadzu) and a static circular dichroism spectrometer (J-810, Jasco) sample integrity is ensured.

As the solvent environment has a strong impact on the structure and the electronic states in DNA, the choice of the solvent is important. Here, DNA is investigated under the intention to study biologically relevant processes. Therefore the solvent conditions should mimic those of living organisms. Thus physiological phosphate buffered saline is used. It is a solution of ultra pure water with 0.135 mol/l NaCl, 0.0027 mol/l KCl and 0.01 mol/l Na₂HPO₄ and gives pH of 7.4 [122]. In order to inhibit stacking experiments in a methanol-water solution following the description of Chen et al. [8], with 80vol% of methanol and 20vol% of Milli-Q water were performed. The samples were prepared to have an optical density of 0.75 OD at the absorption

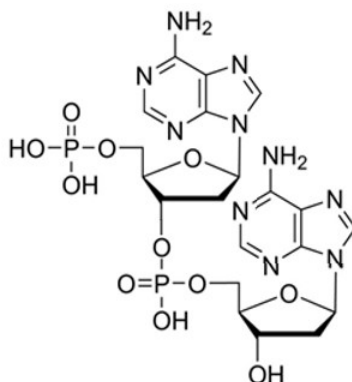


Figure 4.1: Schematic showing a dimer (dA_2), which consists of two dAMP units who are covalently linked via phosphate group to the deoxyribose at the 3' carbon of the next dAMP. The figure is adapted from [121] .

peak at 260 nm in a 300 μm thick jet (see chapter 3.2.3) were the measurements took place.

The static absorption was measured in a UV-vis spectrometer (see chapter 3.1.1). The time-resolved measurements were taken in a deep-UV-transient absorption setup (see chapter 3.2.2). The pump pulses at 266 nm were obtained by third harmonic generation of the fundamental frequency of the laser. Pump pulses at 285 nm were created by narrow-band second harmonic generation of a fraction of the NOPA output. All measurements presented in this chapter were performed under both parallel and perpendicular polarization between pump and probe. In this chapter only the calculated magic angle results will be presented. The instrument response function (IRF) was below 300 fs (FWHM) over the whole spectral range for both pump wavelengths. For excitations with 266 nm the pump was focused to 80 μm (FWHM) leading to a fluence of 4 mJ/cm^2 . For excitations with 285 nm the pump was focused to 50 μm (FWHM) resulting in a fluence of 6 mJ/cm^2 .

In order to be less sensitive to beam-pointing fluctuations and to sample a uniformly-pumped region, the pump beam focus was two times larger than the probe focus.

All data have been corrected for GVD using the data from the neat solvent (cf. figure 4.2). The data were taken with both parallel and perpendicular polarization between pump and probe back-to-back for each time delay. 30 000 individual shots were acquired to average one spectrum. After each spectrum the polarization of the pump pulses was switched with a fast motorized half wave plate. When both polarizations were acquired, the delay was moved. To avoid seeing artefacts of long term drifts on the data multiple scans with were averaged. Magic angle data has been calculated from the parallel $\Delta OD \parallel$ and perpendicular spectra $\Delta OD \perp$.

To account for probe fluctuations, reference spectra has been recorded, by splitting the probe spectrum with a fused silica plate before the sample. Each probe spectrum was referenced to its corresponding reference spectrum (see equation 3.3).

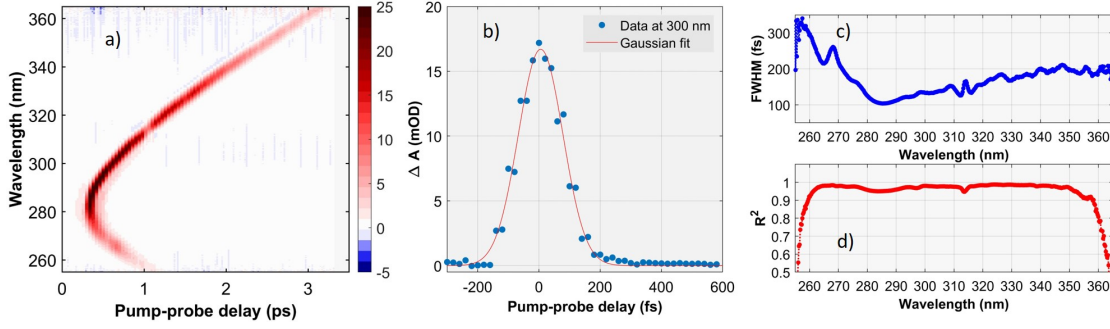


Figure 4.2: Instrument response function (IRF) pumped at 288 nm. a) shows the spectrally resolved transient absorption signal for time delays close to the pump-probe overlap. b) shows an exemplary time trace at a probe wavelength of 300 nm. c) shows spectrally resolved the FWHM of a Gaussian fit to the data in a) and d) shows the respective R^2 value as a measure of the goodness of the fit.

Global analysis has been applied to fit the datasets using the OPTIMUS toolbox [119]. A sequential model has been executed with the minimum number of exponential components necessary. The exponentials are convoluted with the Gaussian of the IRF to account for the finite temporal resolution of the measurement. As the focus of this study is on the long term evolution of the spectral shapes and not on the short term dynamics the spectra had been cut for short time delays below 400 fs.

Molecular dynamics (MD) simulations are used in this chapter to support the interpretation. As they were not performed in the framework of this thesis, only a brief description of the key points of the simulation follows. The simulations were kindly performed by Rahul Sharma. The molecular structures of dA₂ and dA₂₀ were generated from the NAFlex [123] server with the help of the leap program of AMBERTOOLS [124]. The molecules were solvated in explicit TIP3P [125] water molecules exceeding the solute by at least 11 Å. Na⁺ and Cl⁻ ions were added to reach a 150 mM salt concentration. the solvated system was equilibrated and thermalized for 500 ps. The dynamics were performed using 2 fs steps while the coordinates were saved every 1 ps. For each sample a MD simulations for 400 ns were performed using PARMBSC1 [126] force field in AMBER 18 [124]. To avoid the contribution of possible meta-stable configurations only the last 200 ns were used for the data analysis. AMBERTOOLS 18 was used to determine the coupling element $|J|$ following equation 4.1 (compare equation 2.1):

$$J(R, \beta, \alpha_1, \alpha_2) = \frac{d^2}{R^3} [\cos(\beta) - 3\cos(\alpha_1)\cos(\alpha_2)] \quad (4.1)$$

with d being the transition dipole moment of the base, R the distance between two bases, β the angle between the dipole moments of the bases, and α_i the angle between the respective dipolemoment \vec{d}_i and R . The values for d (2.56 D) were taken from Svozil et al. [127]. In figure 4.5 the coupling elements from the MD simulation are shown. For the histogram equal

portions of each dataset were averaged to be able to compare the dimer (dA_2), the end pairs of the strand (dA_{20} ends) and the mean of the strand (dA_{20} mean).

4.3 Results

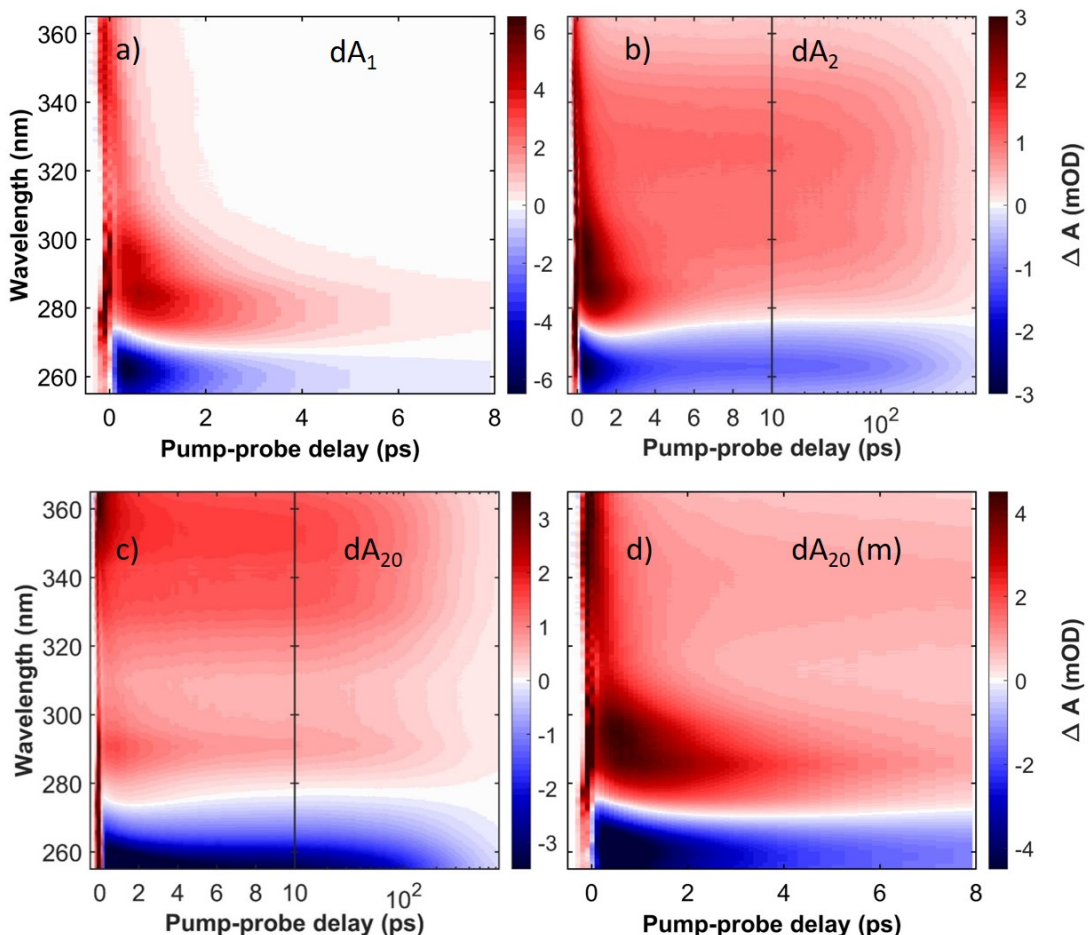


Figure 4.3: Spectrally-resolved transient absorption signal of adenine homopolymers: Monomer dA_1 a), dimer dA_2 b), 20-mer dA_{20} c) and 20-mer in a methanol solution $dA_{20}(m)$ d). All samples except of $dA_{20}(m)$ has been measured in a physiological phosphate buffer solution (see text for details) d). The first 10 ps are displayed on a linear scale. Larger time delays are shown on a logarithmic scale. The samples were excited at 266 nm with an IRF of < 300 fs (FWHM). The dynamics on the ps timescale in the multichromophoric systems are associated with a charge-transfer between neighbouring bases in the molecule. The differences of the spectral shape in the ESA region can be associated to different charge transfer characters in the respective molecules.

Figure 4.3 shows the time-wavelength-resolved transient absorption (TA) spectra of the dA_1 a), dA_2 b), dA_{20} c) and $dA_{20}(m)$ d). In all samples one observes a negative TA signal below 275 nm, which is associated with the ground state bleach (GSB) as well as a positive TA signature above

280 nm associated mostly with the excited state absorption (ESA). The position of the GSB band, as well as the ESA band peak and shape and the dynamics differ amongst the four samples. The monomer dA_1 shows a narrow ESA band with its maximum around 290 nm which decays on the ps timescale. The oligomer samples display a significantly broader ESA band which decays two orders of magnitude slower. This ESA band is therefore associated with long-lived exciton states which are exclusive for oligomers. Please note, that the nomenclature of excited states in multimers might differ in the literature. The definition of an exciton in this work summarizes all excited states, whose origin is the coupling of two or more chromophores. It therefore, includes neutral excitons as well as excitons with a degree of charge transfer (see section 2.2.3). Among the oligomers one can observe different ESA band widths, different GSB positions and also different kinetics. First the early transients will be presented together with the static absorption spectra, which give insights into the excited state formation. A global analysis of the data together with a molecular dynamics simulation is presented in the following. This section is concluded with the analysis of pump probe data of an oligomer after excitation in the low energy tail of the absorption spectrum.

4.3.1 Early transients and static spectra

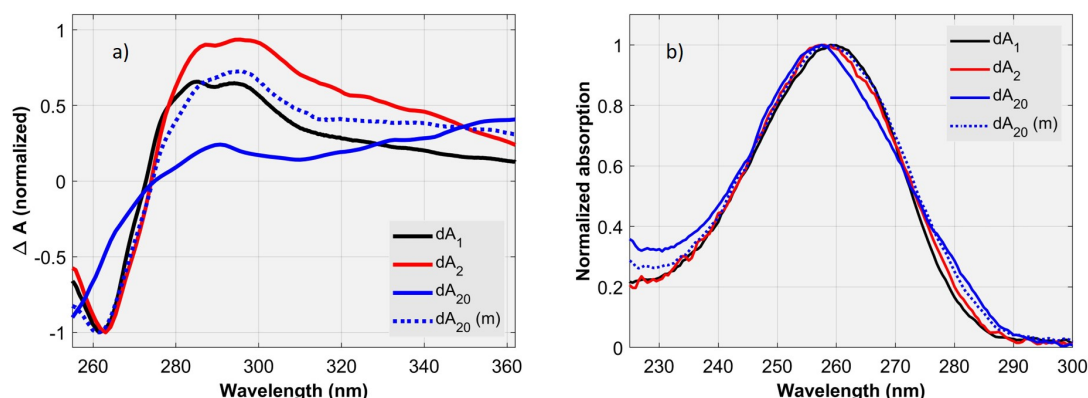


Figure 4.4: a) Spectrally resolved transient absorption spectra of Adenine homopolymers at a pump-probe delay of 500 fs. b) Static absorption spectra of Adenine samples normalized to the absorption maximum of each sample.

As mentioned in chapter 2.2.4, an excitation of the deoxyadenosine monophosphate monomer (dA_1) close to the absorption maximum of the singlet $^1\pi\pi^*$ band at 266 nm in physiological phosphate buffer solution is followed by an ultrafast internal conversion within 200 fs [50] to the vibrationally hot ground state via conical intersections. In figure 4.4 a) the normalized TA spectrum of the monomer after 500 fs pump-probe delay is shown in black. Around 260 nm the bleached ground state transition (GSB) is visible. For wavelengths above 275 nm one observes an excited state absorption (ESA), whose band may overlap at low wavelengths with the GSB signal. The ESA is associated with the vibrationally hot ground state (see above). Furthermore, one can see a ESA tail extending to the near-UV towards 370 nm. This signal

can be associated with the initially excited $L_a \pi\pi^*$ state [128]. In figure 4.3 a) one can see the time-wavelength resolved transient absorption data of dA_1 , where one can see the decay of the vibrationally hot ground state. Figure 4.4 a) shows in red the TA signal of the deoxyadenosine monophosphate dimer (dA_2). Both spectra show almost identical features, especially in the GSB region. Additionally to the signals described for the monomer above, the dimer shows an enhanced ESA signal between 280-340 nm suggesting an extra broad ESA band. The 20-base adenine-homopolymer (dA_{20}) can be seen in figure 4.4 a) in blue. The TA spectrum shows clear differences with the monomer and the dimer. The GSB signal is strongly blue shifted with respect to the monomer and the dimer. The ESA shows much less contribution from a hot monomeric ground state around 290 nm and the ESA is much broader and extends beyond 365 nm. As a comparison a measurement with dA_{20} in a 80:20 methanol-water solution ($dA_{20}(m)$) has been performed, where base stacking is suppressed [8] (figure 4.4 a) blue dotted). The GSB signal mimics that of the monomer, the ESA contains the hot monomeric ground state signal and the broader ESA band, seen in dA_{20} in buffer solution, is missing. The normalized static absorption spectra shown in figure 4.4 b) contain valuable information about the formation of the excited state (see section 4.4 for the discussion). The spectra of the monomer (black) and the dimer (red) are very similar, but slight spectral changes above 270 nm, which can be observed in dA_{20} with stronger expression, are visible. The spectrum of the 20-mer, shown in blue, differs significantly from the mono- and dimer. The shape of the main absorption peak around 260 nm is, due to the hypochromic effect, blue shifted and appears in the normalized plot narrower. Additionally there is an absorption wing below 245 nm and above 275 nm extending to the red (see section 4.3.3 for more details).

Rahul Sharma from the group of John Maddocks (institute of mathematics at EPFL) performed molecular dynamics simulations for this work (see methods section for more details on the simulations). Having the data of the simulation one can compute the dipolar coupling between the bases using equation 2.5. The histogram (figure 4.5) shows the distribution of the dipolar coupling in the dimer (red), the terminal bases of the 20-mer (pink) and in the 20-mer (blue). One can see that the bases in the strand have a stronger dipolar coupling compared to the terminal bases in the strand. The dimer shows slightly lower dipolar coupling than the terminal bases in the strand.

4.3.2 Global analysis

To study the dynamics and the signature of the charge-transfer (CT) state the time-wavelength transient absorption spectra are analysed in the following. The experimental data of all four samples are shown in figure 4.3. As already mentioned above, the monomer dA_1 (4.3 a)) shows a rapid internal conversion of the initially excited state, resulting in the ESA band above 310 nm decaying in the sub-picosecond range. In the few-picosecond timescale the hot ground state undergoes vibrational cooling, leading to a blue shift of the hot ground state ESA band and a decay of both the ESA and the GSB band. The dimer dA_2 (4.3 b)) shows an additional species decaying on the 100 picosecond timescale in the GSB as well as in the ESA region. This is

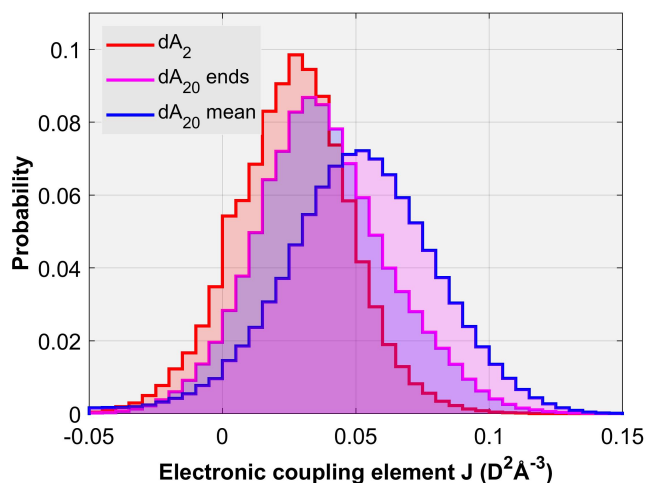


Figure 4.5: Molecular dynamics (MD) simulation of the ground state ensemble of the solvated dA_2 and dA_{20} molecules. The histogram bins configurations, which lead to the same dipolar coupling element $|J|$ and displays the probability for each $|J|$ -value. For each base pair involved for each sample 200 000 values contribute to the histogram. The dimer (dA_2) is depicted in red, the end pairs of the strand (dA_{20} ends) in violet and the mean of the strand in blue (dA_{20} mean). The local environment of the bases in the centre of the strand lead to a higher coupling between the bases. The MD simulations were kindly performed by Rahul Sharma from the laboratory for computation and visualization in mathematics and mechanics at EPFL.

the additional ESA spectral component already observed in figure 4.4 a) which spans from 280 – 340nm and is the non-monomeric ESA spectrum. It is the signature of the CT state in dA_2 (see discussion). dA_{20} shows a significantly broader ESA signal which decays faster than the one of dA_2 . The corresponding band width in the 20-mer in the methanol solution dA_{20} (m) is between those of dA_2 and dA_{20} .

To quantitatively analyse the data and to extract the charge recombination times a global analysis has been performed. For this purpose a sequential model has been applied (see 3.4). The decay associated spectra (DAS) are displayed together with the lifetimes in figure 4.6, the time-wavelength resolved residuals are displayed in figure 4.7 and the results of the fits shown in table 4.1. As the residuals are small compared to the TA signal the error of the fit results is estimated with 10%. For the monomer two exponentials describe the dynamics satisfactorily with lifetimes of $\tau_1^{(1)} = 0.7 \pm 0.1$ ps and $\tau_2^{(1)} = 2 \pm 0.2$ ps. The two exponential components account well for the displayed dynamics, but it has to be noted that a global fit is not an adequate description for vibrational cooling. As the main focus lies on the CT recombination times, which are happening orders of magnitude more slowly, this does not display a big issue. For the dimer and the multimer we get similar results on the few-picosecond range, whereby dA_{20} is slightly slower. Most importantly, both the dimer and the multimer require two additional slow decay components to describe the data: One lifetime τ_3 on the 100 ps timescale and another lifetime τ_4 which exceeds the maximum pump-probe delay of the experiment, which

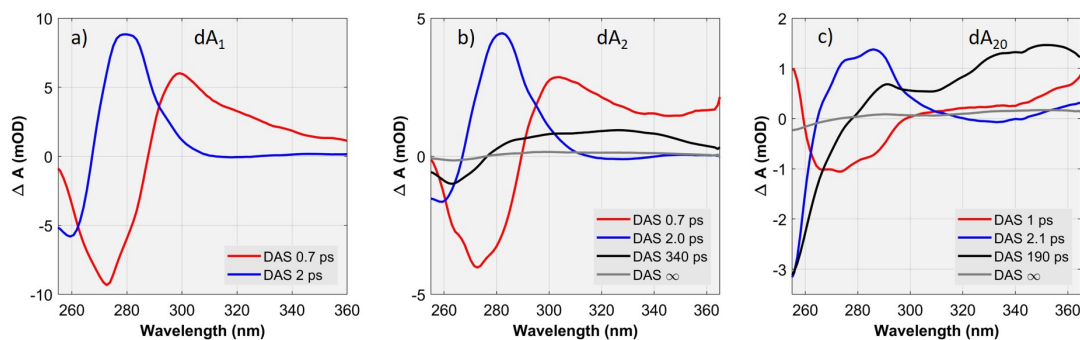


Figure 4.6: DAS of dA₁ a), dA₂ b) and dA₂₀ c) using a sequential model. Compare figure 4.3 for the experimental data. The obtained decay constants are compared in table 4.1.

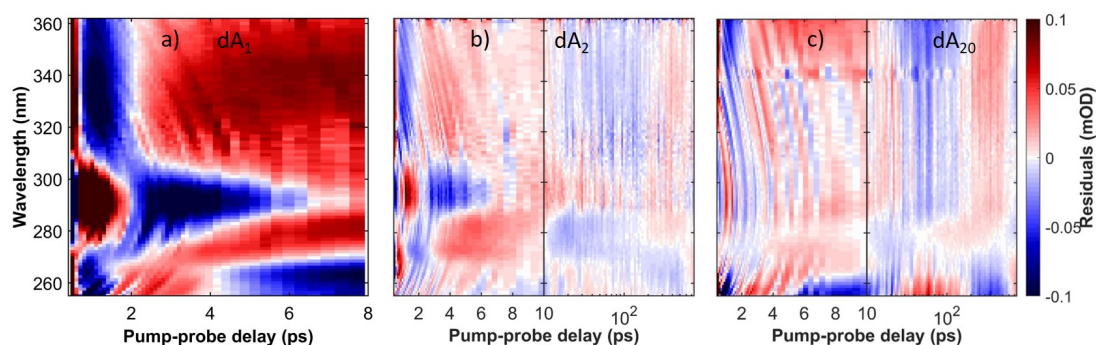


Figure 4.7: Residual from the global analysis displayed in figure 4.6. The corresponding experimental data are shown in figure 4.3.

can therefore not be determined quantitatively. τ_3 is almost 60% faster in dA₂₀ compared to dA₂ (see table 4.1).

4.3.3 20-mer excited in the low energy tail of the absorption spectrum.

In figure 4.4 we can observe an enhanced absorption in the red wing of the spectrum for the 20-mer. This feature is suppressed in the methanol solution (blue dotted). The extended absorption tail below 270 nm is visible in both 20-mer samples and is only weakly affected by the disruption of stacking. In figure 4.8a) we see the spectrally resolved time dependent transient absorption spectrum of dA₂₀ excited at 285 nm (dA_{20 285 nm}), which we will discuss in the following.

Compared to dA₂ and dA₂₀ both pumped at 266 nm (dA_{2 266 nm} / dA_{20 266 nm}), dA_{20 285 nm} shows quantitatively and qualitatively a different behaviour. In both the dA_{2 266 nm} as well as dA_{20 266 nm}, (see figure 4.3 b), c) for the spectrally-resolved transient absorption data) one observes a spectral shift in the first 2-3 picoseconds. By modelling the decay as a sequential decay in a global analysis, this shift appears as two prominent DAS components (see figure 4.6). In dA_{20 285 nm} we do not observe this behaviour (see figure 4.8a) for the spectrally-resolved transient absorp-

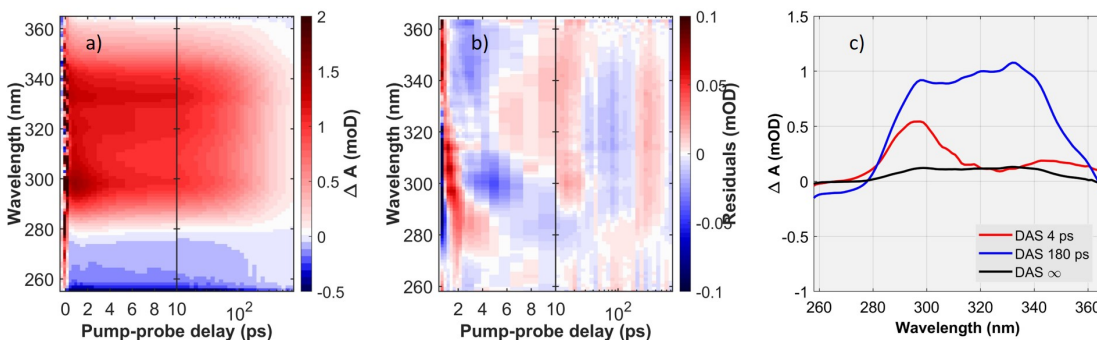


Figure 4.8: a) Spectrally-resolved transient absorption signal dA_{20} after excitation with 285 nm. A global analysis had been performed using a sequential model. The residuals in mOD are shown in b). c) shows the DAS. The life times are depicted and compared in table 4.1.

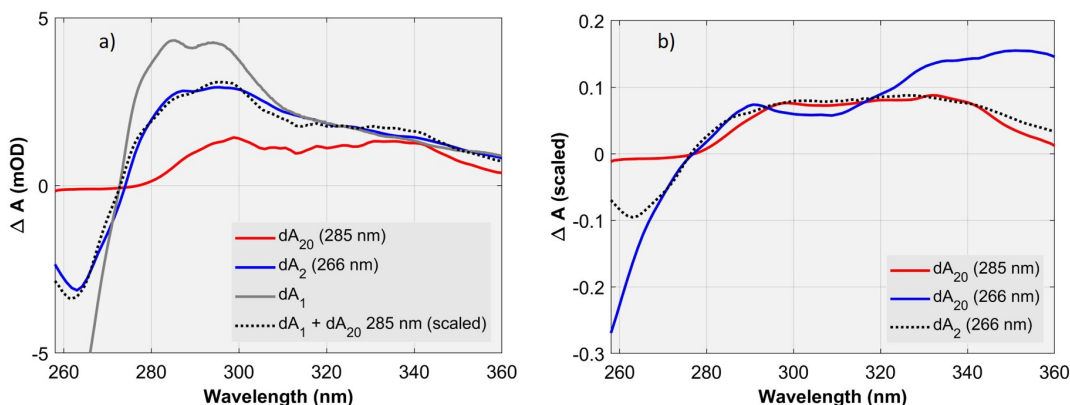


Figure 4.9: a) Transients at 500fs. The scaled sum of dA_1 and dA_{20} 285 nm are compared to dA_2 266 nm. b) Comparison of intermediate time SAS of dA_{20} 285 nm, dA_{20} 266 nm and dA_2 266 nm (scaled for comparison).

tion data and 4.8b) for the DAS analysis). Furthermore, the bleach spectrum of dA_{20} 285 nm differs strongly compared to dA_{20} 266 nm. Figure 4.9a) shows early transients at 500 fs after excitation, which are scaled for better comparability. After excitation at 285 nm the bleach is red-shifted compared to the excitation at 266 nm. Also the bleach signal itself is significantly lower in amplitude. The excited state absorption (ESA) band differs between the two excitations as well (cf. figure 4.9a)). The shape of the ESA band is an indication for the degree of charge transfer. In order to understand the excited state properties reflected in the ESA band, we compare it to the ESA bands associated with the CT state in dA_2 and dA_{20} , which is dynamically formed after 266 nm excitation. By looking at the species associated spectra (SAS) of the intermediate time constant (see figure 4.9b)), one can see that the ESA spectra of dA_{20} 285 nm are very similar to the one of the dimer. The spectrum of the dimer is compared with the scaled sum of monomer and dA_{20} 285 nm at a pump-probe delay of 500 fs in figure 4.8a). The spectrum consists of 0.5 times the amplitude of the monomer added to 0.75 times the amplitude of dA_{20} 285 nm. The factors were determined empirically in order to match the

spectrum as good as possible. Figure 4.8a) shows the striking agreement of the two spectra.

When modelling the dynamics via a sequential decay cascade two lifetimes have been used to empirically describe the fast decay component. This process involves vibrational cooling of a vibrationally hot ground state, which includes a spectral shift of the corresponding ESA band. The lifetimes in the dimer are slightly shorter. As $dA_{20\ 285\text{nm}}$ shows no significant contribution of a monomer-like channel, the ps-timescale is fitted with only one time constant that has a value of 4 ps (see table 4.1. In dA_{20} , This lifetime is within the limits of accuracy of the analysis independent of the excitation wavelength and has a value of 180 ps. As all other samples also $dA_{20\ 285\text{nm}}$ show a signal that does not decay on the timescale of our experiment and has a similar spectral shape compared to the intermediate lifetime.

Table 4.1: Life times of decay channels in the samples

Sample	τ_1 [ps]	τ_2 [ps]	τ_3 [ps]	τ_4 [ps]
$dA_{1\ 266\text{nm}}$	0.7 ± 0.1	2.0 ± 0.2	-	-
$dA_{2\ 266\text{nm}}$	0.7 ± 0.1	2.0 ± 0.2	340 ± 34	∞
$dA_{20\ 266\text{nm}}$	1.0 ± 0.1	2.1 ± 0.2	190 ± 19	∞
$dA_{20\ 285\text{nm}}$	-	4.0 ± 0.4	180 ± 18	∞

4.4 Discussion

4.4.1 Excited state formation

The blue shift of the early GSB spectrum of dA_{20} relative to the monomer and the missing hot monomeric ESA observations are a signature of an excitonic state in the 20-mer (see figure 4.4a)). Therefore, the initially populated Franck-Condon states in dA_{20} is mainly composed from non-monomeric excitonic states. The ESA, whose maximum is expected around 370 nm [91] is therefore associated with the lowest-energy exciton, which is, as suggested by Borrego-Varillas et al., to be delocalized over two bases [91]. The increased static absorption of the 20-mer in buffer solution below 240 nm as well as a blue-shift of the absorption maximum around 260 nm is a signature for a molecular exciton. Hu et al. reported in their theoretical study, that this experimental signatures is in line with adenine strands being H-aggregates [129]. Thus the excitation is a molecular exciton. As the ESA of the neutral exciton, visible in dA_{20} , is missing in the dimer and the GSB corresponds to the one of the monomer in dA_2 a monomeric species gets excited. This observation, gained from time resolved experiments, is surprising, as we can see a coupling of the two chromophores in the CD spectra (see figure 5.2) and also a minor blue shift in the absorption (see figure 4.4). Several reasons could explain this apparent contradiction. There might be a heterogeneity in excitation and a small fraction of the molecules could be excited as neutral excitons. Furthermore, as Chen et al. showed, the appearance of a CD signal might not in all cases coincide with the excitation of an exciton and the observation of an exciton in time-resolved spectra [8]. The transient absorption spectra indicate the population of mainly a monomeric species.

One would expect the formation of a 2-base exciton already in a dimer. The absence of excitonic coupling in dA_2 may therefore be explained by the conformational distribution in the ground state. The dipolar coupling scales inversely with the third power of the distance of the two bases and the angle (see equation 2.5). The dimer is less rigid compared to the 20-mer therefore conformations with a larger distance and angles deviating from a parallel arrangement are more likely to be present. The molecular dynamics simulations (for details of the simulation see section 4.2) shown in figure 4.5, confirm that more frequent nearest neighbour configurations with a large electronic coupling moment are present in the ground state configuration in a 20-mer compared to a dimer. The ground state conformation is therefore responsible for the dominant excitonic interaction in the excited state.

4.4.2 Charge-transfer state relaxation

The broad ESA spectrum which is observed in the 100 ps DAS in the dimer and oligomer samples is the signature of the CT state. Please note, that the nomenclature of the excited states might differ from the literature and refer to section 2.2.3 for the definitions used in this thesis. As in the dimer a monomeric state had been identified as the initial excited state, the CT state is formed dynamically. The ESA band of dA_{20} has been identified by Borrego-Varillas et al. as a fully charge separated adenosine radical ion pair [91]. The observed change in the ESA spectrum of dA_2 , namely a narrower ESA band, is therefore preliminary assigned to a partial charge separation in contrast to dA_{20} . The anisotropy data presented in chapter 5 will help to confirm this assignment. As the ESA bandwidth of dA_{20} (m) is between dA_2 and dA_{20} one can assume a CT character between the one of dA_2 and dA_{20} . Nevertheless, the different polarity of the solvent makes a reliable comparison challenging. As both dA_2 and dA_{20} (m) show no signatures of excitonic coupling but show the signature of the CT state it can be inferred that excitonic coupling is not necessary for the formation of a charge transfer state in DNA. As the associated life time is 60% faster in dA_{20} compared to dA_2 (see table 4.1), the charge recombination is faster in the multimer compared to the dimer. The slower dynamics on the picosecond timescale in the oligomer compared to the dimer can be attributed to the different local solvent environment in dA_{20} , as a base in dA_{20} is due to its neighbouring bases less exposed to the solvent.

David Skowron describes a transient absorption experiment in his PhD thesis [130] with a dimer and a multimer as well. In that work the ground state recovery at 250 nm is probed. He extracts strikingly similar lifetimes from his data in contrast to Sue et al. [29]. He reasons, that in the later study the sample was measured in a cuvette without continuous sample exchange which leads to a heating of the sample to 40°C. In a heated sample, the charge recombination of the dimer speeds up and approaches the one of the multimer with ≈ 180 ps. He argues that in an adenine oligomer the heterogeneous environment could lead to various exciton states with different degree of charge transfer character. As we will see in the next chapter of this thesis in the analysis of the anisotropy spectra the ESA band of the multimer only consists of one excited state species what is in contrast to the above mentioned hypothesis.

In his thesis he explains the different observables between the dimer and the multimer in terms of differences in solvation environment. While we cannot exclude this explanation, our data show that several implications from this reasoning are in contrast to our experimental observations. Stacked bases exclude water molecules in between the two bases of the stack. Therefore, the bases in a strand are differently solvated than in a dimer. This leads to a less polar environment for a base stack in a multimer compared to a dimer. The polarity will affect the nature of the CT state as the thermodynamic driving force for charge separation is changed. Accordingly the energy of the CT state will be lower. As we saw in this chapter with the ESA spectrum, opposing to the explanation above, the CT character of the dimer is lower than in the oligomer. In the next chapter this assignment will be supported by anisotropy spectra which confirm the lower CT character of the dimer.

The difference in solvation is leading, according to Skowron, to a different coupling to vibrational modes of the solvent with the vibrational modes of the amino groups which would lead to a less efficient back-electron transfer. As a result the life time of the excited state is longer. While we cannot exclude this mechanism, we will come to a different conclusion using solvent dependent measurements in the next chapter.

4.4.3 Direct excitation of charge-transfer state

It has been suggested that exciting at the low energy tail of the absorption spectrum leads to states which have a lower excitonic but stronger charge transfer character [46] [131]. Calculations predict the maximum of the charge transfer excitations to be blue shifted compared to the $\pi\pi^*$ transitions. Nonetheless, we can isolate these excitations in the red wing of the spectrum as these states show stronger inhomogeneous broadening. This implies that we are investigating a specific sub-ensemble of conformations, which is the lowest energy configuration. The charge transfer band overlaps the whole $\pi\pi^*$ band, but due to the low oscillator strength, the direct charge transfer (CT) excitation is negligible when exciting at the peak of the $\pi\pi^*$ band. To confirm this assignment as well as investigating the nature and the fate of the excited CT states a transient absorption experiment has been performed, exciting in this spectral region. When exciting with 266 nm the CT state is transiently formed. Here, by exciting the lowest energy CT state through a ground state transition, it is investigated if the directly excited and the transiently excited state are identical. The results are compared to the measurements performed with an excitation at 266 nm in the previous section. For the multimers excited at 266 nm two DAS components are necessary to describe the dynamics on the picosecond timescale. This is due to a monomeric decay pathway, where the electronically excited state is transferred into a vibrationally excited ground state via a conical intersection (see subsection before). When exciting at 285 nm only one DAS component is necessary for the picosecond timescale. A decay pathway, which includes a conical intersection to the hot ground state, seems to be not accessible with that excitation. More importantly no monomeric transitions can be excited at 285 nm. This can be explained by the different nature of the two excitations. When exciting at 266 nm we are predominantly pumping the $\pi\pi^*$ transition,

which has a strong oscillator strength. When pumping at 285 nm, we almost exclusively excite a transition, which leads to a direct charge transfer. The charge transfer excitation has a low oscillator strength as well as a pronounced inhomogeneous broadening compared to the $\pi\pi^*$ transition. These attributes are reflected in the broad and weak bleach band. The first DAS component may correspond to an initial relaxation process of the Frank-Condon state to the lowest energy excited state configuration similar to the initial exciton component observed by Borrego Varrilas et al. [91]. The SAS of $\text{dA}_{266\text{ nm}}$ and $\text{dA}_{285\text{ nm}}$ of the intermediate time constant look alike (see figure 4.9b)). The SAS can be associated in this case with the CT state. We could see in the previous subsection that the bases in the dimer are weakly coupled (bleach band looks monomer-like) and that the degree of charge transfer is lower compared to $\text{dA}_{20\text{ 266 nm}}$. As these experimental observables are very similar, it is concluded that by exciting the oligomer at 285 nm a CT state with a similar degree of charge transfer as in the dimer is induced. The CT state has a strong solvent interaction thus different molecular geometries and different solvation have strongly different electronic energies leading to a big inhomogeneous broadening of the state. By exciting at 285 nm we may select the lowest energy conformation from the distribution of ground state geometries. Therefore it is likely that the 285 nm CT state represents a state that is very well solvated (hence the low energy) and that this is also the case for most dimer states due to the full solvent exposure. In contrast to $\text{dA}_{20\text{ 285 nm}}$ the dimer shows contributions of the hot ground state on the sub-picosecond to picosecond timescale. To demonstrate that the dimer spectrum on the short time scales consists of monomeric excited states and solvent-stabilized CT states equivalent to the lowest energy CT state in dA_{20} , the dimer spectrum and a scaled sum of the monomer and $\text{dA}_{20\text{ 285 nm}}$ are compared in figure 4.9a) (for details see the results section). The striking agreement of the two spectra in figure 4.8a), suggests that excitation of the dimer at 266 nm results in the direct excitation of solvent-stabilized CT states. This most likely implies that in most dimer systems the nucleobases are separated by a thicker solvent layer compared to most adjacent bases in the 20-mer. This is consistent with the fact that dipolar coupling is significantly less pronounced in the dimer system (see figure 4.5).

The intermediate lifetime corresponds to the charge transfer state and independent of the excitation wavelength has a value of 180 ps. This lifetime is determined by the recombination rate of the charge transfer state. It is independent of the degree of charge transfer but depends on the length of the strand. This is because the dimer shows a similar degree of charge transfer (compared to dA_{20} excited at 285 nm), but has roughly a two times longer lifetime. This strongly indicates that the CT recombination rate is increased through the presence of further bases adjacent to the CT state. It is likely that the underlying process dominates the recombination rate in dA_{20} , since the rate is independent of the CT character or solvent configuration of the CT state. This surprising finding will be investigated further in the next chapter. All samples show a signal that does not decay on the timescale of our experiment. This signal has a very similar spectral shape compared to the intermediate lifetime. This suggests, that a significant fraction of the formed CT states does not recombine on an ultrafast timescale.

Figure 4.10 shows the decay pathway after excitation. By exciting at 266 nm one populates

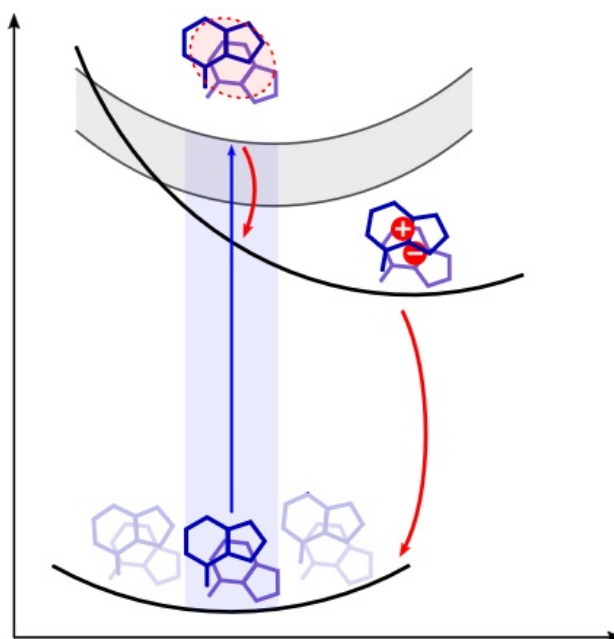


Figure 4.10: Model showing the decay pathways of an excited electronic state. The curves show cuts along the reaction coordinates of the potential energy surfaces (figure courtesy of Malte Oppermann).

bright excitons, which decay either directly to the ground state via a conical intersection or change their character to charge transfer states. By exciting at 285 nm one populates directly charge transfer states. As this charge transfer state is on a different position on the multidimensional potential energy surface one reaches a different local lowest energy excited state compared to the excitation at 266 nm. This charge transfer state is very similar to the charge transfer state in the dimer after 266 nm excitation.

4.5 Conclusion

It had been found that the excitation of a multimer in a physiological buffer solution leads to a exciton state which spans two bases. Surprisingly this exciton state is not excited in a dimer. It seems that the structural rigidity of the multimer is needed that the bases approach each other and the dipolar coupling therefore enables the formation of an exciton. The transiently populated charge transfer state shows a full CT character in the case of the multimer, and shows a lower CT character for the dimer. The charge recombination takes place at an almost 60% faster rate in the case of the multimer compared to to dimer. The nature of the charge recombination process remains unknown and will be addressed in the following chapter.

Furthermore, it had been found that the excitation of an adenine oligomer in the red part of the spectrum relative to the prominent $\pi\pi^*$ transition leads to the direct excitation of a charge transfer state. The first experimental proof, that the CT band has a high degree of

inhomogeneous broadening, had been provided by observing the broad bleach signal of dA_{20 285 nm}, confirming the theoretical calculations. The nature of the CT state resembles the CT state seen for adenine dimers after excitation at 266 nm. The dynamics of charge recombination is a property of the sample regardless of the excitation energy and the following degree of charge transfer. The early time spectra of the dimer can be modelled as a weighted sum of monomer and dA_{20 285 nm} spectra.

5 Structural dynamics and intrastrand proton charge transfer

For photo-induced molecular dynamics, transient conformational changes on the ultrafast timescale play a paramount role. With established experimental techniques it remains difficult to unravel the underlying structural dynamics. Here, the conformational dynamics of adenine mono, di- and 20-mer in water and heavy water buffer solutions are investigated by using broadband transient absorption anisotropy in the deep-UV. First the excited state population dynamics in the heavy water buffer solution are probed and compared to the results in the water buffer solution. It is found that the deactivation of the CT state takes place via a proton transfer. The anisotropy in both solvent environments is examined. It is found that, despite the deuteration of the amino group in the nucleobase, the electronic states and the dipolar coupling are not substantially changed, thus a CT state indistinguishable from the one in H₂O solution is reached. Nonetheless the charge recombination is slowed down by more than a factor of two. The fast rotational diffusion is explained by the flexibility of the 20-mer. The CT character is reached after less than 300fs and no structural rearrangement is involved in its formation. Also no change in character follows on the few ps timescale. Therefore, the ground state conformation determines the CT character which is on average stronger in the 20-mer than in the dimer. In the 20-mer an additional time constant is observed, which can be interpreted as a structural relaxation due to the CT state.

5.1 Introduction

The functionality of biomolecules rely on their local structure. In DNA the structure is determined by the base sequence, hydrogen bonded base pairs and the stacking of neighbouring bases in a strand. Those motives not only influence the structure but also the electronic states of the molecule. Electronically excited states can drive the nuclear degrees of freedom and induce local conformational changes. As functional structural dynamics are common in biological systems [9] they had been suggested to play a key role in the photoprotection mechanism in DNA [35]. To date there is no experimental evidence for excited state induced conformational changes in DNA. As there is a lack of experimental methods to study conformational changes with the required time resolution, so far mainly population dynamics have

been studied.

The structural dynamics in single strands as well as the impact of hydrogen bonding will be discussed in this chapter. In order to study the impact of the solvent the transient absorption and static spectra in heavy water are presented. Furthermore the anisotropy in water and heavy water solutions are shown and analysed.

5.2 Experimental details

The data presented in this chapter are taken with the same setup under alike conditions (see section 4.2) as the data presented in the previous chapter and are therefore analysed together with those data. The pump had a wavelength of 266 nm and was focused to 90 μm (FWHM) leading to a fluence of 2.4 mJ/cm². To investigate proton transfer, experiments in a buffer solution with heavy water (D₂O) have been performed. In order to counteract evaporation and keep the sample concentration in the jet constant the solvent replenishment rate was adapted according the different vapour pressure of D₂O (see section 3.2.3). The monomer, dimer and multimer solutes are the same as described in section 4.2.

5.3 Results

5.3.1 Static spectra and population dynamics of oligomers in a heavy water solution

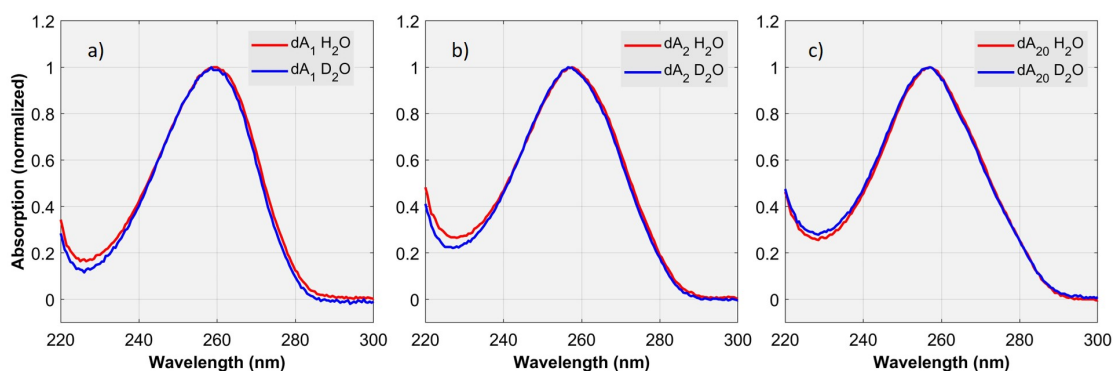


Figure 5.1: Static absorption of a) dA₁ b) dA₂ and c) dA₂₀ in buffer solutions. The buffer is mixed with water/ heavy water shown in red/blue. The change in solvent has barely any influence on the absorption spectrum.

Static spectra First the static absorption spectra are presented. In figure 5.1, the static absorption spectra of the monomer a), the dimer b) and the 20-mer c) are shown in a water/heavy water phosphate buffer solution in red/blue. All spectra are normalized to their absorption maximum close to 260 nm. The purpose of this figure is to highlight the possible impact on the spectra of the two solvent environments. To see the impact of the covalently bonded bases and

therefore the difference between monomer, dimer and 20-mer one can refer to figure 4.4b). As this was already described in the previous chapter it will not be discussed here anymore.

All three spectra show qualitatively the same behaviour in both solvents. The monomer and the dimer in heavy water solution show slightly stronger absorption in the low energy tail of the main absorption peak from 265 nm on. They also show stronger absorption in the region below 240 nm. It has to be noted that a background subtraction with the spectrum of the pure solvent had been performed. Due to thermal drifts of the static spectrometer such a background subtraction only has a limited precision. The described differences in absolute absorption in the monomer and the dimer are above the uncertainties one would expect of such a background subtraction and are therefore significant. In the 20-mer the differences are limited to a higher absorption of the sample solvated in a H_2O buffer solution in the region below 240 nm. The main absorption peak is identical within the measurement accuracy of the static absorption spectrometer.

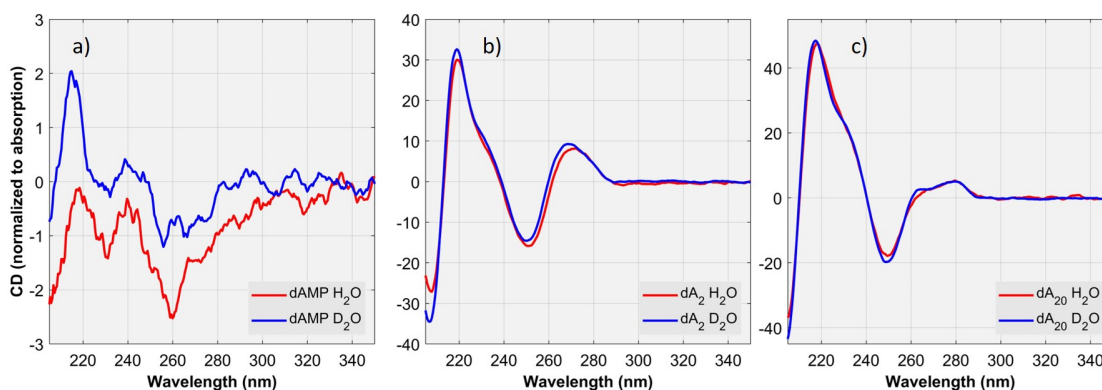


Figure 5.2: Normalized static circular dichroism (CD) spectrum of a) dA_1 b) dA_2 and c) dA_{20} in buffer solutions. Each spectrum is normalized to the absorption of the sample recorded at 260 nm. The buffer is mixed with water/ heavy water shown in red/blue. The solvent has barely any influence on the CD spectrum.

In figure 5.2 the static CD spectra of the monomer a), the dimer b) and the 20-mer in water/heavy water buffer solution are presented in red/blue. The CD spectrometer records the circular dichroism as well as a static absorption spectrum. Each CD spectrum is scaled according to the absorption at its absorption maximum around 260 nm. As there are no dipolar coupled bases in the monomer the CD signal is purely from the individual bases itself and therefore much smaller than the signals of the dimer and the multimer. Both dimer spectra show positive CD peaks around 265 nm and 215 nm and negative CD peaks around 245 nm and 204 nm and are therefore qualitatively very similar but there are small differences. The high energy peaks around 204 nm and 215 nm and the peak at 265 nm are slightly lower in amplitude in the H_2O solution than in the D_2O solution, whereas the peak at 245 nm is higher in amplitude in the H_2O solution. Furthermore, all extrema are blue shifted by approximately one nanometre in the D_2O solution. The CD spectra of the 20-mer show a similar structure as

the ones of the dimer. There are two negative peaks around 200 nm and 245 nm. The positive peak with a maximum around 214 nm shows a shoulder around 230 nm, which is also present in the dimer. The second positive also shows a substructure. There is one maximum at 275 nm and a second pronounced side peak at 259 nm. This side peak is only visible in the spectrum in D₂O solution but not in H₂O solution. The high energy peaks (200 nm, 214 nm, 245 nm) are, like in the dimer, blue shifted by one nanometre in D₂O solution with respect to the H₂O solution. Furthermore, those high energy peaks are slightly lower in amplitude in H₂O solution.

Population dynamics Figure 5.3 shows the spectrally-resolved transient absorption signal of the monomer dA₁ a), the dimer dA₂ b) and the 20-mer dA₂₀ c) in D₂O buffer solution. The first 10 ps are presented on a linear scale and the later time delays are displayed on a logarithmic scale. By comparing figure 5.3 with the equivalent measurement in H₂O shown in figure 4.3 one can see the striking similarities in both solvent systems. In both solvents the multimer samples are displaying dynamics on two different time scales and the dynamics of the monomer are limited to the few picosecond range. Also the shape of the corresponding time resolved TA spectra look alike.

A first impression can be gained from the early transient spectra at 500 fs, which are free from any contributions of the coherent artefact (see figure 5.4). Those transients are normalized to their GSB minimum at this time delay in order to exclude the effect of slightly different pump powers. It can be seen, that transients in all samples qualitatively are not affected by the solvent. The spectrum of the dimer and the 20-mer show a higher relative ESA signal in H₂O than in D₂O. The higher ESA signal is mainly present in the region from 280 – 300 nm. For higher wavelengths the ESA signals in both solvent systems approach each other. On the contrary, the ESA signal of the monomer is higher in H₂O solution than in D₂O for all wavelengths. This is probably an artefact of the normalization, which is challenging for this measurement as the GSB region is not fully accessible. Nonetheless one can conclude that the signal shape in both solvent systems is similar apart from the 280 – 300 nm region.

Global analysis To analyse the spectro-temporal dynamics of the three samples in D₂O a global analysis analogous to the one presented in chapter 4.3.2 was performed. A sequential model was applied to the data presented in figure 5.3 (see chapter 3.4 for details). The decay associated spectra together with the life time of each component are displayed in figure 5.5. Analogous to the data collected in an H₂O solution, two exponential functions with their corresponding decay associated spectra are sufficient to account for the dynamics present in the monomer. An additional component which is not decaying on the timescale of the experiment is added to attribute long lasting signals. In all three samples this life time has only a minor contribution. For the dimer and the multimer sample four exponentially decaying functions were necessary to fit the data, one of which is not decaying on the timescale of the experiment. The resulting decay constants are presented in the inset of each figure and summarized in table 5.1. By comparing the life times in both solvents, one can see that they

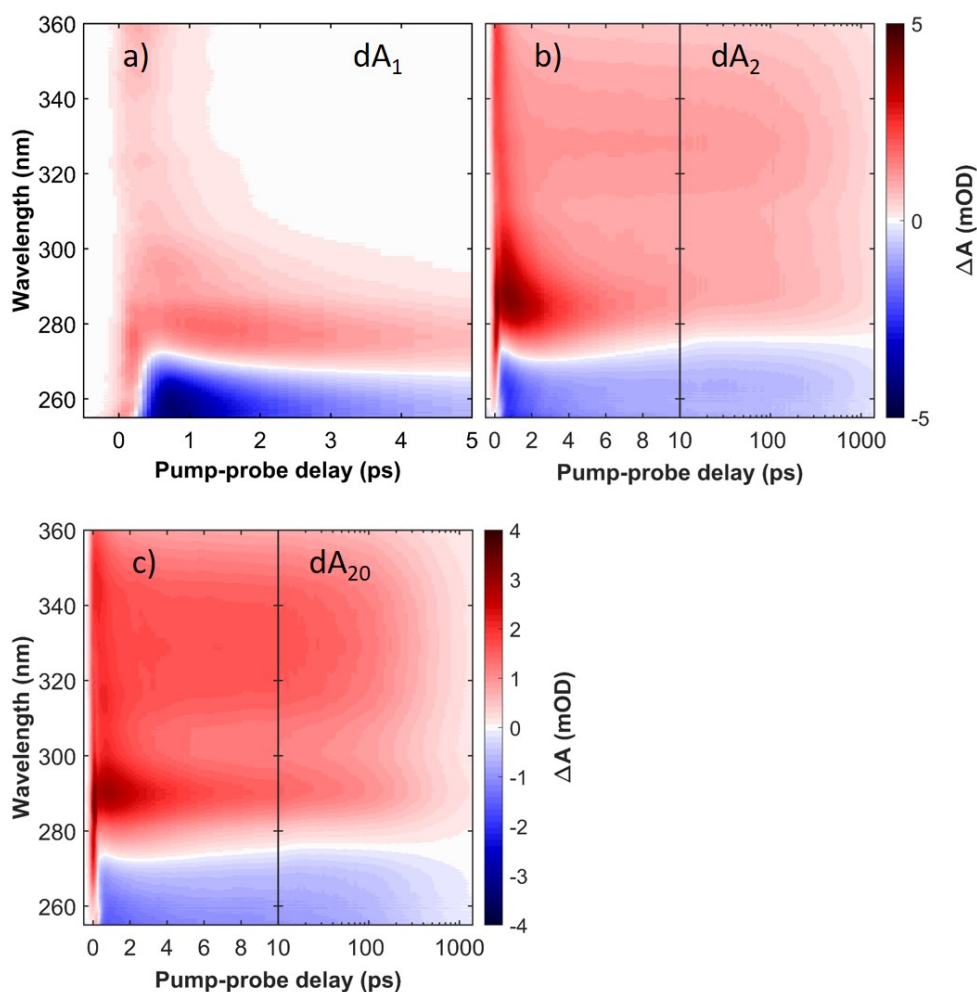


Figure 5.3: Spectrally-resolved transient absorption signal of adenine homopolymers : Monomer dA_1 a), dimer dA_2 b) and 20-mer dA_{20} c). The first 10 ps are displayed on a linear scale. Larger time delays are shown on a logarithmic scale. The samples were excited at 266 nm with an IRF of < 300 fs (FWHM).

are slower in D_2O solution than in the H_2O solution. The first two life times (τ_1 and τ_2) are slightly slower in the monomer and up to 1.5 times slower in the multimers. Most interestingly also the longer life times are slower in the dimer and the 20-mer. In the dimer τ_3 is more than a factor of two (2.15) slower in D_2O than H_2O . In the 20-mer τ_3 is by a factor of 1.7 slower (kinetic isotope effect (KIE)). The DAS spectra on the other hand are almost not affected by the different solvent environments. For the dimer and the 20-mer the DAS corresponding to τ_3 and τ_4 are almost identical.

In order to show that the fit adequately describes the data, the residuals of the fit are presented in figure 5.6 in mOD. The residuals are orders of magnitude smaller than the measured data shown in figure 5.3. Therefore the quality of the fit is very high.

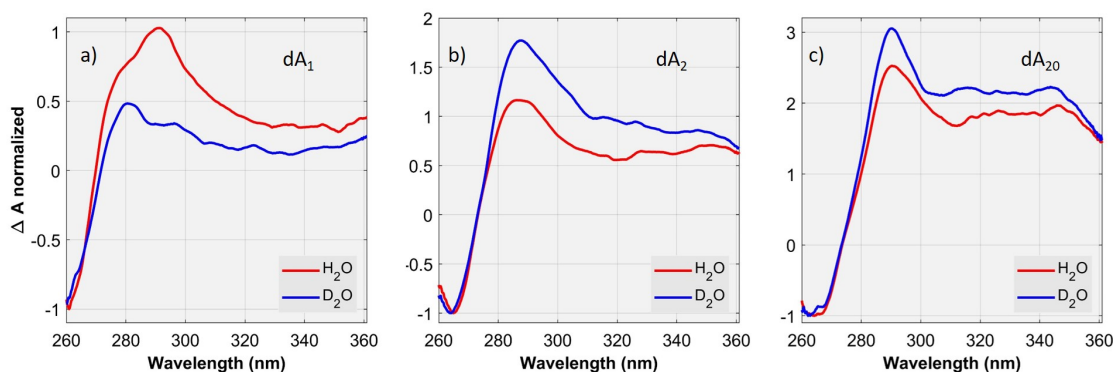


Figure 5.4: Transient absorption spectra at a time delay of 500 fs of a) dA_1 , b) dA_2 and c) dA_{20} in a H_2O/D_2O buffer solution in red/blue.

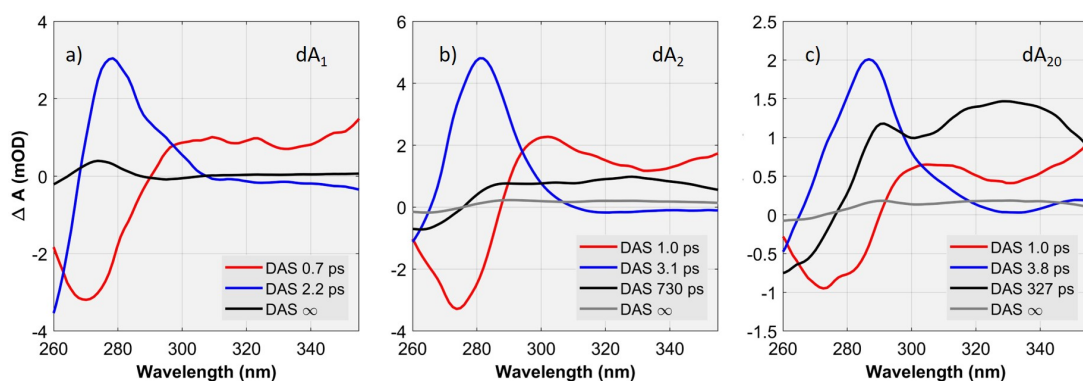


Figure 5.5: Decay associated spectra (DAS) resulting from a sequential global fit of resulting from a spectrally-resolved TA measurement of a) dA_1 b) dA_2 and c) dA_{20} . The corresponding raw data are shown in figure 5.3. The decay constants to each corresponding DAS are indicated in the legend of the figure and are summarized in table 5.1.

Table 5.1: Life times of the different decay channels of the monomer, the dimer and the 20-mer in D_2O -solution.

Sample	τ_1 [ps]	τ_2 [ps]	τ_3 [ps]	τ_4 [ps]
dA_1	0.7 ± 0.1	2.2 ± 0.2	-	∞
dA_2	1 ± 0.1	3.1 ± 0.3	730 ± 73	∞
dA_{20}	1.0 ± 0.1	3.8 ± 0.4	327 ± 33	∞

5.3.2 Anisotropy

Figures 5.7/5.8 show the spectro-temporally resolved anisotropy signal of the monomer a), the dimer b) and the multimer c) in a H_2O/D_2O solution. It has to be noted that the measurements in H_2O were performed in two independent experimental runs. The measurement of dA_{20} in H_2O solution in the experimental run where both solvent configurations were measured did not had sufficient data quality to perform the analysis shown below. All measurements except for dA_{20} in H_2O solution were performed back to back. All measurements of the two

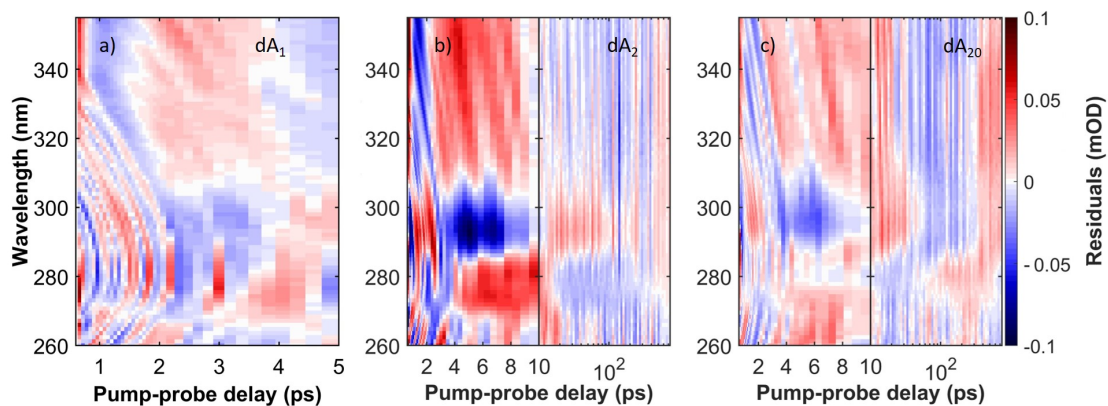


Figure 5.6: Residuals of the global fit shown in figure 5.5 of a) dA_1 b) dA_2 and c) dA_{20} in mOD.

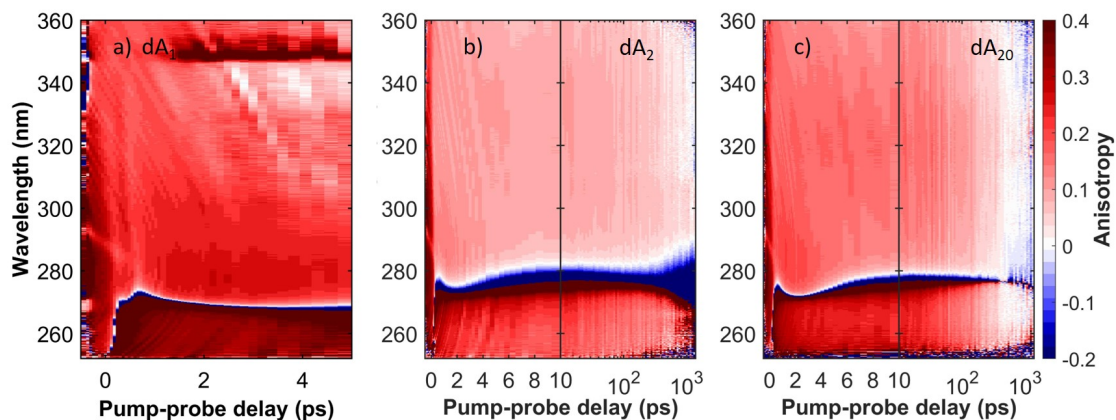


Figure 5.7: Spectrally-resolved transient anisotropy absorption signal of a) dA_1 b) dA_2 and c) dA_{20} in a water buffer solution.

independent experimental runs were consistent. As explained in section 3.2.4 the anisotropy of a single electronic transition can reach values between 0.4 and -0.2. For transitions where excited and the probed transitions are parallel one gets a value of 0.4 and for a perpendicular orientation the value of -0.2. One can see that for early time delays the anisotropy value in the GSB region is close to 0.4. In the ESA the initial anisotropy value is smaller. As the anisotropy is calculated as the difference of parallel and perpendicular pump-probe measurements (compare equation 3.5) the data quality of the original pump-probe data is of great importance. When the pump-probe signal decays to zero, the anisotropy signal diverges. This can for example be seen in figure 5.8a) for long wavelengths and time delays longer than 4 ps. The pump-probe signal is zero in the region where the ESA and the GSB bands overlap. The anisotropy signal thereby diverges to a negative value coming from a positive pump-probe signal and diverges to a positive value coming from a negative one. The anisotropy signal is mostly uniform over each of the whole ESA and the whole GSB band. Only for short time delays, where vibrational cooling plays a role, does the anisotropy signal have a higher value in wavelength regions, where vibrational cooling is visible.

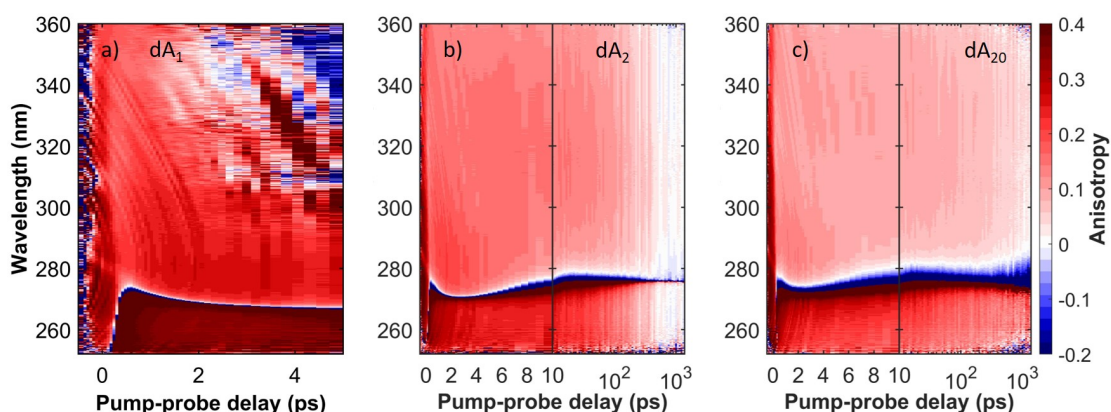


Figure 5.8: Spectrally-resolved transient anisotropy absorption signal of a) dA_1 b) dA_2 and c) dA_{20} in a heavy water buffer solution.

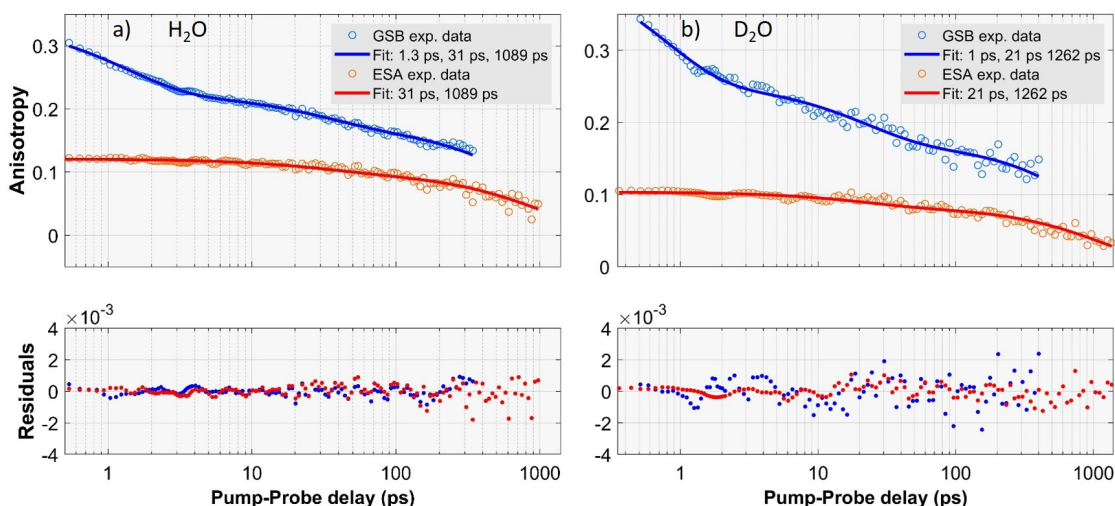


Figure 5.9: Fit of the anisotropy signal of the 20-mer in a water/ heavy water buffer solution a)/b). The averaged GSB/ESA signal and the corresponding fit are depicted in blue/red. The wavelength range for averaging the bands had been chosen in order to avoid regions high noise, singularities or effects of vibrational cooling (see main text for details). The lower part of the figure shows the residuals of the fit.

Analysis To be able to compare the different data sets the data were quantitatively analysed. For this purpose the data shown in figure 5.7/5.8 were fitted. As described in the previous paragraph, the GSB and ESA bands individually have a uniform anisotropy value. Therefore, the anisotropy value of each band was averaged in order to be able to fit the data. The upper and lower limits for the averaging were chosen in such a way, that as many data points as possible are taken into account, but areas which disturb the signal are avoided. Therefore, wavelengths, where vibrational cooling is present (< 310 nm), as well as the areas of very low pump probe signal have been excluded from the anisotropy signal used for the analysis. For

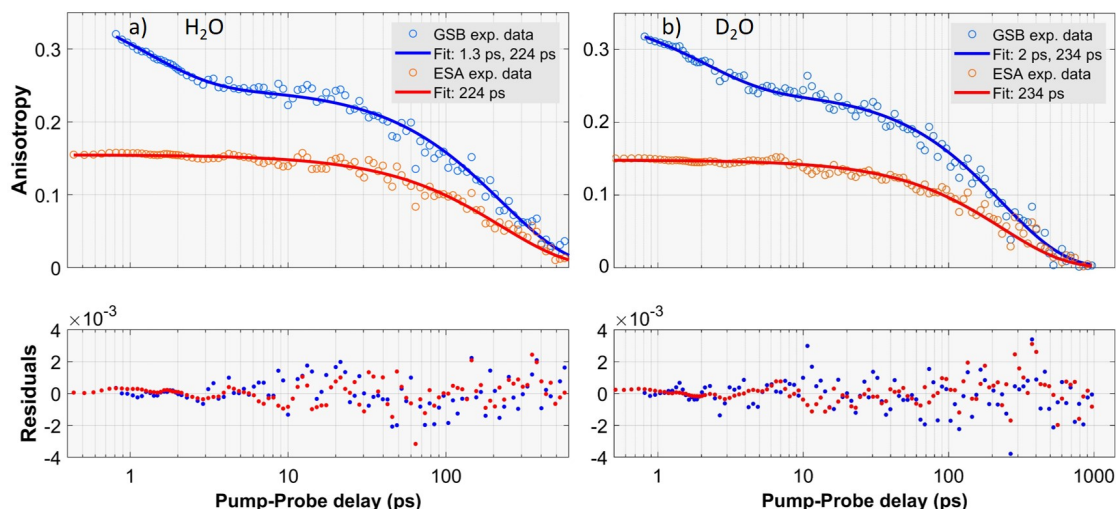


Figure 5.10: Fit of the anisotropy signal of the dimer in a water/ heavy water buffer solution a)/b). The averaged GSB/ESA signal and the corresponding fit are depicted in blue/red. The wavelength range for averaging the bands had been chosen in order to avoid regions high noise, singularities or effects of vibrational cooling (see main text for details). The lower part of the figure shows the residuals of the fit.

late time delays, the pump-probe signal approaches very low signal levels and therefore the noise of the anisotropy signal increases strongly. The data were therefore cut for long time delays that the high noise did not distort the fit. The magic angle signal in the dimer decays to zero more slowly. Therefore more time points could be taken into account and the longest time constant therefore has a lower error. To be able to judge the reliability of the values gained by the fits, the range of included values was systematically varied and the effect was evaluated. The best fits of the dimer and the 20-mer are presented in figures 5.9 and 5.10 in H₂O- in a) and in D₂O-solution in b). The lower part of the figure displays the residuals of the fits. The ESA and GSB time constants were fitted globally, so that both regions have common decay constants ρ but individual prefactors. The data were fit with a sum of exponentials. This is assuming that all processes leading to the decay of the anisotropy take place in parallel. It should also be noted that this assumes that for each process the anisotropy is decaying to zero. For a state with strong charge transfer one expects the transition dipole being perpendicular to the plane of the bases, leading to a negative anisotropy value for example. Nonetheless the assumption that the anisotropy decays to zero with all processes leads to a good description of the data. The lowest number of exponentials necessary to describe the data was used for the best fits. Fits with different number of time constants were tried out in order to find the best fit. In case of the 20-mer three time constants in the GSB region and two time constants in the ESA region were necessary independent of the solvent. For the dimers two time constants in the ESA- and one time constant in the GSB region were enough. The time constants are shown in table 5.2. The long life times are in both, the dimer $\rho_2^{(2)}$ and the multimer $\rho_3^{(20)}$ longer in D₂O- than in H₂O-solution. Furthermore, the long life time is by approximately a factor

of five faster in the dimers than in the 20-mers. The intermediate time constant, that only appears in the multimer, is on the other hand faster in H₂O than in D₂O. Because of the small contribution to the overall anisotropy signal, the relative error of this component is higher than for the other components. The value of the fast component is very sensitive on how the short time points are cut. In order to exclude the influence of the IRF early points have to be excluded from the fit. As only very few time points are available to determine that time constant only few outliers can change the time constant strongly.

Table 5.2: Anisotropy life times of the dimer and the 20-mer in H₂O and D₂O.

Sample	ρ_1 [ps]	ρ_2 [ps]	ρ_3 [ps]
dA ₂ H ₂ O	1.3 ± 0.2	224 ± 10	-
dA ₂ D ₂ O	2 ± 0.5	234 ± 10	-
dA ₂₀ H ₂ O	1.3 ± 0.2	31 ± 10	1089 ± 200
dA ₂₀ D ₂ O	1.0 ± 0.2	21 ± 15	1262 ± 200

5.4 Discussion

5.4.1 Electronic states of oligomers in heavy water solution

The solvation of a molecule can change the energetic position of an electronic level and with it also the energy of the transition between two levels. As shown above, the absorption spectrum of the $\pi\pi^*$ transition is slightly modified for the monomer and the dimer (compare figure 5.1). This is due to the exchange of the hydrogen atoms by the deuterium atoms in the amino group of the adenine [132]. From the point of view of the static absorption, the electronic spectrum is only very slightly modified.

In line with this the static circular dichroism spectra (compare 5.2) also show only minor differences. Circular dichroism is sensitive to the dipolar coupling between chromophores. The purpose of this measurement is to check if the dipolar ground state coupling between the chromophores differ in the two solvent conditions. The CD spectra of the dimer and the 20-mer are nearly not dependent on the solvent. The slight blue shift that is seen in the static absorption spectrum of the dimer is also seen in the static CD spectrum and is therefore consistent. The shoulder in the CD spectrum of the 20-mer in D₂O around 260nm, which is missing in H₂O might hint to a small variation in dipolar coupling. As this change is very minor and even the absolute CD values are identical in almost all regions one can conclude that the electronic coupling is not perturbed in D₂O compared to H₂O.

The transients for short pump probe delays after the influence of the IRF (compare 5.4) indicate which electronic states are initially populated. As the ultrafast excited state deactivation of the monomeric $\pi\pi^*$ state is faster than our IRF, also contributions from the vibrational cooling of the hot ground state influence the early transients. From the strong similarity of the spectra one can conclude that the same excited states get populated. This becomes clear when comparing the DAS spectra in H₂O (see figure 4.6) and D₂O (see figure 5.5). The DAS spectra

are very similar but the time constants differ. The first two time constants mainly attribute for the vibrational cooling of the hot ground state molecules. In H_2O the vibrational cooling is very efficiently taking place via high frequency modes [29] and the cooling times are therefore short. In D_2O , due to the different mass, the frequencies of the modes are different and the cooling slower. As the DAS on the 100 ps timescale and long lived DAS have an almost identical shape in H_2O and D_2O we can conclude that the lowest energy charge transfer state is independent of the solvent. That the life time is much longer (compare the results section above) shows that the charge recombination is slowed down in D_2O even if the CT state is identical. This is especially remarkable in the light of the results when exciting the charge transfer state directly (see chapter 4) and reaching a different low energy CT state, where the charge recombination rate was not dependent on the state but on the strand itself. Here, we see that the charge recombination rate depends on the local solvent environment. There are several possible reasons why the decay rate of the CT state is slower in D_2O . The different solvent environment can directly influence the rates, as seen for the vibrational cooling rates. The relative change of the life time is higher for the τ_3 than for the first two. As the hydrogen in the amino group is replaced by a deuterium atom, a motion of the amino group is expected to be slower. Plasser et. al predict that such a motion is necessary for the CT state to return to the ground state [65]. The deuteration could also alter energy gaps, which could be involved in a decay mechanism. Conti et al. predict an excited-state proton transfer to be responsible for the decay of the CT state [133]. A proton is thereby exchanged between the amino groups. The kinetic isotope effect for the long time constant is stronger for the dimer than for the 20-mer. As the 20-mer is closer packed than the dimer the distance between the amino groups is shorter. Also due to better solvation of the dimer more solvent molecules are in the vicinity of the bases as in a strand the nearest neighbours shield the bases from solvent molecules. The proton transfer is proportional to the distance and the polarity [134]. Therefore, the bigger KIE for the dimer is explained by charge recombination by proton transfer.

Even though the simulation done by Conti et al. showed that a proton transfer mechanism in principle exists, the authors disfavoured that channel [133]. As they calculated a barrier of 0.9 eV for intrastrand proton transfer, it would make it improbable. If the barrier on the other hand is overestimated by this theory, this channel is a very good candidate for a charge recombination mechanism on the 100-ps timescale. Another possible explanation for the slower charge recombination in heavy water solution is given by Skowron in his thesis [130]. He regards proton transfer as an improbable mechanism and assigns the kinetic isotope effect of the charge recombination to a change in the coupling of vibrational modes due to deuteration of the amino group, which are responsible for back-electron transfer.

It should be noted that Crespo-Hernandez et. al have investigated an alternating and a non-alternating adenine-thymine double strand in heavy water [98]. Surprisingly they did only observe a KIE for this time constant, for the alternating adenine-thymine double strand which may indicate that proton transfer only occurs in the alternating duplex. Therefore, in the non-alternating duplex the intras-strand proton transfer might be quenched by the base-pairing. In the more recent study of Zhang et al. the same group demonstrated, that proton coupled

electron transfer takes place in a non-alternating adenine-thymine double strand but not in a alternating one [102].

5.4.2 Structural dynamics

Due to rotational diffusion the anisotropy decays to zero. Therefore the longest observable time constant is caused by rotational diffusion. As we can see in figure 5.9 and 5.10 in all samples the anisotropy for both the GSB and the ESA decays to zero. Therefore ρ_2^2 and ρ_3^{20} in both solvents are rotational diffusion time constants. The rotational diffusion is by approximately a factor of five faster in the dimer than in the 20-mer. The rotational diffusion is in its simplest description inversely proportional to the viscosity and to the third power of the radius of the object. The viscosity of water and heavy water at 298.15 K is $\eta_{H_2O} = 0.89$ and $\eta_{D_2O} = 1.09$ [135]. Therefore the rotational diffusion times in heavy water should be approximately 20% slower assuming that all other parameters are the same. The results in table 5.2 follow this trend although especially for the dimer the rotational diffusion is less than 20% slower. Due to a different solvent environment the effective size of the solvated dimer could change slightly so the simple proportionality with the viscosity would not describe the scenario fully. It is remarkable that the rotational diffusion constant is only a factor of 5 bigger in the 20-mer systems compared to the dimer systems. Assuming that the 20-mers are by a factor of 10 larger than the dimers, one would expect a rotational diffusion time constant which is by 1000 bigger in the 20-mers than in the dimers. When one assumes the 20-mer curly unordered object, which could reduce the size to for example three times the size of a dimer. Due to the third power to the size one would still expect the rotational diffusion time to be by a factor of 27 bigger than the one in the dimer. Therefore we can conclude that the 20-mer does not act as a stiff rod but more like a flexible string. Therefore locally the rotational diffusion takes place faster than expected.

The GSB band as well as the ESA band have each one uniform value over the whole band. This is another indication that the ESA band originates from a single excited state species, which is the CT exciton [136].

The anisotropy of the ESA band probes the orientation between the photoexcited ground state configuration, which are selected by the pump pulse and the excited state transition dipole. In case of the monomer (see figure 5.7a) and 5.8a)) this signal originates from the hot ground state molecules. The only decay that can be observed is the rotational diffusion. As the focus of this chapter is not on this aspect this data will not be further discussed. In case of the dimer and the 20-mer the ESA signal is associated with the CT exciton. For the dimer the anisotropy value is 0.15 in both solvents and decays mono-exponentially. The 20-mer has a lower value of 0.12 in H_2O and 0.11 in D_2O with a bi-exponential decay (see section 5.3.2). As mentioned above all data presented here were measured back to back. For dA_{20} in H_2O the data of independent measurement runs are shown here as the data quality in the other measurement runs did not allow for the analysis presented here, especially for longer

pump-probe delays. Nonetheless, the early anisotropy values can be analysed. The initial value of the ESA of dA_{20} in H_2O which was measured back to back with the measurement with dA_{20} in D_2O showed a value of 0.11 as well. The differences of initial anisotropy values is therefore not an effect of the sample but might be explained by small deviations of the configuration of the polarisers between the two measurement sets. As described above, the longest time scale can be attributed to rotational diffusion. Furthermore, two processes can contribute to the change of orientation of the transition dipole moment of the CT exciton and thereby change the anisotropy value: a conformational change of nucleobases in a strand and a change in CT character. In the CT state the charge transfer takes place between two neighbouring bases. The associated transition dipole moment is therefore perpendicular to the plane of the nucleobases and a stronger CT character results in a lower anisotropy value. The ESA anisotropy of the dimer and the 20-mer does not show a change during the first three picoseconds, which implies that neither a conformational change nor a change in CT character is taking place on this time scale. Therefore the CT character has to be fully developed in less than 300 fs which is the temporal resolution of the measurement (compare figure 4.2). This rules out the possibility that the CT state forms within the first 3 ps as discussed before [46],[91]. Therefore it is concluded that the CT state may form via the following two pathways. A small fraction of CT states is formed directly upon excitation (see section 4.4.3). The majority of CT states are formed via a rapid sub-ps inter-base electron transfer before any structural rearrangement is taking place. The CT character is therefore determined by the ground state conformation prior to photoexcitation. The closer packed 20-mer leads to an on average stronger CT character compared to the dimer which results in a lower anisotropy value of the ESA band.

In the GSB region one probes the ensemble average of the bleached $^1\pi\pi^*$ ground state transitions, which are parallel to the molecular plane of the nucleobases. One sees a rapid decay in the first three picoseconds in all three samples. The dimer shows an additional time constant in the GSB in the 100 ps range and the 20-mer shows an intermediate time constant in the 10 ps range and a longer time constant in the 1000 ps range (see section 5.3.2). The longest time constants in each sample are the rotational diffusion time constants (for details see the discussion at the beginning of the section) and are therefore fitted simultaneously in the ESA and the GSB (for details compare section 5.3.2). The intermediate time constant can be observed for the 20-mer samples in the ESA and the GSB region as well and are therefore also fitted globally. The fast first time constant is seen in all three sample systems. It is difficult to assign it to a physical process. In the dimer the initial photo-excitation is localized on one base. Therefore this decay could be assigned to a delocalization of the excited state after CT exciton formation. In the 20-mer ultrafast internal conversion among exciton states had been observed, which could result in an anisotropy decay. This process is finished in less than 200 fs [91] and can therefore not be the reason for the fast decay seen in the 20-mer. As this signal is seen in all three sample systems one cannot distinguish between ultrafast monomeric processes or ultrafast energy transfer processes. The ESA and GSB bands overlap and vibrational cooling affects the dynamics in the overlap region. As there is access for the

whole ESA band, this effect can be avoided for the former. In case of GSB the accessible area is too small to fully avoid vibrational cooling. Most probably the first time constant seen in the anisotropy of the GSB band is an artefact of vibrational cooling. This artefact still affects later time points of the GSB band to a certain extent and is one reason why the error estimation of the intermediate time constant is done very conservatively (see below).

With the rotational diffusion already assigned, the intermediate time constant of the anisotropy seen in the 20-mer $\rho_2^{(20)}$ needs a process where the initially excited transition moves from its position: For this several processes are plausible. A charge hopping along the strand could take place [137]. A migration of the CT state can only happen in the 20-mer as there are no further bases in the dimer to which the CT state can migrate. That charge transport through DNA plays a role has been shown previously [138] [139]. In a stacked strand each base is rotated by 36° pitch angle in respect to the neighbouring bases. To further investigate this assignment one can analyse how a twist would impact the anisotropy of the ESA and the GSB band. As mentioned above, anisotropy of the GSB probes the motion of the bleached ground state transitions which are in plane of the nucleobases. The anisotropy of the ESA on the other hand has a component perpendicular to this plane. A twist will therefore have a stronger contribution to the GSB anisotropy signal than to the ESA one. One can see in figure 5.9 that the intermediate component ρ_2^{20} is more pronounced in the GSB region than in the ESA region. Therefore the dominant conformational change is taking place in the plane parallel to the base, which is could be consistent with a twist due to the migration of the CT state. On the other hand the CT state is energetically a trap state. A migration of such a state is therefore not very likely. A second possible option would be a structural relaxation to a minimal energy conformation. In stacked perylene bisimides (PBI) systems such structural changes have been observed on a similar timescale [140] [141] [2]. The chromophores approach each other and the driving force is the charge separation. In a dimer system one would in a simple model expect the same dynamics to happen. As discussed in the previous chapter the interactions between the bases are because of the different solvation significantly weaker in the dimer. This option is therefore the most likely cause of the intermediate time constant. A third possibility for the intermediate time constant are local fluctuations [142] of a single base as shown by Jean et al. [143]. A base locally unstacks and the lifetime seen in their experiment is associated with the rotational diffusion of this single base. As their lifetime also lies in the range of the lifetime observed here it has to be considered. Such a single base fluctuation one would expect to see in the dimer where one cannot observe it in this dataset. Therefore this explanation can be excluded.

5.5 Conclusion

In this chapter the excited state dynamics of the adenine mono, di- and 20-mers in a heavy water buffer solution were compared to the dynamics in a water buffer solution. The change in solvent leads to a deuteration of the amino group. The electronic states and the dipolar coupling are not substantially changed, which leads to a CT state which is indistinguishable to

the one in H₂O. Due to the different solvent modes, the vibrational cooling is slower. Most interestingly the decay of the CT state is by more than a factor of two slower in D₂O. This is rationalized with intrastrand proton transfer being responsible for the charge recombination.

Furthermore the structural dynamics of the adenine mono, di- and 20-mers in both solvent systems are investigated with the help of transient anisotropy. From the rotational diffusion constants it is shown that the 20-mer acts as a flexible string. As the ESA anisotropy is constant for the whole ESA band it is shown that it consists most likely of one single excited state species for longer pump probe delays - the charge transfer exciton. As the ESA value does not significantly change within the first 3 ps after the IRE, it can be concluded that the CT character is fully developed in less than 300 fs and no conformational change or change in CT character is taking place during its formation. Therefore the ground state conformation determines the CT character, which leads to a stronger CT character in the closely packed 20-mer reflected in its lower initial anisotropy signal. The 20-mer shows an additional intermediate time constant, which is interpreted as a structural relaxation due to the CT state minimum energy conformation.

6 Energy and charge transfer between adenine and 2AP bases in a single strand

2-aminopurine (2AP) is a fluorescent base analogue of adenine. As the quenching of the bright state is sensitive to its local environment the fluorescence yield is sensitive to the local structure of the DNA. 2AP is thus commonly used as a local structural probe which does not disturb the structure of the strand. By changing the position of the amino-group in respect to adenine, the electronic structure changes significantly. As its $\pi\pi^*$ transition is strongly red shifted it acts as a energy trap in DNA strands. Effective energy transfer from other DNA bases to 2AP is shown. In this chapter a 2AP monomer, dimer and two 12-mer strands, with an alternating sequence of 2AP and adenine monomers and with an alternating sequence of 2AP and adenine dimers were measured in order to investigate the sequence dependence of energy and charge transfer processes. A static characterisation of four samples is performed ensuring the coupling of the bases, the energy transfer and quenching processes. Transient absorption anisotropy is used to temporally resolve the energy transfer to the 2AP bases and to observe the transient charge transfer states. By pumping the 2AP transition the signature of the bright 2AP-monomer state as well as 2AP-2AP and 2AP-A charge-transfer states could be identified. The charge-recombination dynamics are the fastest in the 2P-dimer, followed by the alternating dimer, the alternating monomer. Pumping the adenine bases reveals an energy transfer in less than 0.7 ps to the 2AP bases and leads to the same species associated spectra on the 100 ps timescale compared to pumping the adenines and the same dynamics after energy transfer.

6.1 Introduction

2-aminopurine (2AP) is a fluorescent base analogue of adenine. The change of the amino group from the 6 position in adenine to the 2 position in 2AP barely changes the local structure of DNA when included into a strand [144]. In contrast to adenine, 2AP is highly fluorescent. The fluorescence yield of 2AP is sensitive to its local structure: when 2AP stacks with other bases, especially adenine, the fluorescence of 2AP is quenched [145] [81] [146] [147]. Therefore it is used as a local structural probe in biologically relevant DNA samples. Regardless of the minor changes in the structure of 2AP with respect to adenine, its electronic properties strongly

change. As mentioned above, the fluorescent yield is increased by orders of magnitude. It reaches 0.68 for the isolated 2AP [75]. The absorption spectrum shows two separate $\pi\pi^*$ transitions. One of them is lower in energy than all other DNA bases [143]. Therefore 2AP can act as an energy sink. The fluorescence of 2AP stems from a bright electronically excited $\pi\pi^*$ state as the conical interaction to the ground state, present in adenine, is not accessible [59]. Nordlund et al. have shown that energy is effectively transferred from DNA bases to 2AP [145] [81] [146] [147]. The energy transfer with adenine, with a transfer efficiency of up to 57% is especially efficient [146]. Regardless of its different electronic structure, the direction of the transition dipole is barely changed between adenine and 2AP [143]. Base stacking sequences modulate the efficiency of the energy transfer, as it may take place over the distance of up to four nearest neighbour bases, acting as spacers between 2AP and a donor base [146]. As thermally induced stacking dynamics happen on the timescale of the excited state of 2AP, the multiexponential decay of the fluorescence is governed by the stacking dynamics [148] [149]. Kelley et al. and Wan et al. have shown that the quenching dynamics of the electronic excited state depends on the redox potentials of the neighbouring bases [82] [150]. As 2AP is an energy sink, further energy transfer can be excluded and an electron transfer is the origin of the quenching [73] [151] [84]. 2AP can thereby either be oxidized or reduced. With adenine it undergoes oxidative charge transfer. Experiments in D₂O excluded the participation of a proton transfer [150].

Johnson et al. showed that the deep-UV CD is a local probe of 2AP conformations [80]. CD is sensitive to stacking. A 2AP exciton is identified in a 2AP dimer and the local structure is of right handedness. It has to be noted that CD is not unambiguous, as different structures can give the same CD signal. As a local probe CD displays the ensemble average of the local structures present in the sample.

The toolset developed in the previous chapters is ideal to investigate energy and charge transfer processes in 2AP containing adenine strands. In order to study time resolved energy transfer between adenines and 2AP's, the adenine bases are excited directly. The broadband deep-UV continuum allows to monitor the bleach band of 2AP, to confirm energy transfer, as well as the signatures of excited states. A comparison between direct excitation of 2AP and excitation via energy transfer will show if the same final states are populated with both excitations. To this end different adenine-2AP model systems were measured. In one set of measurements the adenines and in another the 2AP bases were selectively excited.

6.2 Experimental details

The sample systems investigated in this chapter are 2AP bases and single strands containing 2AP bases. The monomer 2-aminopurine-ribose-5'-monophosphate (2AP) is the 2AP equivalent of dAMP. A dimer, consisting of two 2AP bases linked via the sugar-phosphate backbone and two different oligomers were investigated. Each of the two oligomers contains 12 bases whereof 6 are adenine bases and 6 are 2AP bases. In one sample adenine and 2AP bases are

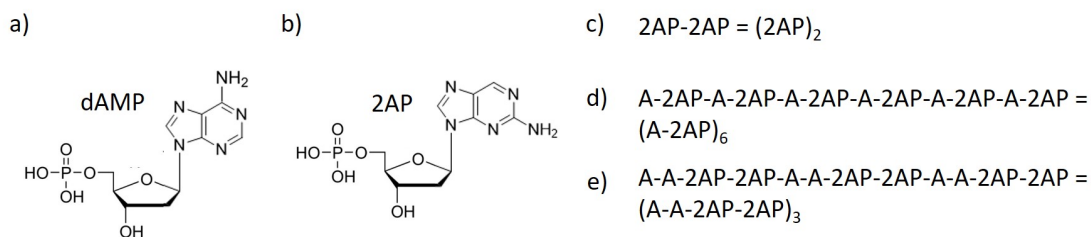


Figure 6.1: Scheme showing the samples measured in this chapter. a) shows the monomeric adenine unit including a sugar and a phosphate (dAMP), which is denoted in the structures in d) and e) as A. b) shows the monomeric 2AP unit with its sugar and a phosphate. c), d) and e) are showing the sequence of bases in the single strands linked via a sugar phosphate backbone. c) is throughout the chapter called 2AP-dimer. d) is called alternating monomer and e) alternating dimer. a) and b) is modified from [121] and [152].

alternating $(A-2AP)_6$ (hereafter referred as alternating monomer), whereas with the second sample adenine dimers and 2AP dimers are alternating $(A-A-2AP-2AP)_3$ (hereafter referred as alternating dimer). The sequence indicated is starting from the 5' and ending at the 3' end. These sequences are chosen with the aim to investigate if the absorption and energy transfer processes take place in a monomeric or in a dimeric unit in the single strand. Furthermore a 2AP dimer was measured $(2AP)_2$. Samples were purchased from Jena Bioscience (2AP), from biomers.net (20-mer (dA₂₀)) and Sangon Biotech ($(2AP)_2$, $(A-A-2AP-2AP)_3$ and $(A-2AP)_6$) and used without further purification. For each measurement a new sample was prepared in a phosphate buffer solution (see section 4.2 for details). As the synthesis of the 2AP-multimers was very challenging only small amounts of sample could be used for the measurements. As the sample volume was limited, unlike in the previous chapters, not a wire-guided liquid-jet could be used, but a flow cell. Each measurement was performed with 1.5 ml of sample in a 0.5 mm flow-cell with drilled windows made out of Spectrosil Quartz (Starna scientific). In order to prevent the flow cell windows from burning, the cell was continuously moved in the focal plane by two motorized stages. The sample was continuously refreshed with a peristaltic pump. Before and after the measurement, a static absorption and static CD spectrum was taken to exclude any damage of the sample. Those measurements are shown in the appendix. The associated spectra for measurements with 266 nm / 326 nm excitation can be seen in figure A.2 / A.3. The samples were prepared to have an absorption of approximately 0.15 OD at the 2AP absorption peak around 310 nm, which lead in the adenine-2AP-strands to an absorption of 0.4 OD at the absorption maximum around 250 nm. To have a stable pump-probe overlap and uniform excitation in the probed area, the pump was more than two times bigger than the probe. For the 266 nm excitation the pump was focussed to 90 μm (FWHM) leading to a fluence of 3 mJ/cm². For excitations with 326 nm the pump was focused to 70 μm (FWHM) leading to a fluence of 7 mJ/cm². As mentioned in section 3.2.2, the pump pulses centred at 266 nm were generated from the third harmonic of the fundamental laser frequency. The pump pulses centred at 326 nm were generated by selectively frequency doubling a narrow window of the visible super continuum resulting a pump spectrum narrower than 2 nm FWHM.

6.3 Results

First the static characterization of the samples in absorption, circular dichroism (CD) and static fluorescence is presented. Transient absorption data are shown pumping the adenine bases and pumping the 2-AP bases, respectively. The section is concluded with the associated transient anisotropy spectra.

6.3.1 Static characterisation of the samples

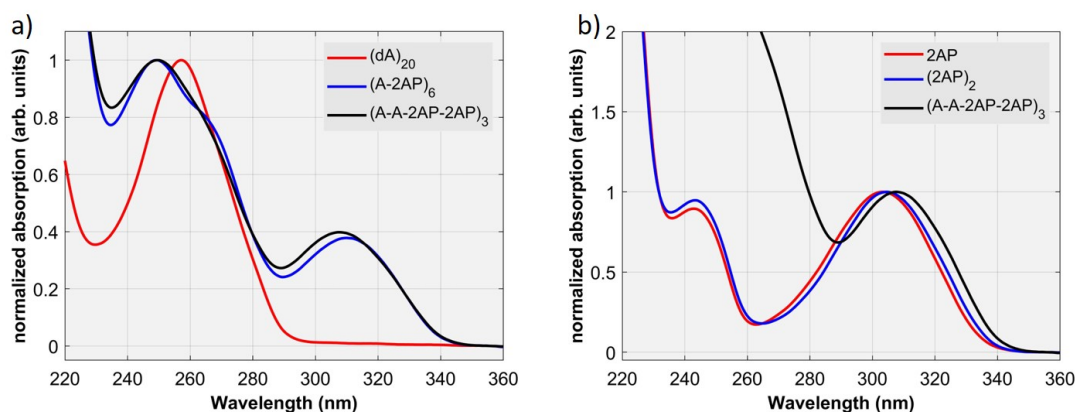


Figure 6.2: Normalized static absorption spectra in phosphate buffer solution: a) dA_{20} , $(A-2AP)_6$ and $(A-A-2AP-2AP)_3$ normalized to the maximum of the $\pi\pi^*$ absorption band of adenine (around 260 nm). b) $(2AP)$, $(2AP)_2$, $(A-A-2AP-2AP)_3$ normalized to the maximum of the absorption peak of 2AP (around 305 nm).

To learn about the basic photophysical properties of the samples a static characterisation is performed. First the static absorption of the samples is presented. Figure 6.2 shows the normalized static absorption of all the samples discussed in this chapter. In figure 6.2 a) the samples containing adenine bases are shown (dA_{20} , $(A-2AP)_6$ and $(A-A-2AP-2AP)_3$). The absorption is normalized to the maximum of the adenine $S_0 \rightarrow S_1$ transition centred around 260 nm. In figure 6.2 b) the two samples containing only 2AP bases (the monomer $(2AP)$ and the dimer $(2AP)_2$) are shown for comparison together with the multimer $(A-A-2AP-2AP)_3$. Here the absorption is normalization to the absorption peak of the 2AP bases around 305 nm.

In figure 6.2 a) one can see the characteristic absorption of dA_{20} presented in the previous chapters. The multimers containing 50% adenine bases ($(A-2AP)_6$ and $(A-A-2AP-2AP)_3$) also show the peak around 260 nm. They show two additional absorption peaks characteristic for 2AP (compare the following paragraph). The adenine absorption peak around 260 nm overlaps with a 2AP absorption centred at 245 nm. Most importantly those multimers have an absorption peak centred around 305 nm.

Those two peaks can also be seen in the monomer $(2AP)$ and the dimer $(2AP)_2$ presented in figure 6.2 b). The monomer and the dimer sample almost resemble each other, except of

a small shift of the peak around 305 nm. The dimer is slightly red-shifted in respect to the monomer. In the multimers ((A – A – 2AP – 2AP)₃ and (A – 2AP)₆ (not shown in this plot)) this red-shift is even more pronounced. The spectrum of the multimers containing adenine as well as 2AP bases is apart of the slightly shifted bands mostly a superposition of the absorption bands of both samples.

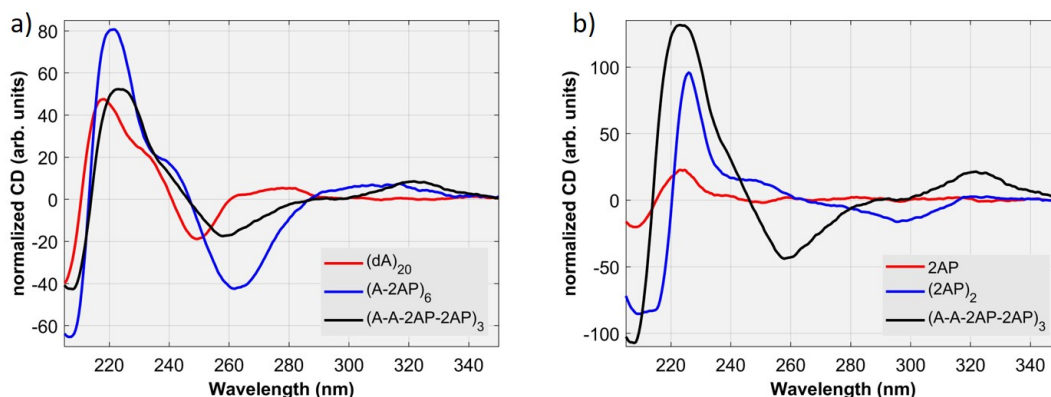


Figure 6.3: Normalized static CD spectra in phosphate buffer solution: a) $(dA)_{20}$, $(A - 2AP)_6$ and $(A - A - 2AP - 2AP)_3$ scaled to the absorption maximum of the $\pi\pi^*$ absorption band of adenine (around 260 nm). b) $(2AP)$, $(2AP)_2$, $(A - A - 2AP - 2AP)_3$ scaled to the absorption maximum of the absorption peak of 2AP (around 305 nm).

Circular dichroism (CD) is sensitive to the dipolar coupling of chromophores. Figure 6.3 shows the CD spectra of the samples described above. In a) the samples containing adenine and in b) the samples only containing 2AP and for comparison the alternating dimer $((A - A - 2AP - 2AP)_3)$ are shown. The spectra are scaled according to the absorption maximum around a) 260 nm and b) 305 nm. In a) all samples show CD couplets around 260 nm and 300 nm. As the hetero-multimers have an additional absorption peak around 240 nm, the CD peak resulting from this transition may overlap with the one stemming from the adenine absorption. In both samples the negative CD peak, observed in dA_{20} below 250 nm is red-shifted and appears at around 260 nm. The positive CD peak seen in dA_{20} from $\approx 260 - 280$ nm may overlap with the negative CD peak stemming from the 2AP absorption peak at 305 nm. There the alternating dimer $((A - A - 2AP - 2AP)_3)$ therefore has a net CD signal around 280 – 290 nm of zero. From 300 – 340 nm it shows a positive CD peak. The alternating monomer $((A - 2AP)_6)$ displays a broader positive CD band from 280 – 330 nm. It also shows an approximately two times stronger negative CD band around 260 nm.

In figure 6.3 b) one can see the CD signal of the 2AP monomer. It shows only a minor CD couplet below 240 nm. The dimer $(2AP)_2$ shows a much stronger CD couplet below 240 nm but more importantly shows a broad negative CD peak from 260 – 320 nm. In comparison with the two other 2AP multimers the CD band of this band has a different shape and sign.

Static fluorescence shows the time averaged emission of a sample after excitation at a defined wavelength. It therefore contains valuable information the dipole allowed transitions of the

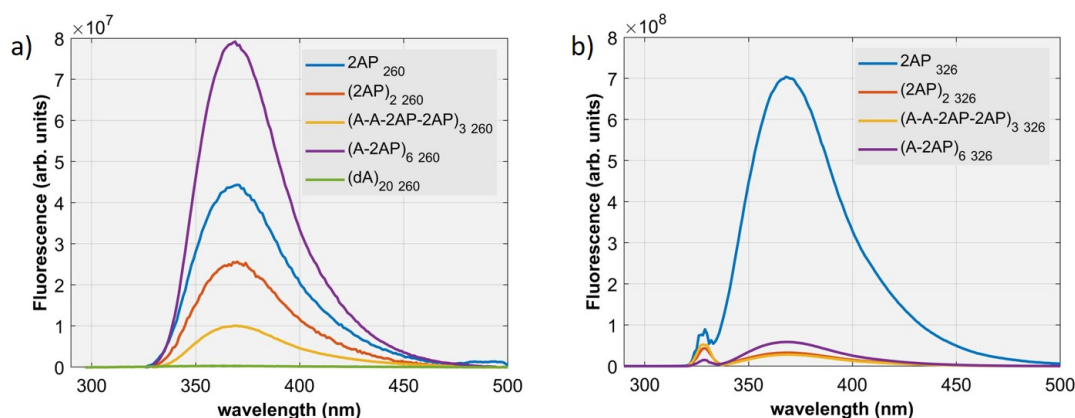


Figure 6.4: Fluorescence spectrum of (2AP), (2AP)₂, (A – A – 2AP – 2AP)₃, (A – 2AP)₆ and dA₂₀ after a) exciting at the absorption maximum of adenine (260nm) and b) in the absorption peak of 2AP (326nm) measured in a phosphate buffer solution. Each spectrum is scaled by dividing by the absorbance of the sample at the excitation wavelength. As the intensity of the excitation light source is not uniform over the whole spectrum the change in peak heights between the two pump wavelengths may result from intensity differences.

excited states. Figure 6.4 shows the static fluorescence of (2AP), (2AP)₂, (A – A – 2AP – 2AP)₃, (A – 2AP)₆ and dA₂₀ after a) exciting at the absorption maximum of adenine (260nm) and b) in the absorption peak of 2AP (326nm). Each spectrum is scaled by dividing by the absorbance of the sample at the excitation wavelength. It has to be noted, that the samples had to be strongly diluted in order to not saturate the fluorescence spectrometer. It was therefore challenging to get a high quality absorption spectrum of the diluted samples and the scaling factor of the fluorescence spectra has therefore a uncertainty of less than 10%. The comparisons made hereafter are therefore significant. After exciting with 260nm one can observe fluorescence from all samples including the two samples only containing 2AP ((2AP) and (2AP)₂). dA₂₀, which shows a very strong absorption peak at 260nm displays only very little fluorescence signal. In contrast, the two hetero-multimers show a strong and broad emission ranging from 330 – 480nm. They show a peak around 370nm with a long tail ranging until 480nm. The emission of the alternating dimer ((A – A – 2AP – 2AP)₃) is by a factor of 8 weaker compared to the alternating monomer. The fluorescence of the 2AP monomer is by approximately a factor of two and the 2AP dimer by approximately a factor of three weaker compared to the alternating monomer. The lower emission of the 2AP monomer compared to the A-2AP alternating monomer seems surprising. In the alternating monomer the lowest lying $\pi\pi^*$ transition is pumped whereas in the monomer a higher lying $\pi\pi^*$ transition is pumped. The emission stems from the lowest lying $\pi\pi^*$ transition (see discussion).

After exciting with 326nm all samples except of dA₂₀ show a strong emission spectrum. As dA₂₀ shows no emission after exciting with 326nm that could be distinguished from noise with our spectrometer, these data are excluded from the figure. The 2AP monomer shows by far the strongest emission. The spectrum of the dimer ((2AP)₂) and the alternating dimer ((A – A – 2AP – 2AP)₃) have almost the same intensity. The emission is more than one order

of magnitude weaker compared to the 2AP monomer. The alternating monomer ((A – 2AP)₆) shows roughly twice as much emission compared to the two dimeric samples. For all samples one can see a peak around 330 nm, which is the scattered excitation.

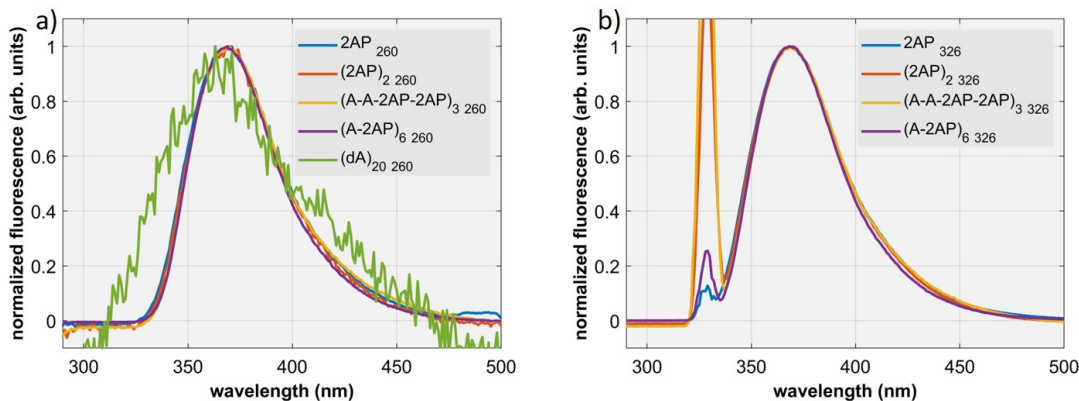


Figure 6.5: Normalized fluorescence spectrum of (2AP), (2AP)₂, (A – A – 2AP – 2AP)₃, (A – 2AP)₆ and dA₂₀ after a) exciting at the absorption maximum of adenine (260 nm) and b) in the absorption peak of 2AP (326 nm) measured in a phosphate buffer solution.

For a comparison of the peak shapes, figure 6.5 shows the normalized fluorescence of the data shown in figure 6.4. The emission peak of dA₂₀ (seen in figure 6.5 a)) has clearly a different shape than the emission peaks of the 2AP containing samples. No difference in lineshape is seen between the two excitations. For both excitations, the alternating monomer shows a slightly less pronounced red emission tail compared to the other three 2AP containing samples.

6.3.2 Population dynamics after exciting the 2AP bases

Figure 6.6 shows the spectrally-resolved transient absorption signal of all samples containing 2AP bases (a) (2AP) b) (2AP)₂, c) (A – A – 2AP – 2AP)₃ and d) (A – 2AP)₆) after excitation at 326 nm. The maximum absorption of 2AP is located around 305 nm (compare figure 6.2). As a flow cell was used in these measurements pump scatter on the detector was unavoidable. The advantage of exciting in the red wing of the absorption spectrum is that the scattering does not block the maximum of the bleach band and it can still be used for analysis. All four samples display dynamics extending beyond 1 ns. Unlike the adenine monomer (compare the two previous chapters) 2AP does not fully decay on the sub-ps to ps timescale, as the electronic structure is fundamentally different [59]. All samples show a bleach band centred around 310 nm (for 2AP around 305 nm). For both the monomer and the alternating monomer ((A – 2AP)₆) this bleach band extends for roughly 20 nm and decays on the ns timescale. For the dimer and the alternating dimer ((A – A – 2AP – 2AP)₃) the band is significantly broader (around 30 nm). The band is within the time-resolution of the measurement present from the beginning but it keeps growing on the 10-ps timescale and decays on the 100 ps timescale. All samples show two regions where an ESA signal is visible. The blue-most ESA is located below

the GSB region. It is starting from 295 nm for the monomer and 305 nm for the alternating monomer and decays on the 1 ns timescale for the monomer and bi-exponentially on the 10 ps and the 1 ns timescale for the alternating monomer. For both, the dimer and the alternating dimer this ESA band is starting below 300 nm, is and is decaying bi-exponentially. The zero-line between GSB and ESA is shifting on the ps time scale displaying either a spectral shift or the different temporal evolution of GSB and ESA. All four samples also display a ESA signal red-shifted from the GSB. As the pump scatter covers the zero-line for almost all of them no statement about the spectra evolution of the zero-line can be made. In all four cases the ESA signal is rising on the ps timescale. In the monomer and alternating monomer the decay takes place on the ns timescale. For the dimeric samples the decay happens bi-exponentially on the 10 ps and 100 ps timescale.

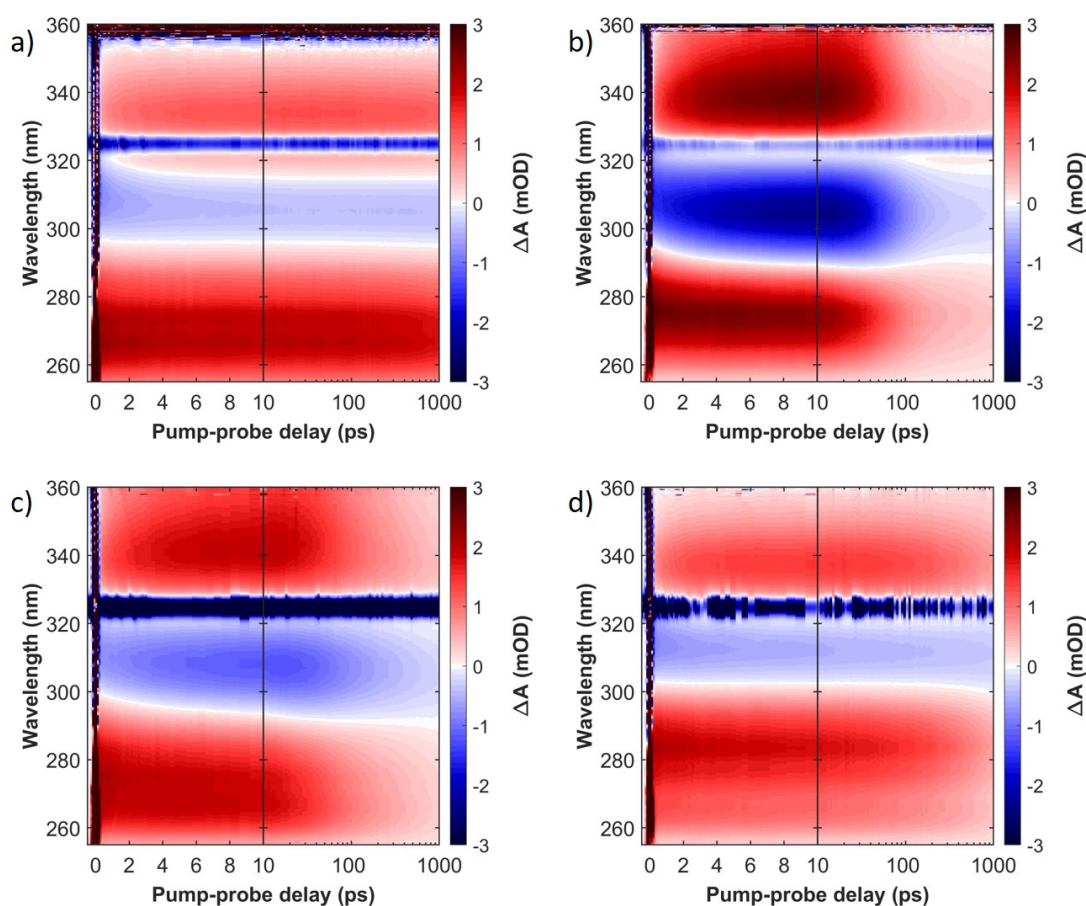


Figure 6.6: Spectrally-resolved transient absorption signal of a) (2AP) b) $(2AP)_2$, c) $(A - A - 2AP - 2AP)_3$ and d) $(A - 2AP)_6$ in a phosphate buffer solution. The scattering signal of the pump can be seen centred at 326 nm.

It has to be noted that the bands most probably overlap and the description given above only displays the evolution of the net signal. This is why a global analysis is necessary. The DAS resulting from the global analysis using a sequential model can be seen in figure 6.7

and the SAS in figure 6.8. The resulting lifetimes are shown in table 6.1. For the global fit the region containing pump scatter ($\approx 320 - 328$ nm) was excluded. To fit the data only three components were necessary in contrast to the dataset where the adenines were excited where four components were needed. As expected, a DAS resembling the early dynamics of photoexcited adenine cannot be observed for any of the samples containing adenines. The DAS of the monomer and the alternating monomer and the DAS of the dimer and the alternating dimer have each strong similarities. The fastest DAS on the few-ps timescale shows a negative value from 300 (in case of the alternating monomer 305) to 350 nm. Below 300 nm both DAS show a positive plateau. For the monomer DAS two is almost purely positive with slightly below zero at 310 nm and having two peaks at 275 and 335 nm. DAS three shows two positive areas from 250–295 nm and 315–350 nm with peaks at 265 and 335 nm and a negative peak from 295–315 nm. For the alternating monomer both DAS show a negative area whereas the longer lived DAS extends further into the blue (305 nm vs 300 nm) resulting into a shift of the band for longer times. The positive peaks resemble the monomer whereby the time constant is by more than a factor of two faster in the strand.

The dimer and the alternating dimer show a DAS on the few-ps timescale. It has a negative value above 320 nm, a broad positive peak which goes to zero around 260 nm for the alternating dimer and reaches negative values from 250–275 nm for the dimer. The lifetimes is almost identical for with 4.4 and 4.6 ps. The second and third DAS show a negative peak from $\approx 290 - 320$ nm and next to it in the red and the blue each a positive peak. In the alternating dimer the bleach band of the longest DAS is slightly blue shifted in respect to the second DAS resulting into a spectral shift of the transient absorption map for long time delays. The second time constant is 50% faster in the dimer than in the alternating dimer. In order to evaluate the quality of the fits, the residuals are shown in figure 6.9. As for the previous data there is a minor structure visible in the residuals which is orders of magnitude lower than the values of the measured data.

6.3.3 Population dynamics after exciting the adenine bases

Figure 6.10 shows the spectrally-resolved transient absorption signal of a) the alternating dimer $((A - A - 2AP - 2AP)_3)$, b) the alternating monomer $(A - 2AP)_6$ and c) the 20-mer dA_{20} after exciting at 266 nm in phosphate buffer solution. The first 10 ps are presented on a linear scale and the later time delays are displayed on a logarithmic scale. All samples are excited close to the absorption maximum of adenine at 266 nm. Below 270 nm one can see the scattering of the pump. As the measurement conditions were different to the previous measurements (flow cell instead of wire-guided liquid jet and lower sample volume) a test run with dA_{20} was done (see figure 6.10 c)) to evaluate the comparability of the measurements. The measurement agrees well with the data presented in chapter 4. Even with the adenine bases being excited, the hetero-multimers in figure 6.10 a) and b) do not display the characteristic bleach below 280 nm seen in dA_{20} (for details see DAS analysis below). Both show a ESA signal decaying on the ps timescale. In $(A - A - 2AP - 2AP)_3$ this signal is very weak and centred around 290 nm

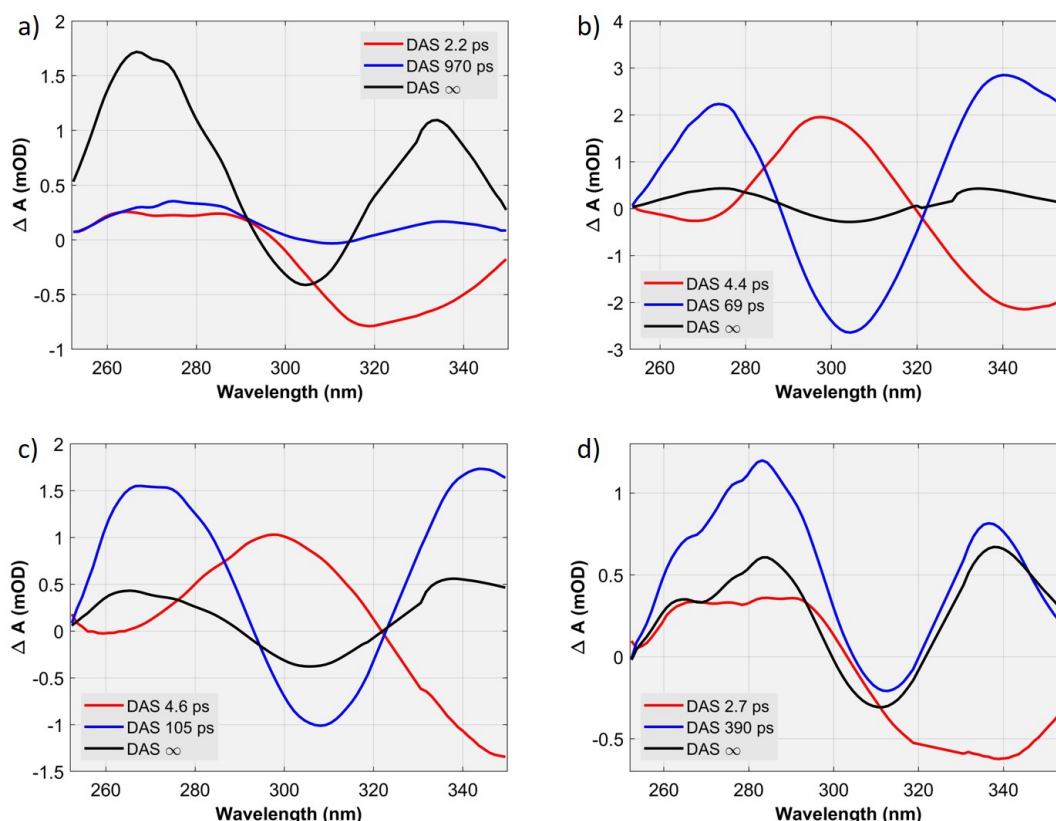


Figure 6.7: Decay associated spectra (DAS) resulting from a sequential global fit of resulting from a spectrally-resolved TA measurement of a) (2AP) b) (2AP)₂, c) (A – A – 2AP – 2AP)₃ and d) (A – 2AP)₆ in a phosphate buffer solution. The corresponding raw data are shown in figure 6.6. The region containing pump scatter ($\approx 320 - 328$ nm) was excluded from the global fit.

whereas in (A – 2AP)₆ it is more notable and centred slightly above 280 nm. Both samples show a bleach signal which is rising on the ps timescale as well as on the 10 – 100 ps timescale. They show an ESA signal decaying on the 100 ps scale as well. The dynamics are in general faster in (A – A – 2AP – 2AP)₃ than in (A – 2AP)₆. The bleach band in (A – A – 2AP – 2AP)₃ is significantly broader.

In order to quantitatively analyse the data, a global analysis of the adenine-2AP samples was performed. The DAS resulting from the global analysis using a sequential model can be seen in figure 6.11 and the SAS in figure 6.12. The resulting lifetimes are shown in table 6.1. For both samples four components, of which one is regarded as infinite on, are necessary to describe the observed dynamics. The first DAS on the sub-ps timescale looks very similar to the DAS observed in the adenine monomer and dimer (compare figure 4.6) including the typical adenine bleach signal. The second DAS decaying on the few-ps timescale has a peak at 290 nm for (A – A – 2AP – 2AP)₃ and at ≈ 280 nm for (A – 2AP)₆ showing a long tail leading to a small negative value for (A – A – 2AP – 2AP)₃ and to nearly zero for (A – 2AP)₆. In (A – A – 2AP – 2AP)₃, DAS three and four have a similar spectral shape. Both show a positive

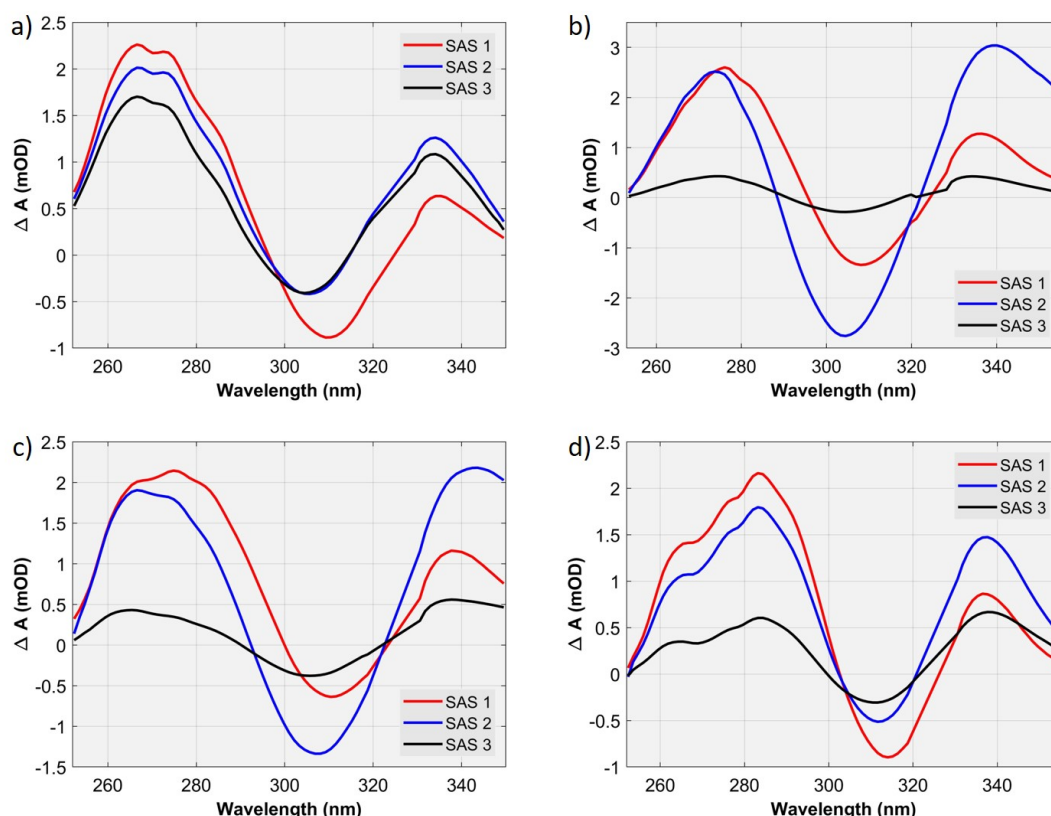


Figure 6.8: Species associated spectra (SAS) resulting from a sequential global fit from spectrally-resolved TA measurement of a) (2AP) b) (2AP)₂, c) (A – A – 2AP – 2AP)₃ and d) (A – 2AP)₆ in a phosphate buffer solution. The corresponding raw data are shown in figure 6.6. The region containing pump scatter ($\approx 320 - 328$ nm) was excluded from the global fit.

peak from 320 – 350 nm and a negative area from 295 – 320 nm. The negative area extends further into the blue for the longer lived DAS resulting into a blue shift of the bleach for longer times. DAS three shows a noticeably stronger positive peak from 270 – 295 nm than DAS four. As a result the blue ESA band decays faster than the red ESA band. For (A – 2AP)₆ DAS three and four have both positive peaks at 285 nm and 335 nm. Towards the blue and red edge of the spectrum the ESA band decreases in amplitude. DAS three has a positive value all over the spectrum reaching a value of zero around 315 nm. DAS four is negative between 300 and 325 nm. Therefore, the rise of the bleach in (A – 2AP)₆ is taking place much slower than in (A – A – 2AP – 2AP)₃. The lifetime of each DAS is shown in the inset of each figure.

In order to evaluate the quality of the fits, the residuals are shown in figure 6.13. It has to be noted, that a minor structure is visible in the residuals. However, the absolute value of the residuals are orders of magnitude lower than the values of the measured data.

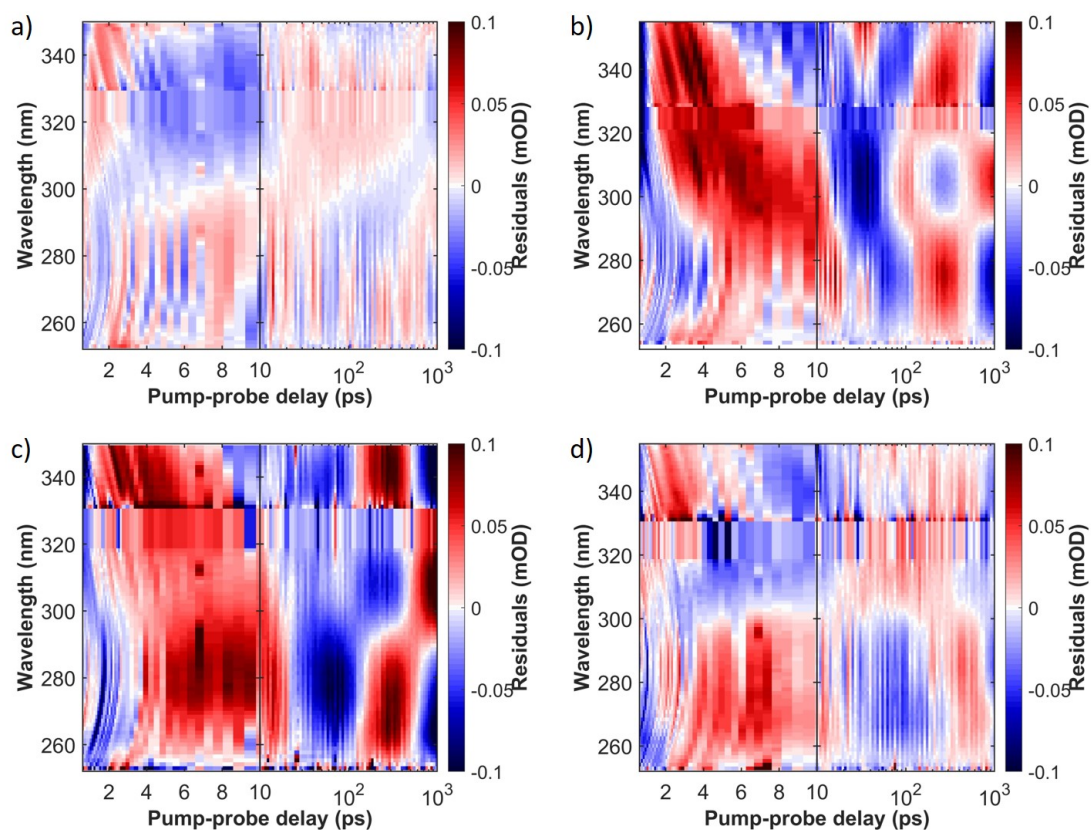


Figure 6.9: Residuals of the global fit shown in figure 6.7 of a) (2AP) b) $(2AP)_2$, c) $(A - A - 2AP - 2AP)_3$ and d) $(A - 2AP)_6$ in mOD.

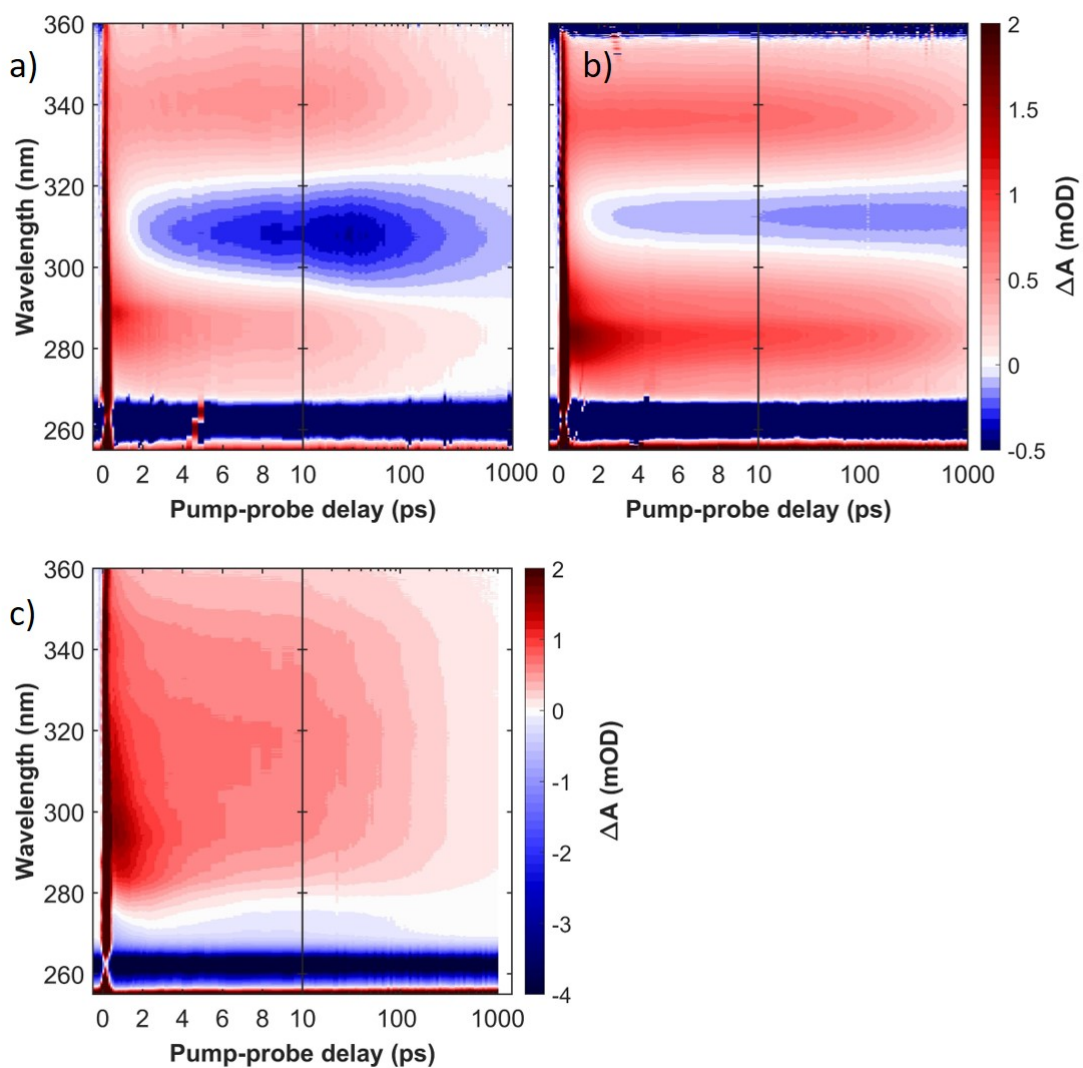


Figure 6.10: Spectrally-resolved transient absorption signal of a) $(A-A-2AP-2AP)_3$ b) $(A-2AP)_6$ and c) dA_{20} after exciting at 266 nm in a phosphate buffer solution. The scattering signal of the pump can be seen below 270 nm.

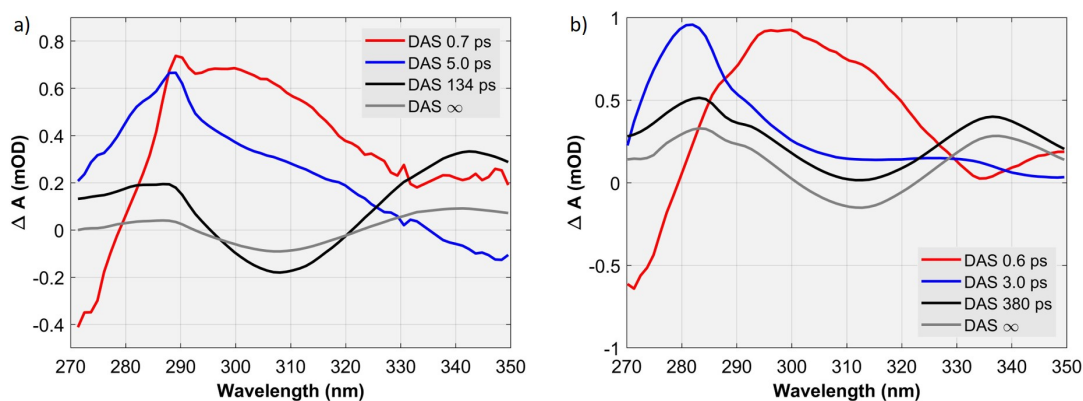


Figure 6.11: Decay associated spectra (DAS) resulting from a sequential global fit of resulting from a spectrally-resolved TA measurement of a) $(A - A - 2AP - 2AP)_3$ and b) $(A - 2AP)_6$ after exciting at 266 nm in a phosphate buffer solution. The corresponding raw data are shown in figure 6.10.

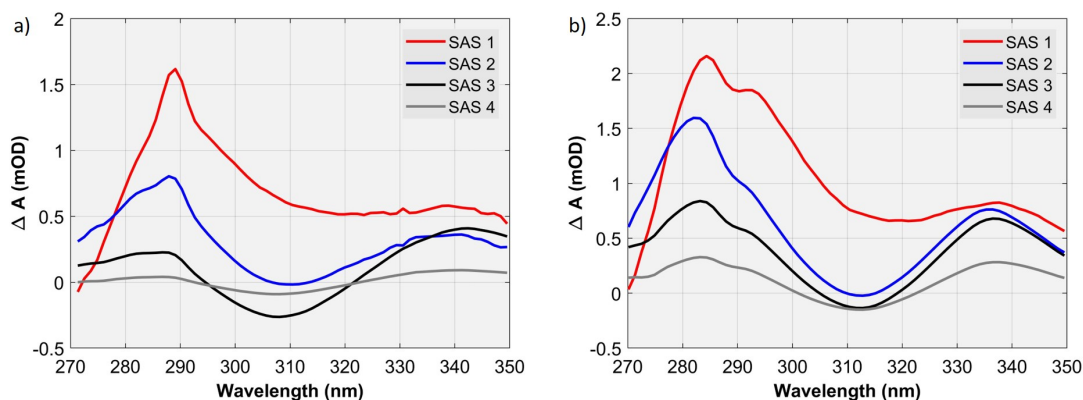


Figure 6.12: Species associated spectra (SAS) resulting from a sequential global fit of resulting from a spectrally-resolved TA measurement of a) $(A - A - 2AP - 2AP)_3$ and b) $(A - 2AP)_6$ after exciting at 266 nm in a phosphate buffer solution. The corresponding raw data are shown in figure 6.10.

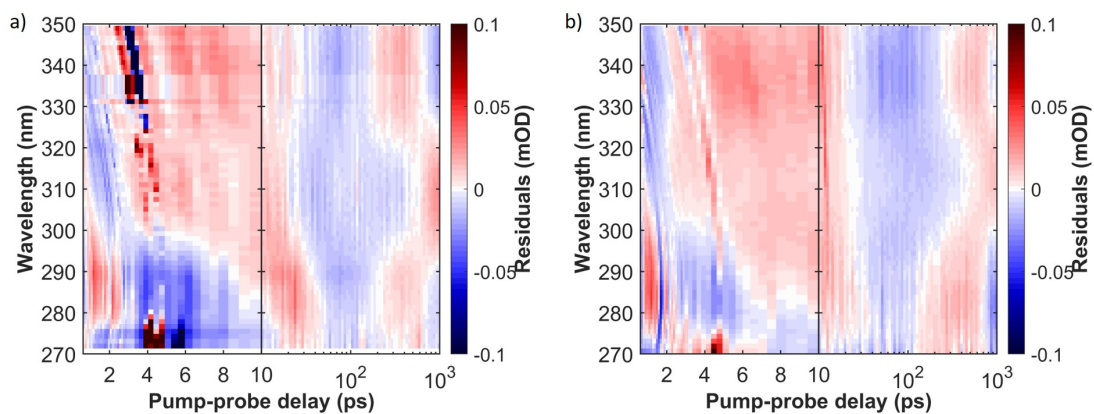


Figure 6.13: Residuals of the global fit shown in figure 6.11 of a) $(A-A-2AP-2AP)_3$ b) $(A-2AP)_6$ in mOD.

Table 6.1: Life times of the different decay channels after excitation of adenine or 2AP bases in strands containing adenine and 2AP bases.

Sample	τ_1 [ps]	τ_2 [ps]	τ_3 [ps]	τ_4 [ps]
(A – A – 2AP – 2AP) ₃ 266nm	0.7 ± 0.1	5 ± 0.5	134 ± 13	∞
(A – 2AP) ₆ 266nm	0.6 ± 0.1	3 ± 0.3	380 ± 38	∞
2AP _{326nm}	-	2.2 ± 0.2	970 ± 97	∞
(2AP) _{2326nm}	-	4.4 ± 0.4	69 ± 7	∞
(A – A – 2AP – 2AP) ₃ 326nm	-	4.6 ± 0.5	105 ± 10	∞
(A – 2AP) ₆ 326nm	-	2.7 ± 0.3	390 ± 39	∞

6.3.4 Anisotropy

Anisotropy after exciting the 2AP bases Figure 6.14 shows the spectrally-resolved transient anisotropy absorption signal of a) (2AP) b) (2AP)₂, c) (A – A – 2AP – 2AP)₃ and d) (A – 2AP)₆ after exciting at 326nm. Strikingly the anisotropy values of the monomer and the alternating monomer display values well above 0.4 in the GSB region. The anisotropy value is even rising on the few ps timescale. As already seen for the anisotropy spectra after exciting at 266nm the bands in all four samples are not uniform within one band. This is due to overlap of more than one band. All samples show positive anisotropies for all bands. The GSB bands show clearly higher anisotropy values as the ESA bands. The decay of the signals is the fastest in the monomer, the second fastest in the dimer and the slowest in the two multimer samples as one can expect for rotational diffusion.

Selected time traces of characteristic areas are shown in figure 6.15.

Anisotropy after exciting the adenine bases Figure 6.16 shows the spectrally-resolved transient anisotropy absorption signal of a) (A – A – 2AP – 2AP)₃ b) (A – 2AP)₆ and c) dA₂₀ after exciting at 266nm. The measurement of dA₂₀ shows the comparability and the feasibility of the experiment under the given experimental conditions. For all samples the scattering covers the region below 270nm. Also the anisotropy below 290nm shows a characteristic positive signature which may be associated with the vibrational cooling of a hot adenine ground state base. The alternating dimer ((A – A – 2AP – 2AP)₃) in a) shows a positive anisotropy signal for the ESA as well as for the GSB region. The anisotropy value for the bleach is higher than for the ESA. The alternating monomer ((A – 2AP)₆) shows a negative anisotropy signal for both ESA regions and a positive signal for the bleach. One can see that both bands do not have a constant value over the band. This is a strong indication for overlapping bands. The strongly different anisotropy values of the both samples indicate transition dipoles which vary in direction relative to the original orientation. Selected time traces of characteristic areas are shown in figure 6.17. As the anisotropy is not constant over a band, as seen in the previous chapter, averaging over a larger area is not meaningful. Nonetheless, to increase the signal to noise ratio the value was averaged over limited area indicated in the inset of the figure.

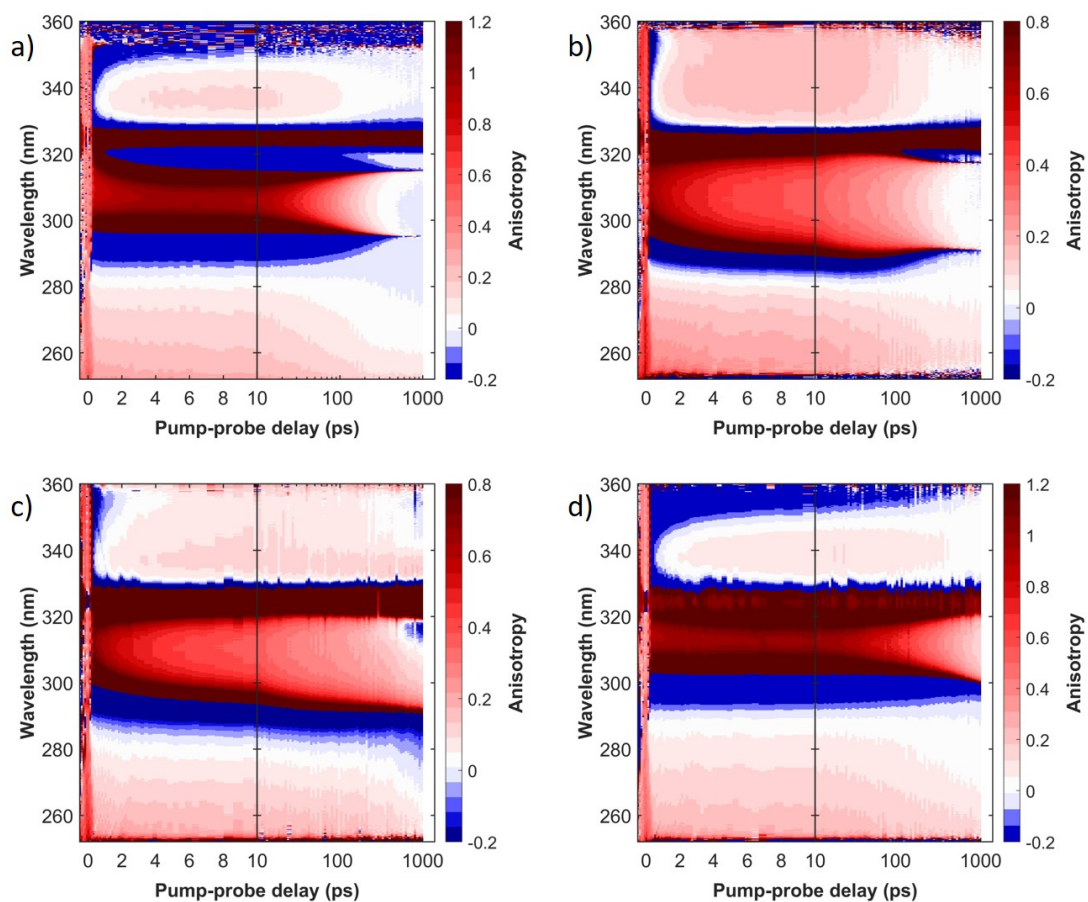


Figure 6.14: Spectrally-resolved transient anisotropy absorption signal of a) (2AP) b) (2AP)₂, c) (A – A – 2AP – 2AP)₃ and d) (A – 2AP)₆ after exciting at 326 nm in a phosphate buffer solution. The scattering signal of the pump can be seen centred at 326 nm.

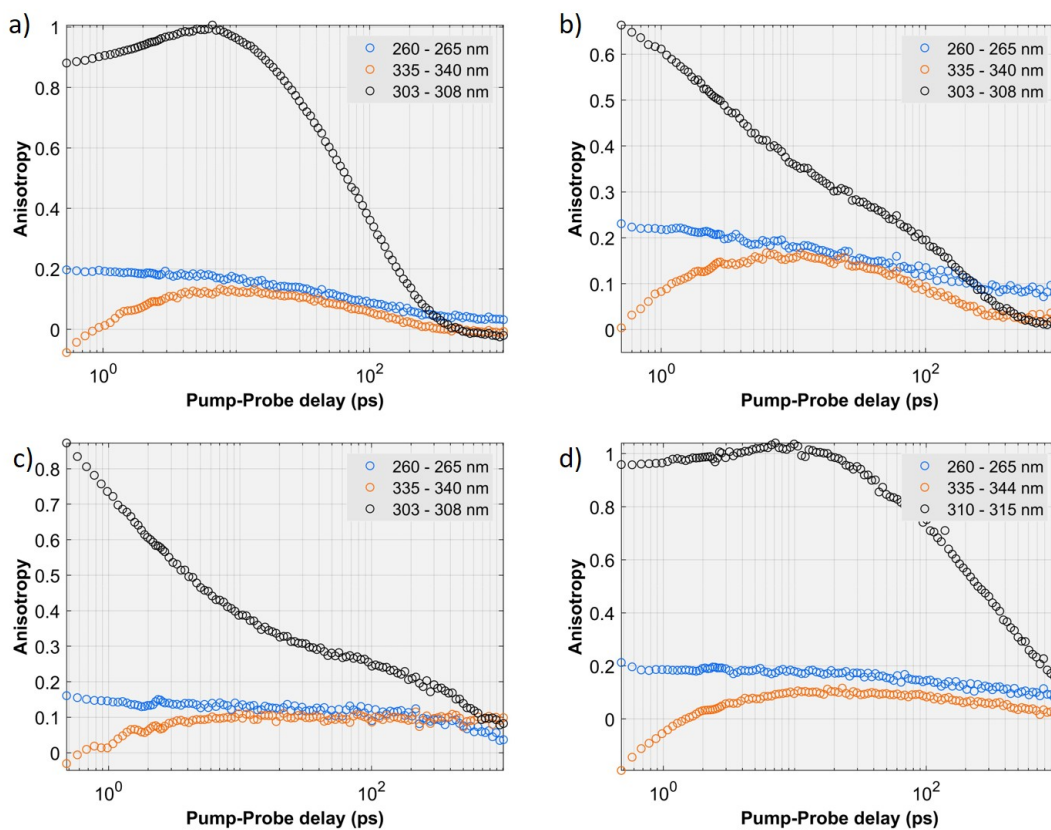


Figure 6.15: Selected anisotropy time traces of a) (2AP), b) (2AP)₂, c) (A - A - 2AP - 2AP)₃ and d) (A - 2AP)₆ after exciting at 326 nm in a phosphate buffer solution shown on a logarithmic timescale.

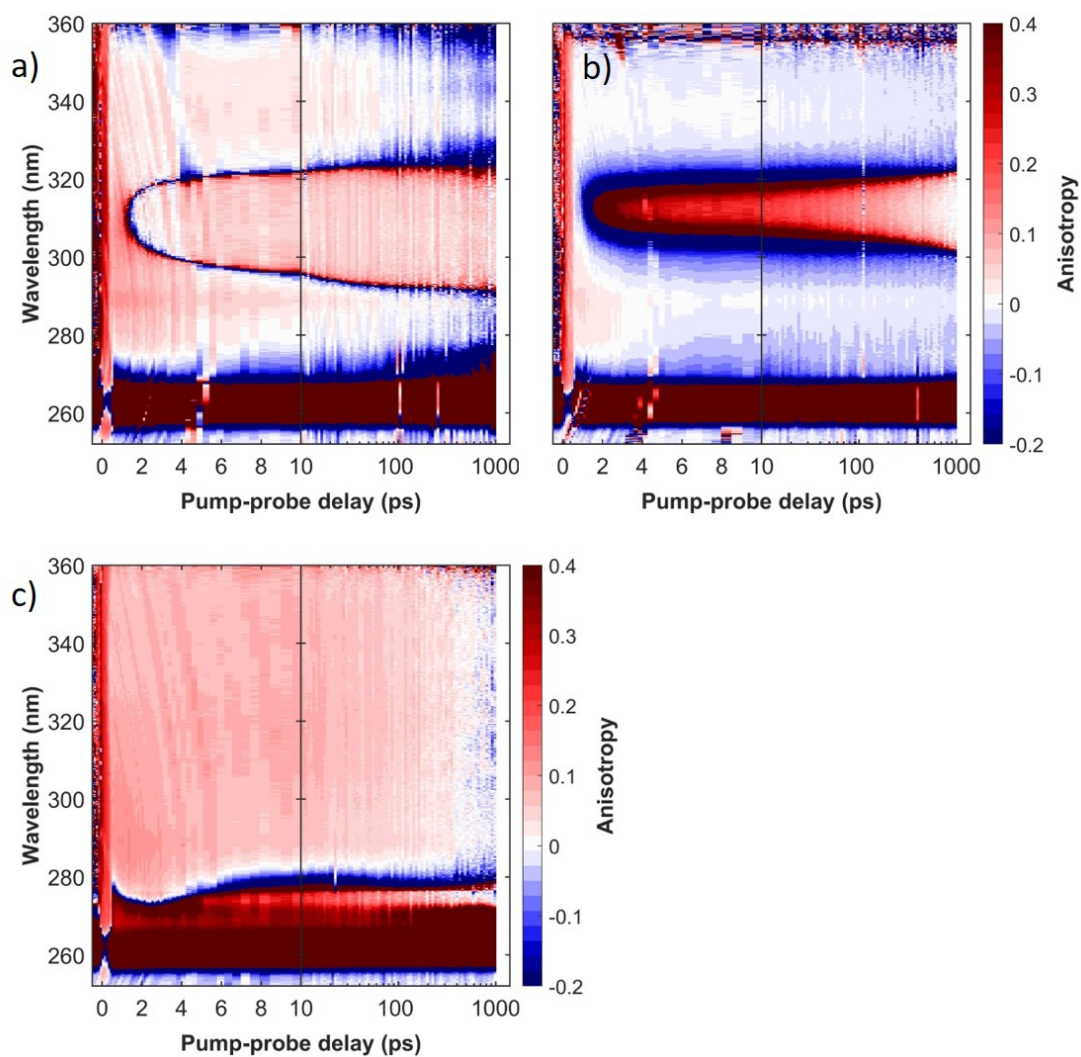


Figure 6.16: Spectrally-resolved transient anisotropy absorption signal of a) $(A-A-2AP-2AP)_3$, b) $(A-2AP)_6$ and c) dA_{20} after exciting at 266 nm in a phosphate buffer solution. The scattering signal of the pump can be seen below 270 nm.

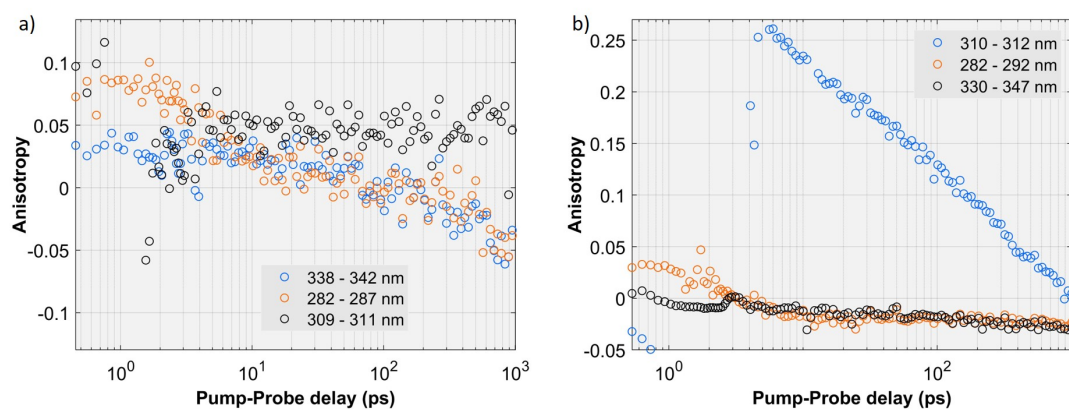


Figure 6.17: Selected anisotropy time traces of a) $(A-A-2AP-2AP)_3$ and b) $(A-2AP)_6$ after exciting at 266 nm in a phosphate buffer solution shown on a logarithmic timescale.

6.4 Discussion

The static absorption, shown in figure 6.2, shows the electronic transitions from the ground state. In the hetero-multimers, both adenine and the 2-AP transitions (one at 245 and one at 305 nm) can be observed. The comparison of 2AP mono- and dimer shows a slight red-shift of the dimer of the main 2AP absorption band. In the hetero-multimers this shift is even more visible. This may be due to stacking with neighbouring bases. This red-shift could be an indicator of excitonic interactions.

The purpose of the CD measurements is to evaluate whether that dipolar coupling is present in the multimers. Furthermore, qualitative implications on the strength of the coupling can be made. A quantitative interpretation of the CD spectrum would need support from computational simulations, which are beyond the scope of this thesis. The monomer shows negligible CD signal as there is no coulombic coupling. The dimer spectra resembles the observations done by Johnson et al. (see introduction) showing that both dimer systems exhibit a similar dipolar coupling [80]. The two multimer samples display a more complex CD spectrum. Three $\pi\pi^*$ transitions (one from adenine and two from 2AP) contribute to the spectrum and the CD bands are probably overlapping. Furthermore CD displays an ensemble average of the local structures present in the sample. The alternating dimer shows a broader absorption peak in the 2AP region and thereby affects the CD couplet. Nonetheless one can conclude that in all three non-monomer samples a coupling of the 2AP transitions is present, as the CD spectrum shows couplets around 300 nm.

Fluorescence measurements were done in order to assess the energy transfer between adenines to 2AP chromophores. From the emission conclusions can be drawn about the bright excited state and the signal strength contains information about quenching channels. As adenine bases show rapid non-radiative relaxation from the excited state, the contribution to the overall fluorescence signal is orders of magnitude less and negligible. Therefore, the fluorescence here is almost entirely caused by excited 2AP bases. The spectral shape of the 2AP fluorescence shows barely any dependence on the sample (see normalized fluorescence spectrum in figure 6.5). Therefore, the bright excited state is very similar in all 2AP containing samples regardless of the excitation wavelength. At 260 nm the absorption of 2AP chromophores have a minimum. As the spectra shown here are scaled according to the absorption (see figure 6.4), the two pure 2AP samples seem to have a strong fluorescence after excitation at 260 nm. The excitation stems from the higher-lying $\pi\pi^*$ and an energy transfer takes place within the chromophore. The emission stems from the lower $\pi\pi^*$ state following Kasha's rule. There might be a non-radiative decay path accessible from this higher lying excited state which is not accessible for the lowest $\pi\pi^*$ state. Therefore the normalized fluorescence spectrum is less intense for the 2AP monomer compared to the alternating monomer.

The absolute absorption of 2AP at 260 nm is less than 10% compared to the absorption of adenine at that wavelength. Directly excited 2AP bases will have a minor contribution to the overall signal and are therefore not further discussed in detail for the time resolved measure-

ments. The alternating monomer shows a 8 times higher fluorescence signal compared to the alternating dimer after excitation of the adenine bases (at 260 nm). This can be due to two effects: Neighbouring bases has been shown to have a higher energy transfer efficiency [146]. Even as the sum of adenine and 2AP bases is the same in the two strands, each 2AP base has two adenine nearest neighbours in the alternating monomer but only one in the alternating dimer. Therefore a lower energy transfer efficiency can be expected. On the other hand excited state quenching, which is present in these strands, affects the total fluorescence yield. Inspecting the fluorescence signal after exciting the 2AP bases (326 nm) still shows a \sim two times higher fluorescence signal for the alternating dimer. This shows that both effects play a role. The fluorescence intensity for 326 nm excitation is a direct probe of quenching and therefore stacking of 2AP. The fluorescence may therefore be a much clearer probe of A-2AP interactions. After exciting the 2AP bases directly all polymer samples show a quenching which results to a 10-20 fold reduction in fluorescence yield. Especially the two dimeric samples show a strong quenching. Therefore, 2AP is more efficiently quenched by another 2AP, rather than an adenine base.

In a single strand not all bases are stacked. Therefore a different propensity for bases stacking in the different model strands can affect the energy transfer efficiency. Unstacked bases for example might not show efficient energy transfer and might not lead to charge transfer states. This might be a reason for the 57% energy transfer efficiency between nearest neighbours in an adenine-2AP strand observed by Nordlund et al. and the lower efficiency of bases which are separated by other bases in the strand [147]. Note that the observation of a CD signal (see figure 6.3) is an indication for some degree of coupling but does not mean that all bases are coupled. Therefore another possible explanation for the differences in fluorescence yield is a different propensity for stacking in the different systems.

When pumping the 2AP transition directly no energy transfer process is expected, thus three decaying components are enough to describe the time resolved dynamics shown in section 6.3.2. In all four samples the bleach signal of the 2AP base is consequently there from the very beginning and no bleach signal from adenine bases can be observed. A spectral evolution of the resulting bleach signals towards the blue is observable in all four samples. This is most probably due to shifts in the overlapping ESA band. The bleach band in the monomeric samples are significantly narrower than the ones of the dimeric samples. Also here overlaps of the ESA bands are a likely cause.

The second species shows a stronger bleach for the dimeric samples leading to a rise of the bleach in these samples on the 10 ps timescale. Nonetheless, both strands show a subtle red shift of the bleach band, leading to a red-shift on the long timescale. The low energy ESA of the second species is much higher in all four samples than for the previous species (SAS 1). Therefore also the low energy ESA shows a rise on this timescale. The last species (SAS 3) in all four cases spectrally mimics the the previous species (SAS 2).

In the 2AP-monomer only bright $\pi\pi^*$ states can be expected [59]. Therefore, the SAS represent

a sum of the bleach band and the signature of the $\pi\pi^*$ excited state ESA. The first SAS for all the other samples looks similar, so on the sub-ps timescale also a $\pi\pi^*$ populated. For the monomer only a shift of the bleach band can be observed. All the other samples show a clear change in the ESA bands, resulting in a rise in the red part of the spectrum. This part is especially pronounced for the 2-AP dimer and the alternating dimer. Thus it is concluded that the red part of the ESA band is a signature of a 2AP-2AP charge-transfer state. For the alternating monomer also a smaller change is visible in this band. This is attributed to the 2AP-A charge-transfer state. Strikingly the charge recombination is fastest in the dimer and second fastest in the alternating dimer. Also the fluorescence is the weakest for the two dimeric systems. Therefore, the coupling of two 2AP bases seems to lead to efficient quenching of the bright state and fast charge recombination.

When pumping the adenine transition at 266nm one can expect an energy transfer to take place. The dA₂₀ TA data were recorded to ensure that the different experimental conditions, relative to the measurements presented in the two previous chapters, lead to the same results and the experiment can be reliably performed under that conditions. Therefore, this dataset will not be further discussed here. In both 2AP-containing strands the first time constant resembles that of adenine. This shows that initially adenine bases are excited. As the bleach is not fully accessible because of pump scattering a distinction between monomeric or excitonic excitation of adenine cannot be made. An energy transfer takes place and 2AP excited states are populated. The lifetime of the adenine-like species can be taken as an upper limit for the energy-transfer time, which is 0.7 ± 0.1 ps in the alternating dimer and 0.6 ± 0.1 ps in the alternating monomer (see τ_1 in table 6.1). There is no significant difference between the two samples. If a Dexter or Förster mechanism is responsible for the energy transfer cannot be concluded from the data (see chapter 2.1.3). As discussed by Nordlund et al. it would require a sophisticated simulation to determine which mechanism is present [147].

Those second species show two ESA peaks around 290 and 340 nm with no absorption around 310 nm, where the bleach band of the 2AP bases would be situated (see second SAS in figure 6.12). Sequentially a second excited state gets populated. Its low energy ESA spectrum is slightly red shifted towards the SAS of the previous one. Both samples shows a GSB signature in the SAS, associated with the bleach of the 2AP bases. The width of the bleach varies between the alternating monomer and the dimer. This might be due to a spectral overlap of GSB and ESA of this species, which covers the GSB. The bleach of the alternating monomer is significantly narrower. The lifetime of this species is more than two times shorter in the alternating dimer than in the alternating monomer. In the light of the previous chapters one can assume that the long living states are charge transfer states. This is in line with previous findings saying that charge transfer states quench excited states in 2AP containing oligomers [82] [150]. This charge transfer state is expected to be oxidative with adenine [150] and there is a 2AP-adenine charge transfer pair. The nearest neighbour of each of this charge transfer bases might affect the electronic configuration of these states and therefore the ESA spectra. The charge recombination, analogous to when pumping the 2APs', takes place on a timescale exceeding our experiment. The associated SAS (SAS number 4) are not significantly different

from the previous ones (SAS number 3). Therefore, on both timescales a similar state is present. The characteristic bleach band of adenine cannot be seen except on the sub-ps timescale. Thus it can be concluded that no long living adenine states are present.

A comparison of the intermediate SAS under both pumping conditions can clarify if different states are populated on this timescale depending on pathways that lead to these states. For the strands, which could be excited at both pump wavelengths, the two long term SAS look strikingly similar. (Note that due to pump scattering in the 266 nm region the data set with excitation of the adenine bases, is cut in the blue.) Therefore, one can assume that the same species are present in both experiments on the longer timescales. Also the decay dynamics are (within the precision of the fitting method) undistinguishable (see table 6.1 for lifetimes). The dynamics in the monomer are the slowest. No quenching of the electronically excited state is expected. In the alternating monomer, where already a considerable effect of quenching can be seen in the static fluorescence (see figure 6.4 b) the dynamics are faster than in the monomer, but slower than in the two dimeric samples. For those two samples quenching is expected, from the fluorescence data, to be similarly pronounced. Still the dimer shows a $\sim 30\%$ faster recombination than the alternating dimer. One can speculate, that for the pure 2AP dimer, where no driving redox-potential between the two bases of the dimer is present, the charge separation is less pronounced and a recombination is therefore quicker.

A thorough analysis of the anisotropy traces would require a careful deconvolution of the overlapping spectral components that contribute to the overall anisotropy signal, which is still in process and no quantitative statements can be done. Therefore, the analysis is limited to a phenomenological description. The anisotropy is sensitive to the transition dipole of the originally excited transition and the transition dipole of the state present at the arrival time of the probe. For the experiment, where adenines get excited and mostly 2APs are probed, the excited and the probed chromophores are not identical. Nonetheless, as Jean et al. [143] showed the direction of the transition dipole for the $\pi\pi^*$ transition is mostly identical in adenine and 2AP. As the magic angle signal has a non-zero value over the whole temporal measurement window one does not observe diverging anisotropy signals for late time delays.

After pumping the 2AP bases several overlapping bands contribute to the ESA signal. Unlike with fluorescence anisotropy, with TA anisotropy one component can have a negative and another a positive value. Therefore, the anisotropy value can lie outside of the usually expected area for a single transition between 0.4 and -0.2. In both monomeric samples an ESA band is strongly overlapping with a GSB band around 310 nm. This leads to anisotropy values as high as 1.2.

When pumping the adenines, both ESA bands in both hetero-multimer start with a small positive anisotropy values, which evolves continuously towards a negative value. In the alternating dimer, the bleach band is after the singularity (zero crossing of the magic angle signal) at ~ 3 ps mostly constant. Surprisingly one does not see a decay due to rotational diffusion. The effect of rotational diffusion could either be covered by an overlapping band

with different dynamics or less likely, the local structure in this strand is less flexible than in the adenine strands discussed in chapter 5 and rotational diffusion takes place on a longer timescale. In the alternating monomer the anisotropy at the centre of the GSB band displays a value of 0.25 after the initial singularity at 5 ps. It decays mono-exponentially to zero within 1 ns. Therefore a higher flexibility is expected in this sample. The anisotropy of the ESA band shows a lower value for this sample hinting to a strong out of plane component of the associated state, which is an indication for a stronger CT character compared to the alternating dimer. As mentioned above, the anisotropy is defined relative to the originally excited transition. Even with the monomeric transition dipole moments of adenine and 2AP having a similar direction, there is a twist angle between neighbouring bases in a stack. Thus, the strikingly different anisotropy values for the hetero-multimers with different pumping conditions is a strong indication for an energy transfer taking place when pumping the adenines.

6.5 Conclusion

In this chapter the energy and charge transfer in different single strand systems containing adenine and 2AP bases were investigated. A static absorption, CD and fluorescence analysis was performed. Two distinct absorption bands of adenine and 2AP bases are present in the hetero-multimers. In all non-monomeric samples CD revealed a dipolar coupling of the bases. Furthermore, fluorescence spectra revealed an energy transfer between the two bases and a quenching of the bright state in all non-monomeric samples, whereas the quenching in the dimeric systems was most efficient. By pumping the 2AP transition the signature of the bright 2AP-monomer state as well as 2AP-2AP and 2AP-A charge-transfer states could be identified. When pumping the adenine bases, time resolved TA spectra showed an initial bleach of the adenine bases. Sequentially the energy is transferred in less than 0.7 ps to the 2AP bases, the adenine bleach disappears and the 2AP bleach rises. To describe the energy transfer another time constant is needed. The energy transfer is supported by a striking difference in anisotropy depending on the excited base. The SAS and the dynamics are apart from the energy transfer dynamics the same, independent which base is excited initially. The charge-recombination dynamics are the fastest in the 2P-dimer, followed by the alternating dimer, the alternating monomer.

7 Conclusion and outlook

In this thesis, the electronic and structural dynamics of adenine single strands have been studied. By comparing different samples, solvents, and excitation conditions, combined with static analysis, several key factors governing the excited state dynamics have been identified.

Transient absorption anisotropy spectroscopy is used in combination with static absorption, static circular dichroism, and static fluorescence to gain insights into the samples' electronic structure and its dynamics. In DNA, the dynamics and structure are governed by two main interactions. Intrastrand stacking and interstrand base pairing. In this thesis, different stacked systems have been investigated. As adenosine shows the highest stacking probabilities among the natural nucleobases, the monomer, dimer and 20-mer of deoxyadenosine monophosphate have been investigated. It is found that in physiological buffer solution, an exciton state spanning over two bases is excited. As this exciton cannot be identified in the dimer, it can be concluded that the structural rigidity in the 20-mer enables more closely packed bases, and thereby stronger dipolar coupling which is needed for the exciton to form. Transiently populated charge transfer states display a complete charge separation in the 20-mer, whereas the dimer only shows partial CT character. By exciting the 20-mer in the oligomer-exclusive red absorption tail overlapping with the terrestrial solar spectrum, a CT state is directly populated and strong inhomogeneous broadening of the CT band is experimentally observed. This CT state does not show a full CT character, and is similar to a CT state in an isolated dimer. Nonetheless, charge recombination takes place at the same rate as for the full CT state in the 20-mer.

The charge recombination rate is by roughly a factor two slower in the dimer compared to the 20-mer. Changing the solvent from a water based buffer solution to a heavy water based buffer solution deuterates the amino group in the nucleobase. This slows down the recombination rate of both dimer and 20-mer. Strikingly, the effect is stronger for the dimer. Therefore, the charge recombination process takes place via a proton transfer between the amino groups. As the distance in the dimer is greater this process is slower. Anisotropy measurements reveal the structural flexibility of the strand. As the anisotropy is constant over the whole ESA band, it reveals that the CT state is one single species and not an average of several species with

different spectral shapes and anisotropies. The CT state is fully formed after 300 fs and the CT character does not continuously develop over several ps. Consequently, the ground state conformation at the moment of excitation determines the CT state character. However, on the 10-ps timescale, a structural relaxation towards the CT state minimum configuration is identified.

In strands with adenosine and 2-aminopurine (2AP) energy and charge transfer processes have been studied. 2AP acts as an energy sink. With a static characterisation energy transfer from adenosine to 2AP and quenching of the bright state had been confirmed in all investigated strands. With direct excitation of the 2AP base the signature of the 2AP-monomer bright state as well as 2AP-2AP and 2AP-A charge-transfer states could be identified. By selectively exciting adenosine, the energy transfer can be time resolved as the initial adenosine bleach disappears in less than 0.7 ps and the 2AP bleach rises. The energy transfer is supported by a striking difference in anisotropy depending on the excited base. The SAS and the dynamics are apart from the energy transfer dynamics the same, independent which base is excited initially. The charge-recombination dynamics are the fastest in the 2P-dimer, followed by the alternating dimer, the alternating monomer.

With the presented techniques and careful analysis of the accessible observables, important scientific questions can be answered but many questions still remain. To confirm the presented result, that charge recombination takes place via proton transfer of the amino-group, a control experiment would be valuable. Hypoxanthine varies to adenine only by the missing amino-group. With such a cross-check the hypothesis could be confirmed. Similarly, the assignment of the intermediate timescale in the anisotropy experiments as a structural relaxation of the CT state would benefit from additional experiments. A variation of the viscosity while keeping the polarity constant or by playing with the polarity while keeping the viscosity constant could help distinguishing simple fluctuations from structural relaxation. Varying the salt concentration or changing the pH of the solvent would be easy and possible realisations. Studying modified bases, especially biologically relevant methylated DNA bases, could be another interesting follow-up experiment, which answer whether epigenetics modulate the photoprotection mechanisms in DNA.

To further investigate the energy transfer process in 2AP systems 2D-UV spectroscopy is an ideal tool [11]. As an ideal pair TA and time resolved fluorescence give the full picture of electronic dynamics [153]. Especially quenching processes can thus be conveniently be studied and dynamical informations gained from both techniques can be combined to better understand the underlying photophysics.

The author of this thesis assisted in the realization of a time resolved circular dichroism setup in the deep-UV [107]. CD is a powerful tool to investigate biological structures. Using time resolved CD as a probe opens the possibility to study dynamics relevant for the functioning of biological samples. Investigating dynamics whose natural cause is not an electronic excitation but a thermal one calls for a different form of temporal trigger [154]. For this, temperature jump

experiments are used. By exciting solvent modes locally, the temperature can be increased on an ultrafast timescale. Combined with time resolved CD this could allow to study time resolved melting of DNA double strands for instance.

This thesis was focused on studying intrastrand processes governed by base stacking. Investigating interstrand processes governed by base pairing could be a promising route. Although there already exists an extended body of work on this topic, the presented observables would add valuable insights.

Bibliography

- [1] V. Balzani, A. Credi, and M. Venturi, *Molecular Devices and Machines—A Journey into the Nano World*. Weinheim, FRG: Wiley-VCH Verlag GmbH & Co. KGaA, Jan. 2003.
- [2] T. Brixner, R. Hildner, J. Köhler, C. Lambert, and F. Würthner, “Exciton Transport in Molecular Aggregates – From Natural Antennas to Synthetic Chromophore Systems,” *Advanced Energy Materials*, vol. 7, no. 16, p. 1700236, 2017. _eprint: <https://onlinelibrary.wiley.com/doi/pdf/10.1002/aenm.201700236>.
- [3] S. Yamazaki and S. Kato, “Solvent Effect on Conical Intersections in Excited-State 9H-Adenine: Radiationless Decay Mechanism in Polar Solvent,” *Journal of the American Chemical Society*, vol. 129, pp. 2901–2909, Mar. 2007. Publisher: American Chemical Society.
- [4] A. W. Lange and J. M. Herbert, “Both Intra- and Interstrand Charge-Transfer Excited States in Aqueous B-DNA Are Present at Energies Comparable To, or Just Above, the 1 pi-pi-star Excitonic Bright States,” *Journal of the American Chemical Society*, vol. 131, pp. 3913–3922, Mar. 2009.
- [5] A. L. Sobolewski and W. Domcke, “Molecular mechanisms of the photostability of life,” *Physical Chemistry Chemical Physics*, vol. 12, no. 19, p. 4897, 2010.
- [6] D. Markovitsi, “UV-induced DNA Damage: The Role of Electronic Excited States,” *Photochemistry and Photobiology*, vol. 92, pp. 45–51, Jan. 2016.
- [7] A. H. Zewail, “Femtochemistry: Atomic-Scale Dynamics of the Chemical Bond Using Ultrafast Lasers (Nobel Lecture),” *Angewandte Chemie International Edition*, vol. 39, no. 15, pp. 2586–2631, 2000. _eprint: <https://onlinelibrary.wiley.com/doi/pdf/10.1002/1521-3773%2820000804%2939%3A15%3C2586%3A%3AAID-ANIE2586%3E3.0.CO%3B2-O>.
- [8] J. Chen and B. Kohler, “Base Stacking in Adenosine Dimers Revealed by Femtosecond Transient Absorption Spectroscopy,” *Journal of the American Chemical Society*, vol. 136, pp. 6362–6372, Apr. 2014.
- [9] K. Henzler-Wildman and D. Kern, “Dynamic personalities of proteins,” *Nature*, vol. 450, pp. 964–972, Dec. 2007. Number: 7172 Publisher: Nature Publishing Group.

- [10] G. Auböck, C. Consani, R. Monni, A. Cannizzo, F. van Mourik, and M. Chergui, "Femtosecond pump/supercontinuum-probe setup with 20 kHz repetition rate," *Review of Scientific Instruments*, vol. 83, p. 093105, Sept. 2012.
- [11] G. Auböck, C. Consani, F. van Mourik, and M. Chergui, "Ultrabroadband femtosecond two-dimensional ultraviolet transient absorption," *Optics Letters*, vol. 37, p. 2337, June 2012.
- [12] M. Nič, J. Jirát, B. Košata, A. Jenkins, and A. McNaught, eds., *IUPAC Compendium of Chemical Terminology: Gold Book*. Research Triangle Park, NC: IUPAC, 2.1.0 ed., June 2009.
- [13] J.-M. Lehn, "Design of organic complexing agents Strategies towards properties," in *Alkali Metal Complexes with Organic Ligands*, Structure and Bonding, (Berlin, Heidelberg), pp. 1–69, Springer, 1973.
- [14] J.-M. Lehn, "Supramolecular Chemistry—Scope and Perspectives Molecules, Supramolecules, and Molecular Devices (Nobel Lecture)," *Angewandte Chemie International Edition in English*, vol. 27, no. 1, pp. 89–112, 1988. _eprint: <https://onlinelibrary.wiley.com/doi/pdf/10.1002/anie.198800891>.
- [15] P. de Rege, S. Williams, and M. Therien, "Direct evaluation of electronic coupling mediated by hydrogen bonds: implications for biological electron transfer," *Science*, vol. 269, pp. 1409–1413, Sept. 1995.
- [16] P. W. Atkins, J. De Paula, and P. W. Atkins, *Physical chemistry*. New York: W.H. Freeman, 2006. OCLC: 1132507116.
- [17] K. M. Guckian, B. A. Schweitzer, R. X.-F. Ren, C. J. Sheils, D. C. Tahmassebi, and E. T. Kool, "Factors Contributing to Aromatic Stacking in Water: Evaluation in the Context of DNA," *Journal of the American Chemical Society*, vol. 122, pp. 2213–2222, Mar. 2000.
- [18] S. Grimme, "Do Special Noncovalent pi–pi Stacking Interactions Really Exist?," *Angewandte Chemie International Edition*, vol. 47, no. 18, pp. 3430–3434, 2008. _eprint: <https://onlinelibrary.wiley.com/doi/pdf/10.1002/anie.200705157>.
- [19] C. R. Martinez and B. L. Iverson, "Rethinking the term "pi-stacking"," *Chemical Science*, vol. 3, pp. 2191–2201, June 2012. Publisher: The Royal Society of Chemistry.
- [20] E. Fermi, *Nuclear physics*. Chicago: Univ. of Chicago Press, rev. ed., reprint ed., 1974. OCLC: 4445652.
- [21] B. Wardle, *Principles and Applications of Photochemistry*. Wiley, 2009.
- [22] D. Dzebo, *Photon Upconversion through Triplet-Triplet Annihilation: Towards Higher Efficiency and Solid State Applications*. PhD Thesis, 2016.

- [23] M. Kasha, "Characterization of electronic transitions in complex molecules," *Discussions of the Faraday Society*, vol. 9, pp. 14–19, Jan. 1950. Publisher: The Royal Society of Chemistry.
- [24] L. Stryer, "Fluorescence Energy Transfer as a Spectroscopic Ruler," *Annual Review of Biochemistry*, vol. 47, pp. 819–846, June 1978. Publisher: Annual Reviews.
- [25] M. Kasha, H. R. Rawls, and M. Ashraf El-Bayoumi, "The exciton model in molecular spectroscopy," *Pure and Applied Chemistry*, vol. 11, Jan. 1965.
- [26] A. Nitzan, *Chemical dynamics in condensed phases: relaxation, transfer and reactions in condensed molecular systems*. Oxford graduate texts, Oxford ; New York: Oxford University Press, 2006. OCLC: ocm62118341.
- [27] M. Montalti and S. L. Murov, eds., *Handbook of photochemistry*. Boca Raton: CRC/Taylor & Francis, 3rd ed ed., 2006. OCLC: ocm61131872.
- [28] G. M. Cooper, *The cell: a molecular approach*. Oxford ; New York: Sinauer Associates, an imprint of Oxford University Press, eighth edition ed., 2019.
- [29] C. Su, C. T. Middleton, and B. Kohler, "Base-Stacking Disorder and Excited-State Dynamics in Single-Stranded Adenine Homo-oligonucleotides," *The Journal of Physical Chemistry B*, vol. 116, pp. 10266–10274, Aug. 2012.
- [30] J. Chen, Y. Zhang, and B. Kohler, "Excited States in DNA Strands Investigated by Ultrafast Laser Spectroscopy," in *Photoinduced Phenomena in Nucleic Acids II: DNA Fragments and Phenomenological Aspects* (M. Barbatti, A. C. Borin, and S. Ullrich, eds.), Topics in Current Chemistry, pp. 39–87, Cham: Springer International Publishing, 2015.
- [31] B. E. Collins, L. F. Ye, D. Duzdevich, and E. C. Greene, "Chapter 12 - DNA curtains: Novel tools for imaging protein–nucleic acid interactions at the single-molecule level," in *Methods in Cell Biology* (J. C. Waters and T. Wittman, eds.), vol. 123 of *Quantitative Imaging in Cell Biology*, pp. 217–234, Academic Press, Jan. 2014.
- [32] A. Rich and S. Zhang, "Z-DNA: the long road to biological function," *Nature Reviews Genetics*, vol. 4, pp. 566–572, July 2003. Number: 7 Publisher: Nature Publishing Group.
- [33] H. Simpkins and E. G. Richards, "Titration Properties of Some Dinucleotides*," *Biochemistry*, vol. 6, pp. 2513–2520, Aug. 1967. Publisher: American Chemical Society.
- [34] N. E. Geacintov, "The Chemical Biology of DNA Damage," *WILEY-VCH Verlag GmbH & Co. KGaA*, p. 473, 2010.
- [35] W. J. Schreier, P. Gilch, and W. Zinth, "Early Events of DNA Photodamage," *Annual Review of Physical Chemistry*, vol. 66, pp. 497–519, Apr. 2015.

- [36] J. Cadet, S. Mouret, J.-L. Ravanat, and T. Douki, "Photoinduced Damage to Cellular DNA: Direct and Photosensitized Reactions†," *Photochemistry and Photobiology*, vol. 88, pp. 1048–1065, Sept. 2012.
- [37] T. Douki, "The variety of UV-induced pyrimidine dimeric photoproducts in DNA as shown by chromatographic quantification methods," *Photochemical & Photobiological Sciences*, vol. 12, pp. 1286–1302, Aug. 2013. Publisher: The Royal Society of Chemistry.
- [38] M. C. Cuquerella, V. Lhiaubet-Vallet, F. Bosca, and M. A. Miranda, "Photosensitised pyrimidine dimerisation in DNA," *Chemical Science*, vol. 2, pp. 1219–1232, June 2011. Publisher: The Royal Society of Chemistry.
- [39] W. J. Schreier, T. E. Schrader, F. O. Koller, P. Gilch, C. E. Crespo-Hernández, V. N. Swaminathan, T. Carell, W. Zinth, and B. Kohler, "Thymine Dimerization in DNA is an Ultrafast Photoreaction," *Science (New York, N.Y.)*, vol. 315, pp. 625–629, Feb. 2007.
- [40] S. Marguet and D. Markovitsi, "Time-Resolved Study of Thymine Dimer Formation," *Journal of the American Chemical Society*, vol. 127, pp. 5780–5781, Apr. 2005. Publisher: American Chemical Society.
- [41] A. Banyasz, I. Vayá, P. Changenet-Barret, T. Gustavsson, T. Douki, and D. Markovitsi, "Base Pairing Enhances Fluorescence and Favors Cyclobutane Dimer Formation Induced upon Absorption of UVA Radiation by DNA," *Journal of the American Chemical Society*, vol. 133, pp. 5163–5165, Apr. 2011.
- [42] B. P. Fingerhut, T. T. Herzog, G. Ryseck, K. Haiser, F. F. Graupner, K. Heil, P. Gilch, W. J. Schreier, T. Carell, R. de Vivie-Riedle, and W. Zinth, "Dynamics of ultraviolet-induced DNA lesions: Dewar formation guided by pre-tension induced by the backbone," *New Journal of Physics*, vol. 14, p. 065006, June 2012.
- [43] J. M. Berg, J. L. Tymoczko, G. J. Gatto, and L. Stryer, *Biochemistry*. New York: W.H. Freeman & Company, a Macmillan Education Imprint, eighth edition ed., 2015.
- [44] T. Gustavsson, N. Sarkar, I. Vayá, M. C. Jiménez, D. Markovitsi, and R. Improta, "A joint experimental/theoretical study of the ultrafast excited state deactivation of deoxyadenosine and 9-methyladenine in water and acetonitrile," *Photochemical & Photobiological Sciences*, vol. 12, no. 8, p. 1375, 2013.
- [45] I. Vayá, T. Gustavsson, F.-A. Miannay, T. Douki, and D. Markovitsi, "Fluorescence of Natural DNA: From the Femtosecond to the Nanosecond Time Scales," *Journal of the American Chemical Society*, vol. 132, pp. 11834–11835, Sept. 2010. Publisher: American Chemical Society.
- [46] A. Banyasz, T. Gustavsson, D. Onidas, P. Changenet-Barret, D. Markovitsi, and R. Improta, "Multi-Pathway Excited State Relaxation of Adenine Oligomers in Aqueous Solution: A Joint Theoretical and Experimental Study," *Chemistry - A European Journal*, vol. 19, pp. 3762–3774, Mar. 2013.

- [47] Z.-Q. You and C.-P. Hsu, "Theory and calculation for the electronic coupling in excitation energy transfer," *International Journal of Quantum Chemistry*, vol. 114, pp. 102–115, Jan. 2014.
- [48] F. Santoro, V. Barone, and R. Improta, "Influence of base stacking on excited-state behavior of polyadenine in water, based on time-dependent density functional calculations," *Proceedings of the National Academy of Sciences*, vol. 104, pp. 9931–9936, June 2007.
- [49] T. Gustavsson, R. Improta, and D. Markovitsi, "DNA/RNA: Building Blocks of Life Under UV Irradiation," *The Journal of Physical Chemistry Letters*, vol. 1, pp. 2025–2030, July 2010.
- [50] D. Onidas, D. Markovitsi, S. Marguet, A. Sharonov, and T. Gustavsson, "Fluorescence Properties of DNA Nucleosides and Nucleotides: A Refined Steady-State and Femtosecond Investigation," *The Journal of Physical Chemistry B*, vol. 106, pp. 11367–11374, Oct. 2002. Publisher: American Chemical Society.
- [51] N. L. Evans and S. Ullrich, "Wavelength Dependence of Electronic Relaxation in Isolated Adenine Using UV Femtosecond Time-Resolved Photoelectron Spectroscopy," *The Journal of Physical Chemistry A*, vol. 114, pp. 11225–11230, Oct. 2010.
- [52] F. Buchner, H.-H. Ritze, J. Lahl, and A. Lübcke, "Time-resolved photoelectron spectroscopy of adenine and adenosine in aqueous solution," *Physical Chemistry Chemical Physics*, vol. 15, pp. 11402–11408, June 2013. Publisher: The Royal Society of Chemistry.
- [53] H. Kang, K. T. Lee, B. Jung, Y. J. Ko, and S. K. Kim, "Intrinsic Lifetimes of the Excited State of DNA and RNA Bases," *Journal of the American Chemical Society*, vol. 124, pp. 12958–12959, Nov. 2002.
- [54] T. Pancur, N. K. Schwalb, F. Renth, and F. Temps, "Femtosecond fluorescence up-conversion spectroscopy of adenine and adenosine: experimental evidence for the pi-sigma-star state?," *Chemical Physics*, vol. 313, pp. 199–212, June 2005.
- [55] T. Gustavsson, A. Sharonov, D. Onidas, and D. Markovitsi, "Adenine, deoxyadenosine and deoxyadenosine 5-monophosphate studied by femtosecond fluorescence upconversion spectroscopy," *Chemical Physics Letters*, vol. 356, pp. 49–54, Apr. 2002.
- [56] B. Cohen, P. M. Hare, and B. Kohler, "Ultrafast Excited-State Dynamics of Adenine and Monomethylated Adenines in Solution: Implications for the Nonradiative Decay Mechanism," *Journal of the American Chemical Society*, vol. 125, pp. 13594–13601, Nov. 2003. Publisher: American Chemical Society.
- [57] J. Peon and A. H. Zewail, "DNA/RNA nucleotides and nucleosides: direct measurement of excited-state lifetimes by femtosecond fluorescence up-conversion," *Chemical Physics Letters*, vol. 348, pp. 255–262, Nov. 2001.

- [58] F. Santoro, R. Improta, T. Fahleson, J. Kauczor, P. Norman, and S. Coriani, "Relative Stability of the L_a and L_b Excited States in Adenine and Guanine: Direct Evidence from TD-DFT Calculations of MCD Spectra," *The Journal of Physical Chemistry Letters*, vol. 5, pp. 1806–1811, June 2014.
- [59] L. Serrano-Andres, M. Merchán, and A. C. Borin, "Adenine and 2-aminopurine: Paradigms of modern theoretical photochemistry," *Proceedings of the National Academy of Sciences*, vol. 103, pp. 8691–8696, June 2006.
- [60] S. Perun, A. L. Sobolewski, and W. Domcke, "Ab Initio Studies on the Radiationless Decay Mechanisms of the Lowest Excited Singlet States of 9H-Adenine," *Journal of the American Chemical Society*, vol. 127, pp. 6257–6265, May 2005. Publisher: American Chemical Society.
- [61] S. Matsika, "Three-State Conical Intersections in Nucleic Acid Bases," *The Journal of Physical Chemistry A*, vol. 109, pp. 7538–7545, Aug. 2005. Publisher: American Chemical Society.
- [62] J. R. Platt, "Classification of Spectra of Cata-Condensed Hydrocarbons," *The Journal of Chemical Physics*, vol. 17, pp. 484–495, May 1949. Publisher: American Institute of Physics.
- [63] M. Barbatti, "Photorelaxation Induced by Water–Chromophore Electron Transfer," *Journal of the American Chemical Society*, vol. 136, pp. 10246–10249, July 2014. Publisher: American Chemical Society.
- [64] A. Broo, "A Theoretical Investigation of the Physical Reason for the Very Different Luminescence Properties of the Two Isomers Adenine and 2-Aminopurine," *The Journal of Physical Chemistry A*, vol. 102, pp. 526–531, Jan. 1998. Publisher: American Chemical Society.
- [65] F. Plasser and H. Lischka, "Electronic excitation and structural relaxation of the adenine dinucleotide in gas phase and solution," *Photochemical & Photobiological Sciences*, vol. 12, no. 8, p. 1440, 2013.
- [66] C. E. Crespo-Hernández, B. Cohen, P. M. Hare, and B. Kohler, "Ultrafast Excited-State Dynamics in Nucleic Acids," *Chemical Reviews*, vol. 104, pp. 1977–2020, Apr. 2004. Publisher: American Chemical Society.
- [67] H. Chen and S. Li, "Theoretical Study toward Understanding Ultrafast Internal Conversion of Excited 9H-Adenine," *The Journal of Physical Chemistry A*, vol. 109, pp. 8443–8446, Sept. 2005.
- [68] C. M. Marian, M. Kleinschmidt, and J. Tatchen, "The photophysics of 7H-adenine: A quantum chemical investigation including spin–orbit effects," *Chemical Physics*, vol. 347, pp. 346–359, May 2008.

- [69] J.-M. L. Pecourt, J. Peon, and B. Kohler, "DNA Excited-State Dynamics: Ultrafast Internal Conversion and Vibrational Cooling in a Series of Nucleosides," *Journal of the American Chemical Society*, vol. 123, pp. 10370–10378, Oct. 2001.
- [70] T. Takaya, C. Su, K. de La Harpe, C. E. Crespo-Hernández, and B. Kohler, "UV excitation of single DNA and RNA strands produces high yields of exciplex states between two stacked bases," *Proceedings of the National Academy of Sciences*, vol. 105, no. 30, pp. 10285–10290, 2008.
- [71] I. Buchvarov, Q. Wang, M. Raytchev, A. Trifonov, and T. Fiebig, "Electronic energy delocalization and dissipation in single- and double-stranded DNA," *Proceedings of the National Academy of Sciences*, vol. 104, no. 12, pp. 4794–4797, 2007.
- [72] K. Kleinermanns, D. Nachtigallová, and M. S. de Vries, "Excited state dynamics of DNA bases," *International Reviews in Physical Chemistry*, vol. 32, pp. 308–342, June 2013.
- [73] A. C. Jones and R. K. Neely, "2-aminopurine as a fluorescent probe of DNA conformation and the DNA–enzyme interface," *Quarterly Reviews of Biophysics*, vol. 48, pp. 244–279, May 2015.
- [74] S. Smirnov, T. J. Matray, E. T. Kool, and C. de los Santos, "Integrity of duplex structures without hydrogen bonding: DNA with pyrene paired at abasic sites," *Nucleic Acids Research*, vol. 30, pp. 5561–5569, Dec. 2002. Publisher: Oxford Academic.
- [75] D. C. Ward, E. Reich, and L. Stryer, "Fluorescence Studies of Nucleotides and Polynucleotides I. FORMYCIN, 2-AMINOPURINE RIBOSIDE, 2,6-DIAMINOPURINE RIBOSIDE, AND THEIR DERIVATIVES," *Journal of Biological Chemistry*, vol. 244, pp. 1228–1237, Oct. 1969. Publisher: American Society for Biochemistry and Molecular Biology.
- [76] J. R. Lakowicz, *Principles of Fluorescence Spectroscopy*. Springer US, 3 ed., 2006.
- [77] J. Liang and S. Matsika, "Pathways for Fluorescence Quenching in 2-Aminopurine π -Stacked with Pyrimidine Nucleobases," *Journal of the American Chemical Society*, vol. 133, pp. 6799–6808, May 2011. Publisher: American Chemical Society.
- [78] S. Lobsiger, S. Blaser, R. K. Sinha, H.-M. Frey, and S. Leutwyler, "Switching on the fluorescence of 2-aminopurine by site-selective microhydration," *Nature Chemistry*, vol. 6, pp. 989–993, Nov. 2014. Number: 11 Publisher: Nature Publishing Group.
- [79] M. Rist, H.-A. Wagenknecht, and T. Fiebig, "Exciton and Excimer Formation in DNA at Room Temperature," *ChemPhysChem*, vol. 3, no. 8, pp. 704–707, 2002.
- [80] N. P. Johnson, W. A. Baase, and P. H. von Hippel, "Low-energy circular dichroism of 2-aminopurine dinucleotide as a probe of local conformation of DNA and RNA," *Proceedings of the National Academy of Sciences of the United States of America*, vol. 101, no. 10, pp. 3426–3431, 2004.

- [81] D. Xu, K. O. Evans, and T. M. Nordlund, "Melting and Premelting Transitions of an Oligomer Measured by DNA Base Fluorescence and Absorption," *Biochemistry*, vol. 33, pp. 9592–9599, Oct. 1994.
- [82] S. O. Kelley and J. K. Barton, "Electron Transfer Between Bases in Double Helical DNA," *Science*, vol. 283, pp. 375–381, Jan. 1999. Publisher: American Association for the Advancement of Science Section: Report.
- [83] O. F. A. Larsen, I. H. M. v. Stokkum, F. L. d. Weerd, M. Vengris, C. T. Aravindakumar, R. v. Grondelle, N. E. Geacintov, and H. v. Amerongen, "Ultrafast transient-absorption and steady-state fluorescence measurements on 2-aminopurine substituted dinucleotides and 2-aminopurine substituted DNA duplexes," *Physical Chemistry Chemical Physics*, vol. 6, pp. 154–160, Dec. 2004. Publisher: The Royal Society of Chemistry.
- [84] M. Narayanan, G. Kodali, Y. Xing, and R. J. Stanley, "Photoinduced Electron Transfer Occurs between 2-Aminopurine and the DNA Nucleic Acid Monophosphates: Results from Cyclic Voltammetry and Fluorescence Quenching," *The Journal of Physical Chemistry B*, vol. 114, pp. 10573–10580, Aug. 2010. Publisher: American Chemical Society.
- [85] C. Wan, T. Xia, H.-C. Becker, and A. H. Zewail, "Ultrafast unequilibrated charge transfer: A new channel in the quenching of fluorescent biological probes," *Chemical Physics Letters*, vol. 412, pp. 158–163, Aug. 2005.
- [86] D. B. Bucher, B. M. Pilles, T. Carell, and W. Zinth, "Charge separation and charge delocalization identified in long-living states of photoexcited DNA," *Proceedings of the National Academy of Sciences*, vol. 111, pp. 4369–4374, Mar. 2014.
- [87] J. J. Nogueira, F. Plasser, and L. González, "Electronic delocalization, charge transfer and hypochromism in the UV absorption spectrum of polyadenine unravelled by multiscale computations and quantitative wavefunction analysis," *Chemical Science*, vol. 8, no. 8, pp. 5682–5691, 2017.
- [88] U. Kadhane, A. I. S. Holm, S. V. Hoffmann, and S. B. Nielsen, "Strong coupling between adenine nucleobases in DNA single strands revealed by circular dichroism using synchrotron radiation," *Physical Review E*, vol. 77, p. 021901, Feb. 2008.
- [89] D. Markovitsi, T. Gustavsson, and A. Banyasz, "Absorption of UV radiation by DNA: Spatial and temporal features," *Mutation Research/Reviews in Mutation Research*, vol. 704, pp. 21–28, Apr. 2010.
- [90] Y. Zhang, J. Dood, A. A. Beckstead, X.-B. Li, K. V. Nguyen, C. J. Burrows, R. Improta, and B. Kohler, "Efficient UV-induced charge separation and recombination in an 8-oxoguanine-containing dinucleotide," *Proceedings of the National Academy of Sciences*, vol. 111, pp. 11612–11617, Aug. 2014.
- [91] R. Borrego-Varillas, G. Cerullo, and D. Markovitsi, "Exciton Trapping Dynamics in DNA Multimers," *The Journal of Physical Chemistry Letters*, vol. 10, pp. 1639–1643, Apr. 2019.

- [92] F. Santoro, R. Improta, F. Avila, M. Segado, and A. Lami, "The interplay between neutral exciton and charge transfer states in single-strand polyadenine: a quantum dynamical investigation," *Photochemical & Photobiological Sciences*, vol. 12, pp. 1527–1543, Aug. 2013.
- [93] V. A. Spata and S. Matsika, "Photophysical deactivation pathways in adenine oligonucleotides," *Physical Chemistry Chemical Physics*, vol. 17, pp. 31073–31083, Nov. 2015.
- [94] D. Markovitsi, F. Talbot, T. Gustavsson, D. Onidas, E. Lazzarotto, and S. Marguet, "Molecular spectroscopy: Complexity of excited-state dynamics in DNA," *Nature*, vol. 441, no. 7094, pp. E7–E7, 2006.
- [95] R. Improta and V. Barone, "Interplay between "Neutral" and "Charge-Transfer" Excimers Rules the Excited State Decay in Adenine-Rich Polynucleotides," *Angewandte Chemie International Edition*, vol. 50, no. 50, pp. 12016–12019, 2011.
- [96] I. Conti, P. Altoè, M. Stenta, M. Garavelli, and G. Orlandi, "Adenine deactivation in DNA resolved at the CASPT2//CASSCF/AMBER level," *Physical Chemistry Chemical Physics*, vol. 12, no. 19, p. 5016, 2010.
- [97] R. Improta, F. Santoro, and L. Blancafort, "Quantum Mechanical Studies on the Photo-physics and the Photochemistry of Nucleic Acids and Nucleobases," *Chemical Reviews*, vol. 116, pp. 3540–3593, Mar. 2016.
- [98] C. E. Crespo-Hernández, B. Cohen, and B. Kohler, "Base stacking controls excited-state dynamics in A·T DNA," *Nature*, vol. 436, pp. 1141–1144, Aug. 2005.
- [99] J. Chen, A. K. Thazhathveetil, F. D. Lewis, and B. Kohler, "Ultrafast Excited-State Dynamics in Hexaethyleneglycol-Linked DNA Homoduplexes Made of A·T Base Pairs," *Journal of the American Chemical Society*, vol. 135, pp. 10290–10293, July 2013.
- [100] D. B. Bucher, A. Schlueter, T. Carell, and W. Zinth, "Watson-Crick Base Pairing Controls Excited - State Decay in Natural DNA," *Angewandte Chemie International Edition*, vol. 53, pp. 11366–11369, Oct. 2014.
- [101] K. de La Harpe, C. E. Crespo-Hernández, and B. Kohler, "Deuterium Isotope Effect on Excited-State Dynamics in an Alternating GC Oligonucleotide," *Journal of the American Chemical Society*, vol. 131, pp. 17557–17559, Dec. 2009.
- [102] Y. Zhang, K. de La Harpe, A. A. Beckstead, R. Improta, and B. Kohler, "UV-Induced Proton Transfer between DNA Strands," *Journal of the American Chemical Society*, vol. 137, pp. 7059–7062, June 2015.
- [103] B. A. Wallace and R. W. Janes, eds., *Modern techniques for circular dichroism and synchrotron radiation circular dichroism spectroscopy*. No. v. 1 in *Advances in biomedical spectroscopy*, Amsterdam ; Washington, DC: IOS Press, 2009. OCLC: ocn326471051.

- [104] Y. Feng, I. Vinogradov, and N.-H. Ge, "General noise suppression scheme with reference detection in heterodyne nonlinear spectroscopy," *Optics Express*, vol. 25, pp. 26262–26279, Oct. 2017. Publisher: Optical Society of America.
- [105] Y. Feng, I. Vinogradov, and N.-H. Ge, "Optimized noise reduction scheme for heterodyne spectroscopy using array detectors," *Optics Express*, vol. 27, pp. 20323–20346, July 2019. Publisher: Optical Society of America.
- [106] M. Oppermann, N. Nagornova, A. Oriana, E. Baldini, L. Mewes, B. Bauer, T. Palmieri, T. Rossi, F. van Mourik, and M. Chergui, "The LOUVRE Laboratory: State-of-the-Art Ultrafast Ultraviolet Spectroscopies for Molecular and Materials Science," *CHIMIA International Journal for Chemistry*, vol. 71, pp. 288–294, May 2017.
- [107] M. Oppermann, B. Bauer, T. Rossi, F. Zinna, J. Helbing, J. Lacour, and M. Chergui, "Ultrafast broadband circular dichroism in the deep ultraviolet," *Optica*, vol. 6, pp. 56–60, Jan. 2019. Publisher: Optical Society of America.
- [108] P. Baum, S. Lochbrunner, and E. Riedle, "Generation of tunable 7-fs ultraviolet pulses: achromatic phase matching and chirp management," *Applied Physics B*, vol. 79, pp. 1027–1032, Dec. 2004.
- [109] P. Baum, S. Lochbrunner, and E. Riedle, "Tunable sub-10-fs ultraviolet pulses generated by achromatic frequency doubling," *Optics letters*, vol. 29, no. 14, pp. 1686–1688, 2004.
- [110] U. Megerle, I. Pugliesi, C. Schrieffer, C. F. Sailer, and E. Riedle, "Sub-50 fs broadband absorption spectroscopy with tunable excitation: putting the analysis of ultrafast molecular dynamics on solid ground," *Applied Physics B*, vol. 96, pp. 215–231, Aug. 2009.
- [111] A. Picchiotti, V. I. Prokhorenko, and R. J. D. Miller, "A closed-loop pump-driven wire-guided flow jet for ultrafast spectroscopy of liquid samples," *Review of Scientific Instruments*, vol. 86, p. 093105, Sept. 2015.
- [112] M. J. Tauber, R. A. Mathies, X. Chen, and S. E. Bradforth, "Flowing liquid sample jet for resonance Raman and ultrafast optical spectroscopy," *Review of Scientific Instruments*, vol. 74, pp. 4958–4960, Oct. 2003. Publisher: American Institute of Physics.
- [113] S. Laimgruber, H. Schachenmayr, B. Schmidt, W. Zinth, and P. Gilch, "A femtosecond stimulated Raman spectrograph for the near ultraviolet," *Applied Physics B*, vol. 85, pp. 557–564, Nov. 2006.
- [114] M. Lorenc, M. Ziolk, R. Naskrecki, J. Karolczak, J. Kubicki, and A. Maciejewski, "Artifacts in femtosecond transient absorption spectroscopy," *Applied Physics B: Lasers and Optics*, vol. 74, pp. 19–27, Jan. 2002.
- [115] A. Ansari, C. Jones, E. Henry, J. Hofrichter, and W. Eaton, "Photoselection in polarized photolysis experiments on heme proteins," *Biophysical Journal*, vol. 64, pp. 852–868, Mar. 1993.

- [116] A. Reuther, A. Laubereau, and D. N. Nikogosyan, "A simple method for the in situ analysis of femtosecond UV pulses in the pump-probe spectroscopy of solutions," *Optics Communications*, vol. 141, no. 3, pp. 180 – 184, 1997.
- [117] C. Ruckebusch, M. Sliwa, P. Pernot, A. de Juan, and R. Tauler, "Comprehensive data analysis of femtosecond transient absorption spectra: A review," *Journal of Photochemistry and Photobiology C: Photochemistry Reviews*, vol. 13, pp. 1–27, Mar. 2012.
- [118] I. H. van Stokkum, D. S. Larsen, and R. van Grondelle, "Global and target analysis of time-resolved spectra," *Biochimica et Biophysica Acta (BBA) - Bioenergetics*, vol. 1657, pp. 82–104, July 2004.
- [119] C. Slavov, H. Hartmann, and J. Wachtveitl, "Implementation and Evaluation of Data Analysis Strategies for Time-Resolved Optical Spectroscopy," *Analytical Chemistry*, vol. 87, pp. 2328–2336, Feb. 2015. Publisher: American Chemical Society.
- [120] C. T. Middleton, K. de La Harpe, C. Su, Y. K. Law, C. E. Crespo-Hernández, and B. Kohler, "DNA Excited-State Dynamics: From Single Bases to the Double Helix," *Annual Review of Physical Chemistry*, vol. 60, pp. 217–239, May 2009.
- [121] "<https://en.wikipedia.org/w/index.php?title=Adenine&oldid=994273409>," Dec. 2020. Page Version ID: 994273409.
- [122] R. Dulbecco and M. Vogt, "PLAQUE FORMATION AND ISOLATION OF PURE LINES WITH POLIOMYELITIS VIRUSES," *Journal of Experimental Medicine*, vol. 99, pp. 167–182, Feb. 1954. Publisher: The Rockefeller University Press.
- [123] A. Hospital, I. Faustino, R. Collepardo-Guevara, C. González, J. L. Gelpí, and M. Orozco, "NAFlex: a web server for the study of nucleic acid flexibility," *Nucleic Acids Research*, vol. 41, pp. W47–W55, July 2013.
- [124] D. e. a. Case, "Amber 2018," 2018.
- [125] W. L. Jorgensen, J. Chandrasekhar, J. D. Madura, R. W. Impey, and M. L. Klein, "Comparison of simple potential functions for simulating liquid water," *The Journal of Chemical Physics*, vol. 79, pp. 926–935, July 1983. Publisher: American Institute of Physics.
- [126] I. Ivani, P. D. Dans, A. Noy, A. Pérez, I. Faustino, A. Hospital, J. Walther, P. Andrio, R. Goñi, A. Balaceanu, G. Portella, F. Battistini, J. L. Gelpí, C. González, M. Vendruscolo, C. A. Laughton, S. A. Harris, D. A. Case, and M. Orozco, "Parmbsc1: a refined force field for DNA simulations," *Nature Methods*, vol. 13, pp. 55–58, Jan. 2016. Number: 1 Publisher: Nature Publishing Group.
- [127] D. Svozil, P. Jungwirth, and Z. Havlas, "Electron Binding to Nucleic Acid Bases Experimental and theoretical studies. A review.," *Collection Of Czechoslovak Chemical Communications*, vol. 69, no. 7, pp. 395–1428, 2004.

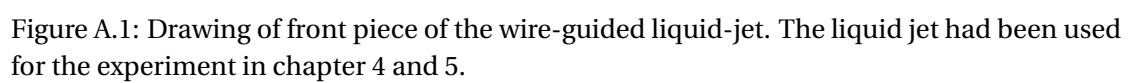
- [128] U. C. Stange and F. Temps, "Ultrafast electronic deactivation of UV-excited adenine and its ribo- and deoxyribonucleosides and -nucleotides: A comparative study," *Chemical Physics*, vol. 515, pp. 441–451, Nov. 2018.
- [129] L. Hu, Y. Zhao, F. Wang, G. Chen, C. Ma, W.-M. Kwok, and D. L. Phillips, "Are Adenine Strands Helical H-Aggregates?," *The Journal of Physical Chemistry B*, vol. 111, pp. 11812–11816, Oct. 2007.
- [130] D. J. Skowron, *Subnanosecond emission from model DNA oligomers characterized through time-correlated single-photon counting spectroscopy*. PhD thesis, Montana State University, May 2017.
- [131] H. Yin, Y. Ma, J. Mu, C. Liu, and M. Rohlfing, "Charge-Transfer Excited States in Aqueous DNA: Insights from Many-Body Green's Function Theory," *Physical Review Letters*, vol. 112, p. 228301, June 2014. Publisher: American Physical Society.
- [132] D. G. Cross, "Hydrogen exchange in nucleosides and nucleotides. Measurement of hydrogen exchange by stopped-flow and ultraviolet difference spectroscopy," *Biochemistry*, vol. 14, pp. 357–362, Jan. 1975.
- [133] I. Conti, A. Nenov, S. Höfner, S. F. Altavilla, I. Rivalta, E. Dumont, G. Orlandi, and M. Garavelli, "Excited state evolution of DNA stacked adenines resolved at the CASPT2//CASSCF/Amber level: from the bright to the excimer state and back," *Physical Chemistry Chemical Physics*, vol. 17, pp. 7291–7302, Mar. 2015. Publisher: The Royal Society of Chemistry.
- [134] N. Mataga, H. Chosrowjan, and S. Taniguchi, "Ultrafast charge transfer in excited electronic states and investigations into fundamental problems of exciplex chemistry: Our early studies and recent developments," *Journal of Photochemistry and Photobiology C: Photochemistry Reviews*, vol. 6, pp. 37–79, Apr. 2005.
- [135] K. R. Harris and L. A. Woolf, "Temperature and Volume Dependence of the Viscosity of Water and Heavy Water at Low Temperatures," *Journal of Chemical & Engineering Data*, vol. 49, pp. 1064–1069, July 2004.
- [136] T. Takaya, H.-o. Hamaguchi, and K. Iwata, "Femtosecond time-resolved absorption anisotropy spectroscopy on 9,9'-bianthryl: Detection of partial intramolecular charge transfer in polar and nonpolar solvents," *The Journal of Chemical Physics*, vol. 130, p. 014501, Jan. 2009. Publisher: American Institute of Physics.
- [137] R. Pant and S. Wüster, "Excitation transport in molecular aggregates with thermal motion," *Physical Chemistry Chemical Physics*, vol. 22, pp. 21169–21184, Sept. 2020. Publisher: The Royal Society of Chemistry.
- [138] R. E. Holmlin, P. J. Dandliker, and J. K. Barton, "Charge Transfer through the DNA Base Stack," *Angewandte Chemie International Edition in English*, vol. 36, no. 24, pp. 2714–2730, 1997. _eprint: <https://onlinelibrary.wiley.com/doi/pdf/10.1002/anie.199727141>.

- [139] N. Renaud, M. A. Harris, A. P. N. Singh, Y. A. Berlin, M. A. Ratner, M. R. Wasielewski, F. D. Lewis, and F. C. Grozema, "Deep-hole transfer leads to ultrafast charge migration in DNA hairpins," *Nature Chemistry*, vol. 8, pp. 1015–1021, Nov. 2016. Number: 11 Publisher: Nature Publishing Group.
- [140] J. M. Lim, P. Kim, M.-C. Yoon, J. Sung, V. Dehm, Z. Chen, F. Würthner, and D. Kim, "Exciton delocalization and dynamics in helical π -stacks of self-assembled perylene bisimides," *Chemical Science*, vol. 4, pp. 388–397, Nov. 2012. Publisher: The Royal Society of Chemistry.
- [141] M. Son, K. H. Park, C. Shao, F. Würthner, and D. Kim, "Spectroscopic Demonstration of Exciton Dynamics and Excimer Formation in a Sterically Controlled Perylene Bisimide Dimer Aggregate," *The Journal of Physical Chemistry Letters*, vol. 5, pp. 3601–3607, Oct. 2014.
- [142] D. Markovitsi, T. Gustavsson, and F. Talbot, "Excited states and energy transfer among DNA bases in double helices," *Photochemical & Photobiological Sciences*, vol. 6, no. 7, pp. 717–724, 2007. Publisher: Royal Society of Chemistry.
- [143] J. M. Jean and B. P. Krueger, "Structural Fluctuations and Excitation Transfer between Adenine and 2-Aminopurine in Single-Stranded Deoxytrinucleotides," *The Journal of Physical Chemistry B*, vol. 110, pp. 2899–2909, Feb. 2006. Publisher: American Chemical Society.
- [144] L. C. Sowers, G. V. Fazakerley, R. Eritja, B. E. Kaplan, and M. F. Goodman, "Base pairing and mutagenesis: observation of a protonated base pair between 2-aminopurine and cytosine in an oligonucleotide by proton NMR," *Proceedings of the National Academy of Sciences*, vol. 83, pp. 5434–5438, Aug. 1986. Publisher: National Academy of Sciences Section: Research Article.
- [145] T. M. Nordlund, D. Xu, and K. O. Evans, "Excitation energy transfer in DNA: Duplex melting and transfer from normal bases to 2-aminopurine," *Biochemistry*, vol. 32, pp. 12090–12095, Nov. 1993.
- [146] D.-G. Xu and T. M. Nordlund, "Sequence Dependence of Energy Transfer in DNA Oligonucleotides," *Biophysical Journal*, vol. 78, pp. 1042–1058, Feb. 2000.
- [147] T. M. Nordlund, "Sequence, Structure and Energy Transfer in DNA[†]," *Photochemistry and Photobiology*, vol. 83, no. 3, pp. 625–636, 2007.
- [148] J. M. Remington, A. M. Philip, M. Hariharan, and B. Kohler, "On the origin of multiexponential fluorescence decays from 2-aminopurine-labeled dinucleotides," *The Journal of Chemical Physics*, vol. 145, p. 155101, Oct. 2016. Publisher: American Institute of Physics.
- [149] J. M. Remington, M. McCullagh, and B. Kohler, "Molecular Dynamics Simulations of 2-Aminopurine-Labeled Dinucleoside Monophosphates Reveal Multiscale Stacking

- Kinetics,” *The Journal of Physical Chemistry B*, vol. 123, pp. 2291–2304, Mar. 2019. Publisher: American Chemical Society.
- [150] C. Wan, T. Fiebig, O. Schiemann, J. K. Barton, and A. H. Zewail, “Femtosecond direct observation of charge transfer between bases in DNA,” *Proceedings of the National Academy of Sciences*, vol. 97, pp. 14052–14055, Dec. 2000. Publisher: National Academy of Sciences Section: Physical Sciences.
- [151] M. A. O’Neill, C. Dohno, and J. K. Barton, “Direct Chemical Evidence for Charge Transfer between Photoexcited 2-Aminopurine and Guanine in Duplex DNA,” *Journal of the American Chemical Society*, vol. 126, pp. 1316–1317, Feb. 2004. Publisher: American Chemical Society.
- [152] “2-Aminopurine-2’-deoxyriboside Oligonucleotide Modification.”
- [153] A. Cannizzo, O. Bräm, G. Zgrablic, A. Tortschanoff, A. A. Oskouei, F. van Mourik, and M. Chergui, “Femtosecond fluorescence upconversion setup with broadband detection in the ultraviolet,” *Optics Letters*, vol. 32, p. 3555, Dec. 2007.
- [154] O. Cannelli, C. Bacellar, R. A. Ingle, R. Bohinc, D. Kinschel, B. Bauer, D. S. Ferreira, D. Grolimund, G. F. Mancini, and M. Chergui, “Toward time-resolved laser T-jump/X-ray probe spectroscopy in aqueous solutions,” *Structural Dynamics*, vol. 6, p. 064303, Nov. 2019. Publisher: American Institute of Physics.

A Appendix

A.1 Drawing of the wire-guided liquid-jet



A.2 UV-vis spectra before and after the 2AP time resolved experiments

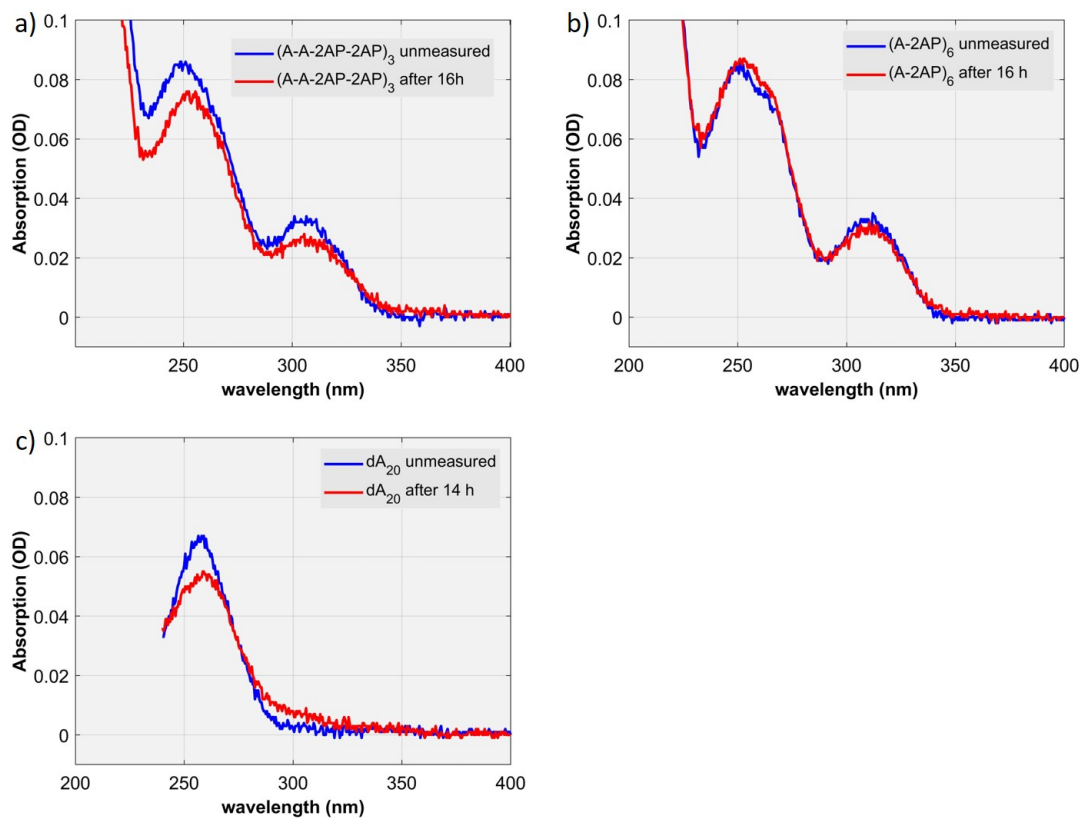


Figure A.2: UV-vis spectra of a) $(A-A-2AP-2AP)_3$, b) $(A-2AP)_6$ and c) $(dA)_{20}$ before and after measurements excited at 266 nm (see figures 6.10 and 6.16). Due to the low sample volumes a small fraction of the molecules are damaged during the experiment.

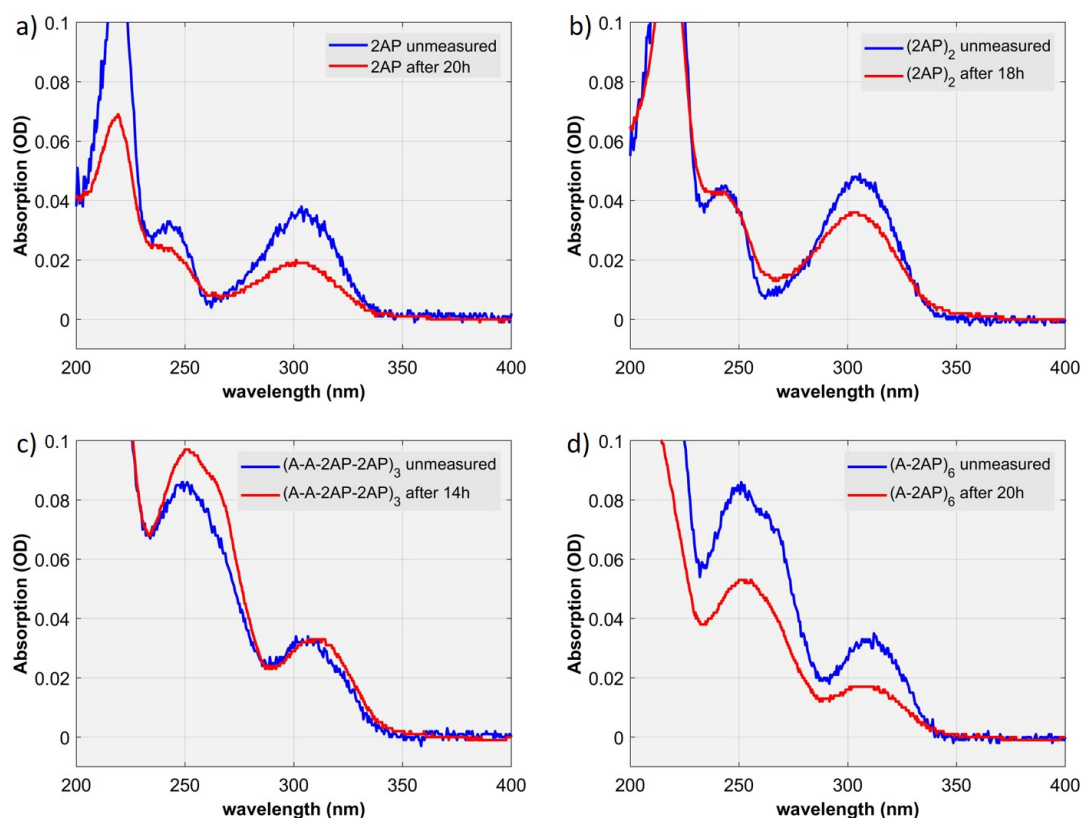


Figure A.3: UV-vis spectra of a) $(2AP)$, b) $(2AP)_2$, c) $(A-A-2AP-2AP)_3$ and d) $(A-2AP)_6$ before and after measurements excited at 326 nm (see figures 6.6 and 6.14). Due to the low sample volumes a small fraction of the molecules are damaged during the experiment.

Curriculum Vitae



Personal details

name **Benjamin Bauer**
adress **Rue Dr. César-Roux 26**
1005 Lausanne, Switzerland
mobile **+41(0)76 746 8699**
e-mail **Benjamin.Bauer@epfl.ch**
date of birth **18.12.1989, Lahr/Schwarzwald, Germany**

Education

- 07/2016 - current **Doctoral program in photonics**, *École polytechnique fédérale de Lausanne EPFL*, “*Electronic and structural dynamics in DNA single strands*”
chair: Prof. Majed Chergui - Laboratory of Ultrafast Spectroscopy (LSU)
specialties: Multi-dimensional femtosecond spectroscopy: 2DUV and circular dichroism. Planing, preparation, performing and analyzing of time resolved spectroscopic measurements. Operation of a cutting edge Ti:Sa laser system. Design and implementation of innovations in the setups.
- 10/2013-09/2015 **Master’s program physics**, *University of Constance*
specialties: laser physics and non-linear optics, solid state nano-structures
- 09/2014-09/2015 **Master thesis**, “*Pump-probe-spectroscopy of single quantum dots in high magnetic fields*”
chair: Prof. Alfred Leitenstorfer - Ultrafast Phenomena and Photonics
specialties: Handling a cutting edge femtosecond fiber laser system and a superconducting magnet cryostat system. Performing and analyzing pump-probe experiments. Preparing nano-structured samples in a clean room.
- 10/2010-09/2013 **Bachelor’s program physics**, *University of Constance*
- 04/2013-09/2013 **Bachelor thesis** “*Structure and electronic properties of graphene / Ni / Ir(111) sandwich compounds*”
chair: Prof. Mikhail Fonin
specialties: preperation, measurements (STM) and analysis of solid state nano-structures in ultra high vacuum.
- 09/2009-05/2010 **Civilian service**, *Ludwig-Frank-Haus Lahr/Schwarzwald (senior center)*, administrative work, elderly care
- 2000-2009 **Scheffel-Gymnasium Lahr in Lahr/Schwarzwald**,
high school graduation

Practical experience

— Teaching activities

Supervision of semester project (09/2018-06/2019) · Atoms and Radiation (02/2019-06/2019 and 2/2018-06/2018) · Electronic spectroscopy (09/2018-01/2019, /09/2017-01/2018 and 09/2016-01/2017) · Physics for chemists (10/2014-04/2015) · Physics for biologists (10/2013-04/2014)

— Activities as assistant

02/2016-06/2016 Group for Ultrafast Electron Imaging Dr. Peter Baum - MPQ-LMU Munich
10/2015-12/2015 Chair for Ultrafast Phenomena and Photonics Prof. Alfred Leitenstorfer - University of Constance
10/2013-09/2014 Chair Prof. Mikhail Fonin - University of Constance

Publications (selection)

B. Bauer, M. Chergui, and M. Oppermann, "Anisotropy of single stranded DNA in aqueous solutions", in preparation

B. Bauer, M. Chergui, and M. Oppermann, "Energy transfer between 2AP and adenine bases in a single strand", in preparation

B. Bauer, R. Shama, M. Chergui, and M. Oppermann, "Excited state dynamics of adenine single strands", in preparation

B. Bauer, M. Oppermann, and M. Chergui, "Exciton dynamics in DNA oligomers studied by broadband deep-UV transient absorption spectroscopy", EPJ Web Conf. **205**, 10006 (2019)

M. Oppermann, B. Bauer, T. Rossi, F. Zinna, J. Helbing, J. Lacour, and M. Chergui, "Ultrafast broadband circular dichroism in the deep ultraviolet", Optica **6**, 2334–2536 (2019)

M. Oppermann, J. Spekowius, B. Bauer, *et al*, "Broad-Band Ultraviolet CD Spectroscopy of Ultrafast Peptide Backbone Conformational Dynamics", J. Phys. Chem. Lett. **10**, 2700–2705 (2019)

O. Cannelli, C. Bacellar, R. Ingle, R. Bohinc, D. Kinschel, B. Bauer, *et al*, "Toward time-resolved laser T-jump/X-ray probe spectroscopy in aqueous solutions", Struct. Dyn. **6**, 064303 (2019)

M. Oppermann, N. Nagornova, A. Oriana, E. Baldini, L. Mewes, B. Bauer *et al.*, "The LOUVRE laboratory: State-of-the-art ultrafast ultraviolet spectroscopies for molecular and materials science", CHIMIA **71**, 288-294 (2017)

L. Wang, T. Rossi, M. Oppermann, B. Bauer, *et al*, "Slow Charge Carrier Relaxation in Gold Nanoparticles", J. Phys. Chem. C **124**, 24322-24330 (2020)

C. Hinz, P. Gumbsheimer, C. Traum, M. Holtkemper, B. Bauer *et al*, "Charge and spin control of ultrafast electron hole dynamics in single CdSe/ZnSe quantum dots", Phys. Rev. B **97**, 045302 (2018)

C. Hinz, C. Traum, J. Haase, B. Bauer, A. Leitenstorfer, and D. Seletskiy, "Femtosecond Hole Relaxation and Biexcitonic Transient Absorption in Single CdSe/ZnSe Quantum Dots", proceedings of CLEO-QELS, FM2B.7 (2015)

Oral presentations (selection)

XXI International Conference on Ultrafast Phenomena (Hamburg, 2018)

Annual meeting of the Swiss Physical Society (Lausanne, 2018)

Fall meeting of the Swiss Chemical Society (Lausanne, 2018)

Grants

PIER Travel Grant - UFP 2018 · Chemistry Travel Award 2018 (SCS)

Additional qualifications

— language skills

german - native · **english** - fluent · **french** - good command · **latin** - proficiency certificate

— IT

program language **MatLab** (good), **Fortran** (basic knowledge), **C** (basic knowledge)

graphic **Origin** (good), **Qti Plot** (good), **Inkscape** (good)

various **SolidWorks** (good), **Inventor** (good), **L^AT_EX** (very good)

— Hobbys and interests

triathlon, **alpin sports**, **trumpet**

Lausanne, 03.02.2021

Benjamin Bauer